COMPUTATIONAL FLUID DYNAMICS (CFD) MODELING OF SOLAR STEAM METHANE REFORMER AND DESIGN OF AN INTEGRATED NOVEL SOLAR COLLECTOR

BY

MUHAMMAD IBRAR HUSSAIN

A Thesis Presented to the
DEANSHIP OF GRADUATE STUDIES

KING FAHD UNIVERSITY OF PETROLEUM & MINERALS
DHAHRAN, SAUDI ARABIA

In Partial Fulfillment of the
Requirements for the Degree of

MASTER OF SCIENCE

In

MECHANICAL ENGINEERING

NOVEMBER 2013

KING FAHD UNIVERSITY OF PETROLEUM & MINERALS

DHAHRAN, SAUDI ARABIA

DEANSHIP OF GRADUATE STUDIES

This thesis, written by **Muhammad Ibrar Hussain** under the direction of his thesis advisor and approved by his thesis committee, has been presented to and accepted by the Dean of Graduate Studies, in partial fulfillment of the requirements for the degree of **MASTER OF SCIENCE in MECHANICAL ENGINEERING**.

Thesis Committee

Thesis Advisor

Dr. Esmail M. A. Mokheimer

Member

Dr. Shakeel Ahmed

Department Chairman

Dr. Zuhair Gasem

Member

Dr. Mohamed A. Habib

Dean of Graduate Studies

Dr. Salam A. Zummo

Date 17/2/14

Dedicated to my parents, my brothers and my sisters

ACKNOWLEDGEMENTS

In the Name of Allah, the Most Beneficent, the Most Merciful.

> Praise belongs to Allah, the Lord of all the worlds (2) The All-Merciful, the Very-Merciful. (3) The Master of the Day of Requital. (4) You alone do we worship, and from You alone do we seek help. (5) Take us on the straight path (6) The path of those on whom You have bestowed Your Grace, Not of those who have incurred Your wrath, nor of those who have gone astray. (7)
>
> Al-Fatiha

I begin with the name of Allah, the most beneficent, the most merciful. May Allah bestow peace on our beloved Prophet Mohammed (*peace and blessings of Allah be upon him*), and his family. I would not have able to complete this work without the help of Allah who endowed me with health, courage, aptitude and patience.

During this work my parents were a constant source of motivation and support. Their prayers, love and encouragement helped me to arrive at this milestone.

Acknowledgements are due to *King Fahd University of Petroleum and Minerals* which gave me the opportunity to pursue a graduate degree and also for all the support I received in carrying out this research. I am also grateful to the *Center for Clean Water and Clean Energy* at *KFUPM* and *MIT* for its support during this research.

I would like to express my gratitude to my thesis advisor Dr. Esmail M. A. Mokheimer for all he taught me, for his patience when I couldn't get things done and for his help when I needed it. I am also very thankful to my thesis committee members Dr. Shakeel Ahmed and Dr. Mohamed A. Habib for their involvement and encouragement.

Special thanks to my friends Osama Hasan and Khalid Nasim for all the “technical resources” they provided without which this work would not have been possible. Thanks also to all my colleagues in the Mechanical Engineering department for making my time in ME graduate room memorable.

TABLE OF CONTENTS

LIST OF TABLES

LIST OF FIGURES

ABSTRACT (ENGLISH)

NAME:	Muhammad Ibrar Hussain
TITLE:	CFD Modeling of Solar Steam Methane Reformer and Design of an Integrated Novel Solar Collector
MAJOR FIELD:	MECHANICAL ENGINEERING
DATE OF DEGREE:	NOVEMBER 2013

A comprehensive two dimensional axi-symmetric Computational Fluid Dynamics (CFD) based homogenous Steam Methane Reforming (SMR) model is developed in the present work. The developed model is capable of predicting the extent of SMR reaction over wide range of operating conditions. The model is also capable of predicting all previously reported trends in SMR process. It includes most comprehensive kinetic model along with all physicochemical phenomena that happen in SMR process. The developed model is used for parametric studies of SMR process. Effects of various flow parameters such as temperature, pressure, feed velocity and inlet feed composition on the SMR process are studied. To drive the SMR process, heat required is provided by solar energy. It is also recognized that SMR process requires the solar energy in a specific distribution for its efficient operation. For this purpose, a novel solar collector is developed. The solar collector can provide required flux distribution over a tubular absorber using continuous reflecting surface. It can secure the flux distribution even if the local solar flux changes. To achieve specific flux distribution, reflecting surfaces of various sizes and shapes can be obtained. Finally, SMR model is integrated with developed solar collector and size of most commonly used tubular reformer is optimized for the weather conditions of Dhahran, Saudi Arabia.

ABSTRACT (ARABIC)

ملخص الرسالة

الاسم: **محمد إبرار حسين**

عنوان الرسالة: **محاكاة ديناميكة عددية لمفاعل يعمل بالطاقة الشمسية لإعادة تشكيل وقود الميثان بالبخار وتصميم مجمع أشعة الشمس المطلوب للمفاعل**

التخصص العام : **الهندسة الميكانيكة**

تأريخ التخرج: **نوفمبر 2013**

تم تطوير نموذج رياضي شامل ثنائي الأبعاد مبني علي النمذجة العددية لديناميكا الموائع و انتقال الحرارة و التفاعلات الكيميائية لعملية اعادة تشكيل وقود الميثان الغازي باستخدام البخار مع وجود محفز كيميائي داخل مفاعل اسطواني متماثل حول محوره. و تم تطوير هذا النموذج الرياضي بحيث يمكن استخدامه لاستنتاج نواتج عملية اعادة تشكيل و قود الميثان و البخار تحت مدى واسع من ظروف التشغيل. و لقد تم التحقق من أن نموذج المحاكاة المطور خلال هذا العمل قادر على استنتاج نواتج التفاعلات التى تم الحصول عليها معمليا كما هو منشور في الأبحاث السابقة بدقة عالية. و يحتوي النموذج الرياضي المطور في هذا العمل على كل المعادلات الرياضية التي تصف كيناماتيكا التفاعلات الكيميائية و الظواهر الفيزيوكيميائية الشاملة و الموجودة في عملية اعادة تشكيل الميثان و البخار. و لقد تم استخدام برنامج المحاكاة الذي تم تطويره و التحقق من صلاحيته و قدرته علي محاكاة التجارب المعملية بدقة عالية في دراسة تأثير عوامل و ظروف التشغيل المختلفة مثل الضغط ودرجة الحرارة و سرعة السريان تركيب خليط المكونات عند مدخل المفاعل علي مكونات المنتج عند المخرج. أيضا تم تطوير و أمثلة تصميم مبتكر لمجمعات أشعة الشمس لتوفير الطاقة الحرارية المطلوبة للمفاعل بتوزيع معين كما تم الحصول على الأبعاد المثلى لمفاعلات اسطوانية الشكل كي تعمل بالشكل الأمثل عند استخدامها مع المجمعات الشمسية التي تم تطويرها خصيصا لهذا الغرض.

CHAPTER 1

INTRODUCTION

Greenhouse gases emitted by the burning of fuels have serious environmental issues. Their concentration in atmosphere is increasing day by day. For example, CO_2 content in the atmosphere has increased from 290 to 390 ppm from 1880 till 2006 as shown in Figure 1 [1]. Consequently, due to global warming the earth's average temperature has increased from 13.6 to 14.8°C from 1880 till 2006 as shown in Figure 2 [1].

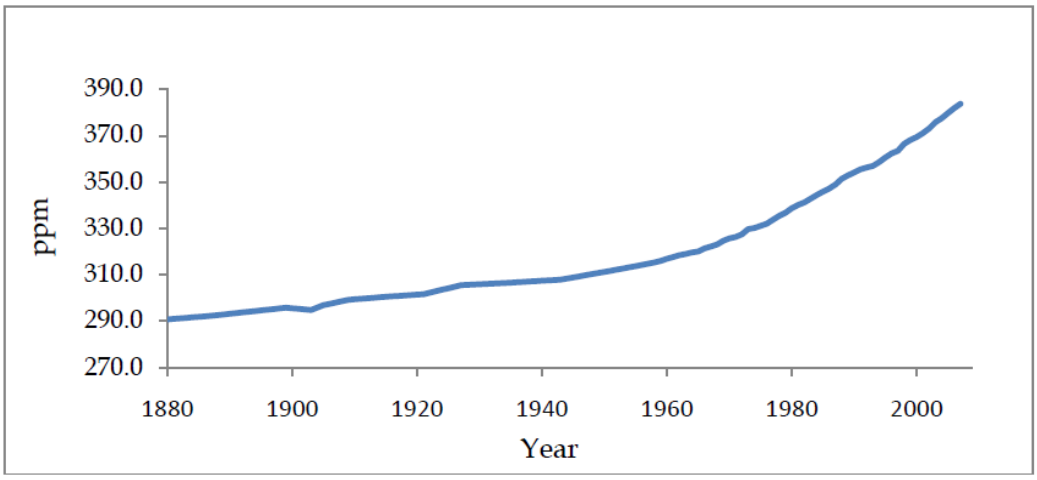

Figure 1 : CO_2 content in atmosphere [1]

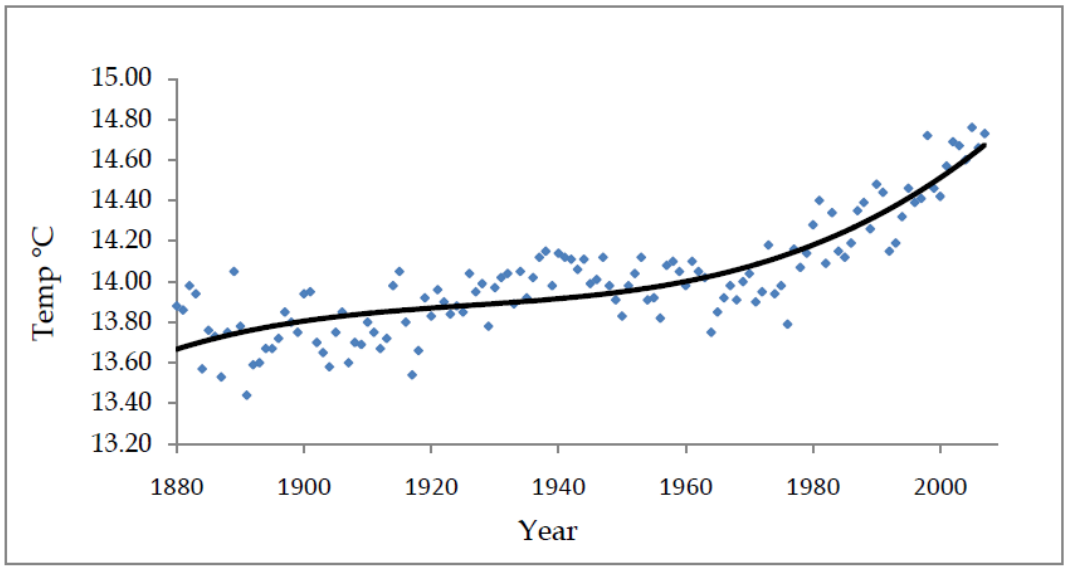

Figure 2 : Global average temperature for various years till 2006 [1]

If uncontrolled release of these harmful gases continues, soon the earth will be no longer suitable to live. The preservation of environment has foremost importance to preserve the life on earth. Therefore, there is a need to look for other resources that either have reduced emission of harmful gases or do not emit them at all.

1.1 HYDROGEN AND REFORMING PROCESS

Hydrogen is the lightest element with atomic number of 1. At the standard temperature and pressure, it exists as a colorless, odorless and diatomic gas. Hydrogen is highly flammable and combusts to produce water only. Therefore, hydrogen is regarded as ultimate fuel for clean combustion. Thus, by combustion of hydrogen, clean energy free of soot, NO_x, CO, and CO_2, can be obtained [1]. Other than combustion, hydrogen is also used for desulfurization in refineries, hydro-treating and for production of chemicals

[2]. Hydrogen can be produced by number of ways such as reforming, electrolysis and gasification as shown in Figure 3.

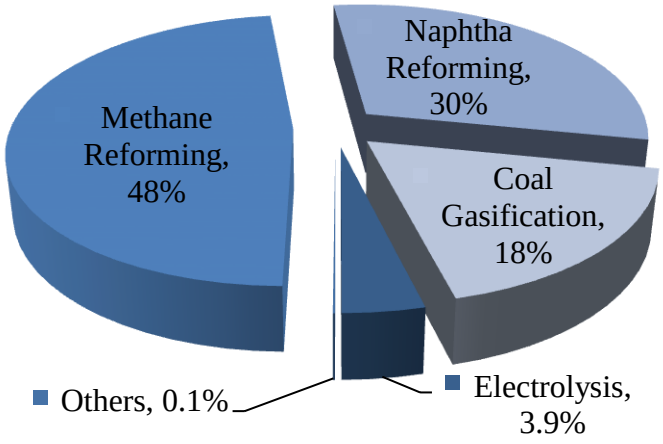

Figure 3 : Hydrogen production technologies [3]

Most commonly used process for hydrogen production is reforming. Reforming is a process that converts fuels into hydrogen rich stream. Appropriate fuels for the reforming are methane, gasoline, methanol and coal [3]. Most commonly used fuel for reforming is methane. It is because of its high hydrogen to carbon ratio. Moreover, the capital cost for hydrogen production plant using methane is three times less than the plant using coal [4]. Some important technologies for production of hydrogen from methane are

- Steam methane reforming (SMR)
- Partial oxidation (POx)
- Dry reforming
- Auto thermal reforming (ATR)

In steam methane reforming, methane reacts with steam to produce CO, CO_2 and hydrogen. In partial oxidation, methane is partially burnt to produce hydrogen. Dry reforming of methane uses carbon dioxide and methane to produce hydrogen in the presence of catalyst. Auto thermal reforming is the combination of steam methane reforming and partial oxidation of methane. Amongst all these processes, SMR has the highest H_2/CO molar ratio and thermal efficiency [3]. SMR is represented by following chemical equations [5].

$$CH_4 + H_2O \rightleftharpoons CO + 3H_2 \qquad \Delta H^{o}_{298} = 206 \text{kJ/mol}$$

$$CO + H_2O \rightleftharpoons CO_2 + H_2 \qquad \Delta H^{o}_{298} = -41.1 \text{kJ/mol}$$

$$CH_4 + 2H_2O \rightleftharpoons CO_2 + 4H_2 \qquad \Delta H^{o}_{298} = 164.9 \text{kJ/mol}$$

The low operating temperature of steam methane reforming makes it less liable to coke formation than POx, ATR and dry reforming. Unlike POx and ATR, no oxygen is required in SMR. On the other hand, it has high emissions and requires relatively high value of H_2O/CH_4 molar ratio to avoid coke formation.

In POx, half mole of oxygen is provided to combust one mole of methane. Thus, methane is partially oxidized due to lack of oxygen as shown in Eq. (1.1) [6]. To fully combust one mole of methane, two moles of oxygen are required as shown in Eq. (1.2) [7].

$$CH_4 + \tfrac{1}{2} O_2 \rightleftharpoons CO + 2H_2 \qquad \Delta H^{o}_{298} = -22.6 \text{ KJ/mol} \qquad (1.1)$$

$$CH_4 + 2O_2 \rightleftharpoons CO_2 + 2H_2O \qquad \Delta H^{o}_{298} = -802 \text{ KJ/mol} \tag{1.2}$$

No use of catalyst in POx makes it more economical than SMR and ATR. It is more tolerant to sulphur poisoning. However, it gives relatively low value of H_2/CO molar ratio. It also requires oxygen at the inlet feed. Neither oxygen nor steam is required at inlet feed for dry reforming. It is represented by following chemical equations [8].

$$CH_4 + CO_2 \rightleftharpoons 2CO + 2H_2 \qquad \Delta H^{o}_{298} = 247 \text{ KJ/mol}$$

$$CO_2 + H_2 \rightleftharpoons CO + H_2O \qquad \Delta H^{o}_{298} = 41.1 \text{ KJ/mol}$$

Reaction has high operating temperatures giving rise to coke formation. Dry reforming can also be used for recycling of CO_2.

The steam methane reforming reaction is endothermic. The Partial oxidation is exothermic. Auto thermal reforming, which is a combination of both, is thermally neutral process. Chemical equations representing auto thermal reforming are as follows [7].

$$CH_4 + \tfrac{1}{2}O_2 \rightleftharpoons CO + 2H_2 \qquad \Delta H^{o}_{298} = -22.6 \text{ KJ/mol}$$

$$CH_4 + H_2O \rightleftharpoons CO + 3H_2 \qquad \Delta H^{o}_{298} = 206 \text{ KJ/mol}$$

$$CO + H_2O \rightleftharpoons CO_2 + H_2 \qquad \Delta H^{o}_{298} = -41 \text{ KJ/mol}$$

$$CH_4 + 2H_2O \rightleftharpoons CO_2 + 4H_2 \qquad \Delta H^{o}_{298} = 165 \text{ KJ/mol}$$

ATR is usually operated at pressure lower than the operational pressure of POx. Reaction is thermally neutral, negating the use of any external heat source. This reaction can be stopped and restarted rapidly than SMR. POx and ATR requires oxygen at the inlet feed. The supply of purified oxygen at the inlet feed requires a costly oxygen separator. Otherwise, exit gas will be very much diluted with nitrogen. The POx and ATR have nearly equal thermal efficiencies but lower than that of SMR. SMR reaction is preferred at the industrial level worldwide. Table 1 summarizes the advantages and disadvantages of these technologies.

Table 1 : Relative advantages and disadvantages of different hydrogen production technologies [3]

Technology	**Advantage**	**Disadvantage**
SMR	• Most extensive industrial experience • High thermal efficiency about 85 % • Oxygen not required • Low process temperature • Best (H_2/C) ratio for H_2 production	• High steam to carbon ratio to avoid coke formation
ATR	• Low process temperature than POx • Thermally neutral • Can be stopped and restarted rapidly	• Requires oxygen • Limited commercial use • Low thermal efficiency about 60 to 75 %
POx	• Sulphur tolerant • No catalyst • No external heat source	• Requires oxygen • Low H_2/CO ratio • Low thermal efficiency about 60 to 75 % • High temperature for coke formation
Dry reforming	• No steam or oxygen is required at the inlet feed	• High temperature for coke formation

1.2 SMR AND OTHER HYDROGEN PRODUCTION TECHNOLOGIES

Ewan and Allen [9] have given a thorough survey of different hydrogen production technologies. The primary sources considered in this study are coal, solar energy, natural gas, nuclear energy, hydro energy, tidal energy and wind energy. Hydro, tidal, solar, nuclear and wind energies are used to produce electricity. This electricity is, then, used to produce the hydrogen through electrolysis process. Solar energy is considered to derive photochemical process. It is also considered to gasify the biomass, from where the hydrogen can be extracted by gas separator. Nuclear energy is considered to provide the heat energy for thermo chemical process such as reforming. The coal and natural gas are considered to produce the hydrogen by gasification and reforming processes, respectively. All these routes have different conversion efficiencies as given in Figure 4.

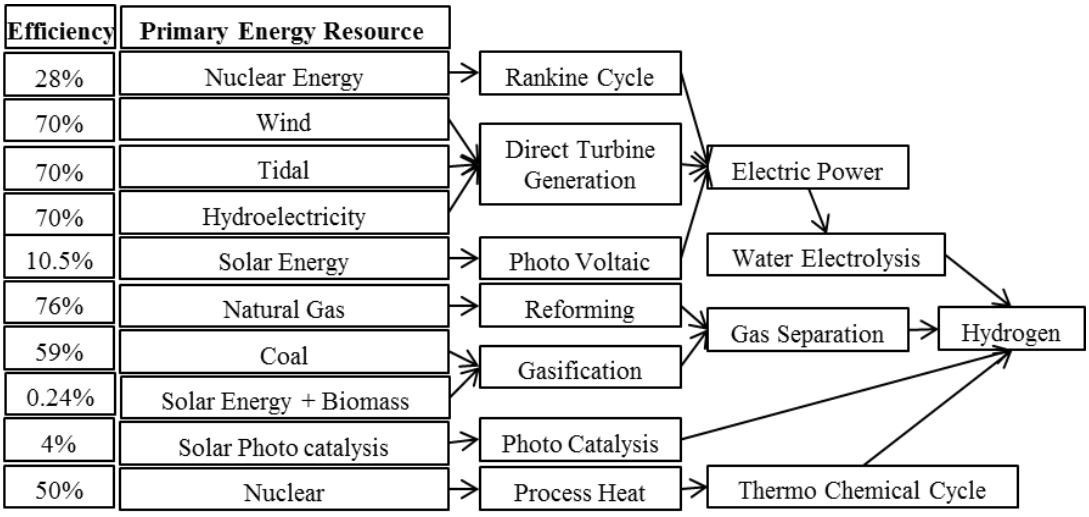

Figure 4 : Efficiencies of various routes to hydrogen [9]

It can be seen from Figure 4 that production of hydrogen from natural gas has the highest efficiency. Therefore, the SMR is the cheapest of all technologies and is used worldwide to produce hydrogen [10].

1.3 SOLAR ASSISTED STEAM METHANE REFORMING

The fossil fuel reservoirs of the world are providing the large portion of the energy needed for our daily lives. These resources are large enough to take care of our needs of energy for many years. For example, the world has totally 177.36 Tm^3 of the natural gas reservoirs [11]. These reservoirs are distributed all over the world in different countries as shown in Figure 5.

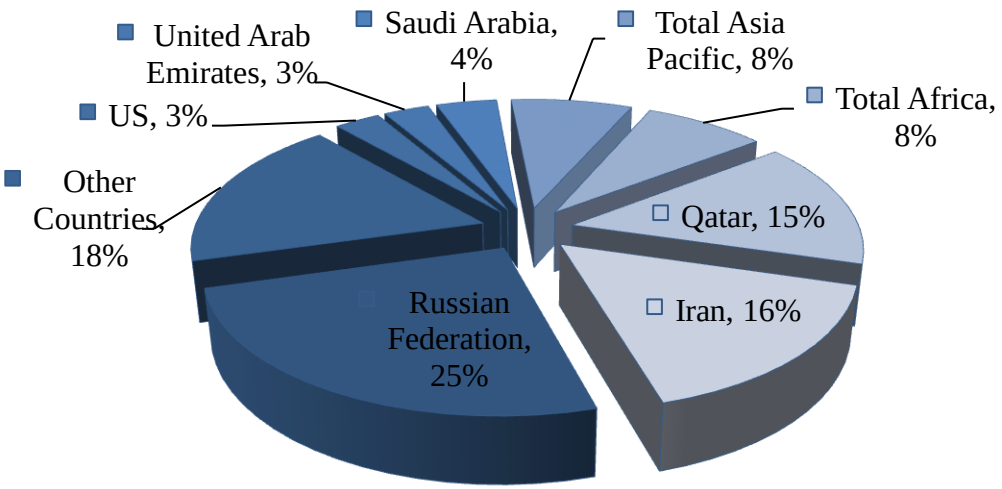

Figure 5 : World's natural gas reservoirs in various countries [11]

However, these energy reservoirs are being used rapidly and inefficiently. The inefficient energy extraction systems are wasting these reserves due to lack of efficient technology. At the present consumption rate, these resources are believed to last for only

60 years. The coal resources of the earth are also about to end. The total coal resources can supply the energy to the earth for only next 133 years at the present consumption rate [11].

These statistics are alarming. Now, it is inevitable to look for new energy resources which can meet our demands with equal ease. The renewable energy resources are the attractive choice. They are abundantly available. They can be accessed all over the world. All the renewable energy resources originate from the energy transferred by sun to the earth. Abbot [12] calculated the energy received by the earth and found it to be 0.85×10^{14} kW. He estimated the world's average energy demand to be 15×10^{9} kW and concluded that the solar energy has enough potential to take care of world's energy demands.

The main problem with the solar energy is that the technologies, converting the solar energy into our required forms, are not fully developed. Therefore, the technologies have not been commercialized yet. A lot of research is being carried out in this area but still these technologies do not provide energy at rates comparable to energy supply rate of fossil fuels. Moreover, the capital costs for most of the solar energy production plants are also high.

The fossil fuels have the advantage of providing the energy at the high rate but they are depleting. While, the renewable energy resources have the advantage of renewability but they cannot provide the energy at high rates. Therefore, there is a need to bridge the supply of energy at high rate by fossil fuels and the renewability of the solar energy. A bridge that can provide a part of required energy from solar as long as the supply rate is not affected. In this way, the available fossil fuels can be used carefully and at the low

rates until the research in the solar technologies is refined enough to meet all the demands.

Steam methane reforming reaction is endothermic in nature. It requires a certain amount of heat to proceed. This heat is stored in the products as chemical energy. This heat may be provided from sun to store the solar energy. Produced hydrogen can be combusted to obtain heat energy. Thus, steam methane reforming is a process that can provide the required bridge between the use of fossil fuels and solar energy. Thus, SMR process provides the solution to the problems of rapid depletion of fossil fuel, time required for the research in the solar technologies to make them efficient and clean environment.

1.4 SMR: - PROCESS DISCRIPTION

1.4.1 CHEMICAL REACTION

Steam methane reforming is a catalytically promoted endothermic reaction. In this process, mixture of methane and steam is passed over the surface of catalyst. Hydrogen and carbon monoxide are formed as products. The reaction is reversible in nature so methane and steam are also present in the product mixture. Aker and Camp [13] found that carbon monoxide and carbon dioxide are primary products of the reaction. Based on this observation, Allen et al. [14] proposed the following two chemical equations to explain the steam methane reforming reaction.

Reaction 1

$$CH_4 + H_2O \rightleftharpoons CO + 3H_2 \qquad \Delta H^{o}_{298} = 206 \text{kJ/mol}$$

Reaction 2

$$CO + H_2O \rightleftharpoons CO_2 + H_2 \qquad \Delta H^{o}_{298} = -41.1 \text{kJ/mol}$$

Gerhard and Moe [5] argued that at high operating temperatures of steam methane reforming, reaction 2 proceeds in backward direction and will not be in equilibrium. They showed that reaction 3 is also taking place in steam methane reforming reaction.

Reaction 3

$$CH_4 + 2H_2O \rightleftharpoons CO + 4H_2 \qquad \Delta H^{o}_{298} = 164.9 \text{kJ/mol}$$

Thus, the steam methane reforming reaction is world widely accepted to be explained by above mentioned three chemical equations. Reactions 1 and 3 are endothermic in nature. These reactions are favored by decrease in pressure as the number of moles on the right side of the chemical equations is greater than the number of moles on the left side. Reaction 2 is slightly exothermic in nature. This reaction is not affected by the change in pressure as evident from the balance of number of moles on the both side of reaction 2. Thus, overall reaction is endothermic in nature and favored by decrease in pressure.

1.4.2 OPERATING PARAMETERS

Steam methane reforming reaction takes place in a reactor of certain shape. This reactor is called reformer. The shape of reformers varies largely. The reformer contains the catalyst for SMR reaction. Catalyst consists of pellets of different shapes. Steam methane reforming reaction takes place at certain operating temperature and pressure. The reaction is endothermic in nature, so the operating temperature of the reaction is decided by the heat supplying source. The operating temperature and pressure of the SMR reaction depend on the required range of methane conversion. The inlet feed to the reformer consists of methane, steam and hydrogen. At the exit of the reformer, gases contain CO, CO_2, H_2, CH_4 and steam. The input gases are also found at the exit of reactor due to reversibility of the process. The feed gas composition is usually defined by steam to methane and hydrogen to methane molar ratios. Feed gases have certain mass flow rate. Each reformer operates at certain contact time. The value of that contact time can be obtained by dividing the volume of reactor to the volume flow rate of feed gases. Reformers are, sometimes, characterized by the inverse of contact time that is also called Gas Hour Space Velocity (GHSV).

1.5 OBJECTIVES OF THESIS WORK

The objectives of the present work are

- To develop a computational fluid dynamics model for homogenous steam methane reforming that can predict the steam methane reforming conversion with high accuracy.
- To validate the model using available experimental data and previously published work.
- To use the model for parametric analysis of steam methane reforming reaction.
- To develop a solar concentrator that can give required flux distribution.
- To integrate the steam methane reforming model with solar concentrator to provide a comprehensive design of solar heated steam methane reformer.

CHAPTER 2

LITERATURE REVIEW

Steam methane reforming is a reversible endothermic reaction. The reaction has very complex kinetics. A large number of catalysts have been developed for SMR to speed up the forward reaction rates. Catalysts, used for SMR, face some general problems such cocking and sintering. Lot of research is being carried out to overcome these problems. The SMR reaction also has non monotonic dependence on different operating parameters. Therefore, a number of simulative studies have been performed for parametric analysis of SMR reaction.

The use of solar collector to supply heat energy for SMR reaction requires the critical analysis of the provided temperature ranges by different solar collectors. The effect of flux distribution over the surface of SMR reformer also has severe effects on the catalyst and SMR conversion. The following sections discuss the state of the art for catalysts, kinetic and flow modeling of SMR. The theoretical and experimental temperature ranges for solar collectors are also discussed. The need of design of a novel solar collector that can give the required flux distribution is also highlighted.

2.1 CATALYSTS AND THEIR PERFORMANCE FOR SMR REACTION

The reaction rates of steam methane reforming are very low. Thus, various catalysts are used to accelerate the reaction. Higher reaction rates are required to make the reaction economically feasible. Usually nickel (Ni) and noble metals based catalysts are used for steam methane reforming reaction [4]. Most commonly used catalyst for steam methane reforming (SMR) is Ni. Ni is used as unsupported as well as supported on certain supports such as SiO_2, Al_2O_3, aluminate, ZrO_2 and Ce-ZrO_2 [15].

The ideal conditions for SMR are pure supply of methane, free of high hydrocarbons and sulfur, and low operating pressure. In real life, steam methane reforming reaction takes place far away from ideal conditions. Non ideal conditions, such as presence of higher hydrocarbons, sulfur content and high operating pressure, make the environment severe for catalyst to operate. So, a catalyst needs to circumvent the following four phenomena to be proved suitable for steam methane reforming [16].

- Activity
- Sulfur poisoning
- Coke formation
- Sintering

Commercially used Ni supported on Al_2O_4, Al_2O_3 and SiO_2 supports are reported to deactivate severely due to oxidation of Ni. Miguel et al. [17] showed that Ni/Al_2O_3 catalyst deactivated severely even when operated under different reaction conditions.

Activity of catalyst is found to be affected to a large extent by pretreatment. For example, Rhodium (Rh) Supported over Al_2O_3 is found to give higher activity than the fresh catalyst after subsequent oxidation reduction of catalyst at elevated temperature [18]. Reduction of catalyst prior to use recover the Ni oxides that are usually produced when Ni is supported on certain supports such as alumina and silica. For example, Ni supported on silica, alumina and zirconia supports has been tested with different reduction temperatures and it is found that the silica supports deactivated soon due to formation of Ni oxide. Ni supported on alumina does not reduce completely at 500°C and is found to be inactive. Ni reduced at 700°C is fairly active whereas Ni supported on zirconia is found to give the highest activity amongst all [19,20]. Supports also affect the catalyst's activity other than providing the high surface area to the active metal. A comparative study of Ni supported over Ce–ZrO_2, ZrO_2, CeO_2, $MgAl_2O_4$ and Al_2O_3 showed that Ni over Ce-ZrO_2 catalyst has the highest activity due to high interaction between Ni and Ce-ZrO_2 support as shown in Figure 6. The high activity of catalyst can also be attributed to the high oxygen carrying capacity of catalyst [21].

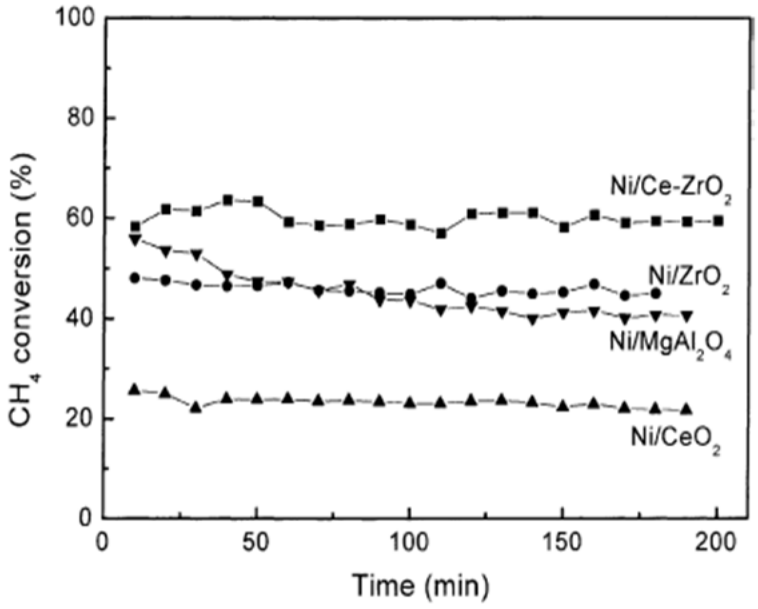

Figure 6 : Activity of supported Ni catalyst Vs time on stream (reaction conditions: P=1 atm, T= 750°C, S/C=3, GHSV=288000 $cm^3/g_{cat}h$) [21]

The methods of preparation of supports are found to have a strong influence on the activity of catalyst due to its influence on energies of active metals and supports. For example, Ni supported on conventional silica and the silica prepared by novel technique of Dielectric Barrier Discharge (DBD) are compared and conventional silica is found to have the higher activity [22].

Interaction of active metal and support is also a main factor that affects the products of steam methane reforming process. A comparison is reported for $Ni/ZrO_2/Al_2O_3$, Ni/La-Ca/Al_2O_3 and $Ni_{0.5}Mg_{2.5}AlO_9$ catalysts. Higher dispersion of active metal due to strong interaction with support cause the $Ni_{0.5}Mg_{2.5}AlO_9$ catalyst to have higher activity, stability and resistant to coke formation and sintering [23]. On the other hand, the strong interaction of Ni/Al_2O_3 catalyst obtained by increasing the calcination temperature is

found to be unfavorable for reduction of catalyst, thus, decreasing the activity of catalyst [24].

The deactivation of Ni/Al_2O_3 catalyst is also related to the concentration of H_2 gas by operating the steam methane reforming reaction at the temperature of 862 K. Deactivation is observed as usual but at the elevated temperature of 1017 K, when the supply of H_2 gas is stopped, a recovery of activity is observed. So, the deactivation is argued to happen due to the high H_2 concentration and low temperature [25].

Steam treatment studies showed that $Ni/Ce–ZrO_2/\theta\text{-}Al_2O_3$ catalyst deactivated in steam due to formation of inactive Ni/Al_2O_4 but reduced to Ni/Al_2O_3 in presence of H_2. Same effect is reported to be the reason for the deactivation of Ni/Al_2O_3 catalysts but for this catalyst the deactivation is low due the coverage provided by ZrO_2. Thus, the catalyst is highly active with the precautionary measure of not using the high Steam concentration initially [26].

Reaction rates increase by increasing the amount of active metal due to increase of number of active sites. Nickel aluminate catalyst with non stiochoimetric content of Ni, 16% and 49% of Ni loading, is tested and increase in conversion with increase in Ni was found [27]. In steam methane reforming, the loading of active metal is limited due to heat and mass transfer limitations. For example, Roh et al. [28] optimized the Ni loading on reduced Ni/Al_2O_3 catalyst and reported that amongst the samples of 6 to 15%, 12% loading of Ni has proved to be the best as shown in Figure 7. It is also reported that below 3% loading of Ni, inactive Ni/Al_2O_4 is formed.

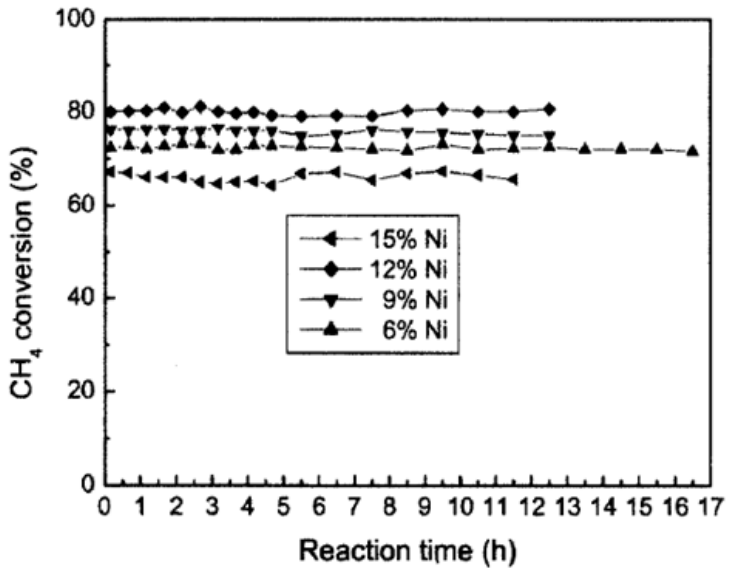

Figure 7 : CH_4 conversion with time on stream over Ni /θ-Al_2O_3 catalysts in SMR (reaction conditions: P=1 atm, T=1023 K, S/C= 1, GHSV=72000 mL/g_{cat}h) [28]

Dong et al. [29] studied the Ni loading on Ce-ZrO_2 catalyst and showed that amongst the samples of 3 to 30 % of loading, 15 % of Ni loading has given the higher activity and stability.

Different techniques have been developed to overcome the phenomenon of coke formation. For example, Ni catalysts are reported to operate in carbon free environment when passivated partly with sulfur. It is due to the fact that sulfur inhibits the coke formation more than the steam methane reforming [30]. Doping with small amount of Sulfur are found to reduce the coke formation strongly [31]. Coking of catalysts has also been reported to be reduced by adsorbing a controlled amount of sulfur on catalyst's surface or by preventing the formation of carbides. The use of small amount of tin or rare earth metals also reduce the coke formation [32,33].

Effect of Boron on the deactivation of conventional Ni/Al_2O_3 catalyst with 0.5% and 1% Boron loading has also been studied. Catalyst is reported to have higher stability with no loss of activity. It is also found that the conversion is higher than that of unsupported Ni catalyst and about 80 % decrease in coke formation is reported [34].

Lanthinia and zirconia (LaO_2, ZrO_2) promoted conventional Ni/Al_2O_3 is found to be more resistant to coke formation and it is also found that catalyst can be activated at low reduction temperature [35]. Coking also depends on the nature of active metal. For example, a comparison of 1 % wt Co, Cu, Fe, Ni, Pt and Pd supported on ZrO_2 showed that amongst all that are tested, Pt/ZrO_2 catalyst is resistant to coke formation [36].

On the other hand, some special supports have proved to be more coke resistant than the conventional supports. For example, $Ni/Ce–ZrO_2$ catalyst is found to be highly coke resistant than the conventional Ni/Al_2O_3 catalyst. It is reported to operate with low S/C ratio of 1 with optimized Ce/Zr: 3/1 ratio amongst the sample of 1/0, 1/1, 1/3, and 3/1. [37].

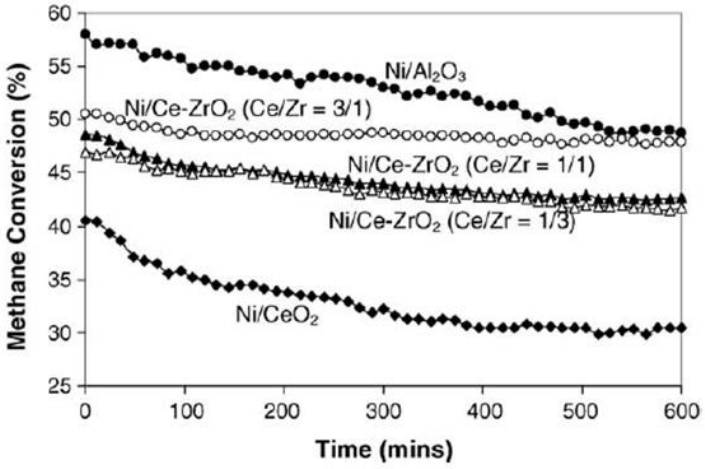

Figure 8 : Steam reforming of methane at 900°C for different catalysts (3kPa CH_4, 3kPa H_2O) [37]

Sintering is another important phenomenon affecting the production of steam methane reforming. It depends on number of parameters. For example, sintering process is found to occur rapidly at the start of reaction and then it slows down. It is more affected by sintering temperature than sintering time. At high temperature, particle migration is dominant and at low temperature atomic migration is dominant [38]. For Ni supported over Mg/Al_2O_4 catalyst, sintering occurs in the initial 200 hours. After that, the change of size of Ni particles is small. Ni particle size limit is also related to the support surface area and Ni loading. It is proportional to Ni loading [39].

2.2 KINETIC MODELING OF SMR

In earlier publications, simple kinetic rate expressions are developed where the rate of reaction is proportional to methane's partial pressure and similar expressions are developed by many authors even in recent years [40–42]. Table 2 shows some of the kinetic models depending only upon the partial pressure of methane.

Table 2 : Kinetic models depending on the partial pressure of methane only

Expressions	Kinetic Parameters	References
$-R_{CH_4} = k_o e^{\frac{-E}{RT}} P_{CH_4}$	k_o=127, E=8778	[13]
	k_o=1×10^6, E=31000	[43–45]
	k_o=1.04×10^6, E=20000	[4]
$-R_{CH_4} = k_o e^{\frac{-E}{RT}} \left(P_{CH_4} - P_{CH_4,e}\right)$	k_o=100-1×10^5, E=10000-26000	[46]
k_o=kmol/(h kg_{cat} atm) E=cal/mol		

Kinetic models based on the power law fit of the experimental data are relatively easy as less insight into the process is required. These models are relatively less accurate. For example in 1972, Steel et al. [47] developed a power law based kinetic model in the temperature range of 773 to 953 K. In this model, the rate of reaction depended on the partial pressure of methane and water but was independent of products' concentrations. The order of reaction rate was positive with respect to steam but negative with respect to the water. Rate expression was reported to be applicable after the 30 seconds of the start of reaction. It was also reported that the consumption of water was not compatible with the consumption of methane and mole fraction of CO_2 was way less than the mole

fraction of CO. This effect was explained by the production of oxygen from the catalyst and error in the measurements of mole fraction of water. Moreover, the rate of reaction was made independent of amount of catalyst used as well as flow velocity and other flow parameters. The power law based kinetic models are also being developed in recent year as by Ko et al. [48]. He developed a kinetic rate expression by taking into account the dependence of methane and steam only in temperature range of 823 K to 1073 K and in the pressure range of 1 to 10 bar. Rate of reaction was found to be the first order in methane and order of reaction rate with respect to steam was -1as shown in Table 3.

Table 3 : Power law based kinetic models

Expressions	**Kinetic Parameters**	**References**
$r_c = k_o e^{\frac{-E}{RT}} P_{CH_4}^n P_{H_2O}^m$	n=1,m=-0.5 k_o=1.78×10^{17} g-mol/g_{cat}.h, E=29 kcal/g mol	[47]
	n=1.104,m=-.9577 k_o=1527 g-mol/g_{cat}.h, E=14.82 kcal/g mol	[48]

One of the main assumptions used in power law based models is the applicability of rate expression after the certain contact time. The limits of that contact time are usually

such that the changes in the concentrations of the species are very small or reaction is close to thermodynamic equilibrium. To predict the rate of reaction right from the beginning, it is required to know how reactants behave when it come in contact with certain amount of catalyst. It requires an insight into the reaction mechanism.

Steam methane reforming reaction is a surface based catalytically assisted endothermic reaction. In this reaction, species are adsorbed on the surface of catalyst and undergo the reaction scheme to form products. The products, then, desorb from the surface of catalyst. How fast the reactants will be consumed, depends upon the slowest process from the adsorption of species, formation of products and desorption of products from the catalyst surface. The slowest process of SMR mechanism is also called the rate determining step. Table 4 shows some of the kinetic models based on rate determining steps.

Table 4 : Kinetic models depending on rate determining steps

Expressions	**Rate Determining step**	**References**
$r_c = k_o e^{\frac{-E}{RT}} P_{CH_4}$	Desorption of CO and CO_2	[14]
$r_c = k_o f\left(K\frac{P_{H_2O}}{P_{H_2}}\right)^n P_{CH_4}$ n=0 for $\frac{P_{H_2O}}{P_{H_2}} > 0.1$, n ≠ 0 for $\frac{P_{H_2O}}{P_{H_2}} < 0.1$	Dissociation of Methane or formation of CO and CO_2	[41]

$r_c = k_o P_{CH4} \Big/ \left(1 + K_A \frac{P_{H_2O}}{P_{H_2}} + K_B P_{CO}\right)^7$	Dissociation of Methane	[49]
$r_c = k_o e^{-\frac{E}{RT}} \left[K_{e3} P_{CH_4} P_{H_2O}^2 - P_{CO_2} P_{H_2}^4 \right]$	$CH_4 + 2H_2O \rightleftharpoons CO_2 + 4H_2$	[50]
$r_c = k_o e^{-\frac{E}{RT}} \left[P_{CH_4} - P_{CO} P_{H_2}^3 \Big/ P_{H_2O} K_{e2} \right]$	$CH_4 + H_2O \rightleftharpoons CO + 3H_2$	[51]
$r_1 = \frac{k_{o,1}}{p_{H_2}^{2.5}} \frac{(p_{CH_4} p_{H_2O} - p_{CO} p_{H_2}^3 / K_{e,1})}{(DEN)^2}$ $r_2 = \frac{k_{o,2}}{p_{H_2}} \frac{(p_{CO} p_{H_2O} - p_{CO_2} p_{H_2} / K_{e,2})}{(DEN)^2}$ $r_3 = \frac{k_{o,3}}{p_{H_2}^{3.5}} \frac{(p_{CH_4} p_{H_2O}^2 - p_{CO_2} p_{H_2}^4 / K_{e,3})}{(DEN)^2}$	Reaction of Carbon Intermediate with Absorbed Oxygen	[52–58]

Allen et al. [14] developed a kinetic rate expression for SMR process by taking the desorption of products (CO and CO_2) as rate determining step. The operating pressure for development of rate expression was varied from 1 to 18 atm and the temperature was kept constant at 1180°F. The initial rate of the reaction was found to be independent of total pressure, thus, the rate was said to be controlled by desorption of products. The proposed reaction mechanism was involving only the adsorption and desorption of species without recognizing the reaction of intermediates separately. Reaction mechanism

considered was very simple. The reaction rate was thought to be a function of total pressure only without recognizing the dependence on relative molar ratios of reacting species and on operating temperature. The constant initial rate can be explained by the constant value of operating temperature and constant inlet molar ratios of reacting species. That's why the model developed had an average error of 7% with a maximum error of 23% [14].

By assuming the simple reaction mechanism of adsorption of methane and desorption of CO with taking the reaction 1 ($CH_4 + H_2O \rightleftharpoons CO + 3H_2$) as the representative reaction of SMR, a kinetic model was developed by Munster et al. [41]. The rate determining step of SMR process was said to be dependent upon the oxygen activity measured by P_{H2O}/P_{H2} ratio. For P_{H2O}/P_{H2} ratio greater than 0.1, rate of reaction was reported to be dependent only upon the partial pressure of methane with adsorption of methane as rate determining step. But at lower values of P_{H2O}/P_{H2} ratio, the absorbed oxygen became the limiting reactant shifting the rate determining step to desorption of CO. Thus, this kinetic model predicted the positive as well as zero order reaction rate with respect to steam depending on the oxygen's activity.

Agnelli et al. [49] developed a kinetic model in temperature range of 640°C to 740°C and at atmospheric pressure by taking the adsorption of methane as rate determining step. Rate of reaction was found to be inhibited by the partial pressure of water whereas hydrogen was found to be the promoter. The rate of reaction also depended upon the partial pressure of CO but the dependence of all species other than methane was found to be very low. Thus, it was reported that, in the operating range of temperature and

pressure, the rate of reaction can be replaced by the first order kinetics involving only the partial pressure of methane. In this model, the values of P_{H2O}/P_{H2} was greater than 0.8. Thus, the rate determining step was the adsorption of methane as predicted by Munster et al. [41]. The rate of reaction was found to have the negative order with respect to steam whereas the rate of reaction was explained to have positive order with respect to steam for P_{H2O}/P_{H2} value less than 0.1 by Munster et al. [41]. Thus, this non monotonic dependence of the rate of reaction on steam's partial pressure needs to be explained clearly by a kinetic model.

The rate determining step varies considerably from model to model. Nikolla et al. [42] showed that over supported Ni the rate determining step is the activation of C-H bond. By eliminating the thermodynamics and transport artifacts, Wei et al. [54] also showed that over the Ni/MgO catalyst the activation of C-H bond is the rate determining step for SMR process. Jones et al. [59] showed that rate determining step in steam methane reforming process is the dissociation of methane but at low temperature the rate determining step changes to formation of CO.

Another important phenomenon that affects the determination of rate of reaction is the diffusion of species due to concentration and temperature gradients. If the rate of reaction is larger than the rate of diffusion, species will not diffuse enough to make the active catalyst site available for reaction, thus, directly reducing the rate of reaction. This reduction of rate of reaction is a function of catalyst's particle size. Smaller the catalyst particle size, lesser will be the decrease of rate of reaction [60]. The size of catalyst

particle can be decreased to a certain extent. It was shown that low particle size increase the deactivation of catalyst [40].

In most of kinetic models, the diffusion limitation are neglected by choosing the particle size small enough such that the diffusion limitation are minimum [40] but for a kinetic model to explain the phenomenon truly, diffusion limitations should be taken into account. Moreover, practically used catalyst has the particle size large enough to ensure the presence of diffusion limitation. Thus, a kinetic model apart from explaining the chemistry should include the diffusion limitation into account.

To handle the diffusion limitations, Oliveira et al. [57] used powered catalyst to minimized the diffusion limitations. Numaguchi et al. [61] developed a kinetic model based on mass and energy balance with pre-assumed rate determining step of adsorption of methane. A pre-assumed rate expression depending on the assumed rate determining step was forced to fit the experimental data to measure the diffusion limitations. As discussed previously, the rate determining step depends on the oxygen activity and can be different under different operating condition. Pre-assumed rate determining step, independent of operating conditions, gives the false explanation of reaction mechanism.

A kinetic model should explain the reaction mechanism correctly by picking the correct reaction path depending on the operating conditions. It should explain the non-monotonic behavior of order of rate of reaction with respect to the partial pressure of steam. It should take into account the diffusion limitations.

Taking the reaction of carbon intermediate with absorbed oxygen as rate determining step, Xu and Froment [52] developed a kinetic model. 21 sets of rate expressions were developed based on possible reaction mechanisms. The best rate expression that explained the experimental data accurately was reported to be the rate of SMR reaction in the operating range of temperature and pressure. Diffusion limitations were catered by taking into account the Knudsen and molecular diffusion. Mass conservation equation was solved on the particle surface by assuming the radial diffusion only. The developed pressure gradients were, then, used to calculate the reduction of rate of reaction due to diffusion [62]. This model also takes care of non-monotonic behavior of rate of reaction with respect to steam and hence it is a more generalized one [63]. It can be seen from Figure 9 that the rate of reactions 1, 2 and 3 are first increasing with increase in steam's partial pressure then, with further increase, it is decreasing. Same effect can be seen in the profile of rate of disappearance of steam and methane in Figure 10**.**

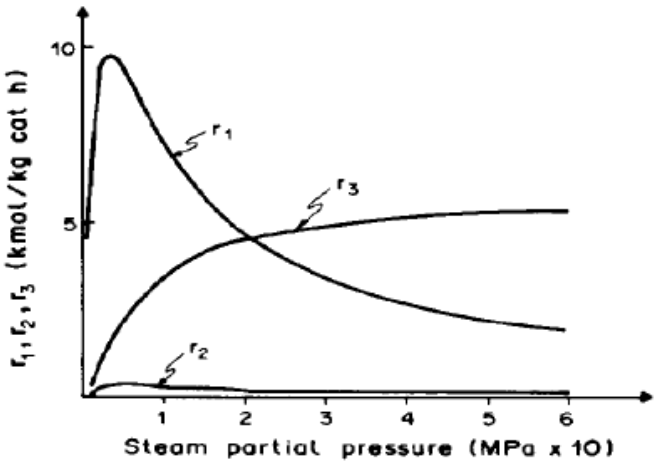

Figure 9 : Dependence of r_1, r_2, and r_3 on steam partial pressure at 900K, P_{CH4}=0.02, P_{CO}=0.01, P_{CO2}=0.01, P_{H2}=0.03 (all in MPa) [63]

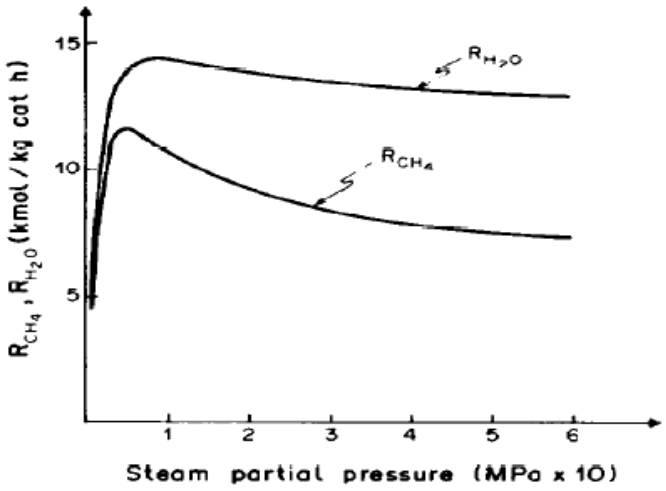

Figure 10 : Dependence of R_{CH4} and R_{H2O} on steam partial pressure at 900K, P_{CH4}=0.02, P_{CO}=0.01, P_{CO2}=0.01, P_{H2}=0.03 (all in MPa) [63]

This model also predicts the previously accepted trends for the order of rate of reaction. One of the main problems with previously developed model is that the range of operating conditions was very narrow. Model by Xu and Froment [52] is developed over the wide range of operating conditions. Thus, it can predict the previous models as well. For example, the model by Bodrov et al. [43–45] was developed for the latter part of range of operating conditions used by Xu and Froment [52] as shown in Figure 11.

The model developed by Dekan et al. [64] has the positive order of rate of reaction with respect to steam. This behavior can also be predicted by the Xu and Froment [52] as the range of operating conditions of model by Dekan et al. [64] was just a part of operating conditions used by Xu and Froment [52] as shown in Figure 12.

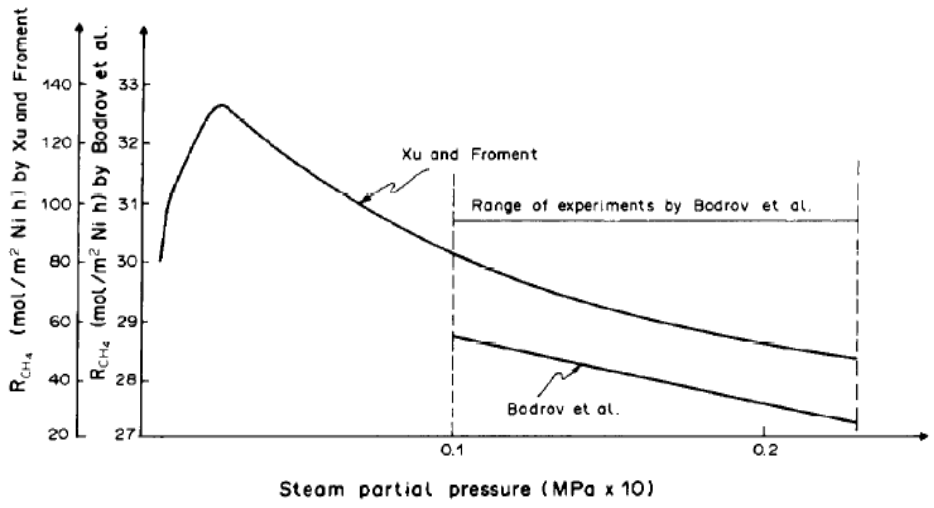

Figure 11 : Comparison of rate expressions by Bodrov et al. [43–45] and Xu and Froment [52], at 1173K, P_{CH4}=0.016, P_{CO}=0.0119, P_{CO2}=0.00261, P_{H2}=0.0462 (all in MPa) [63]

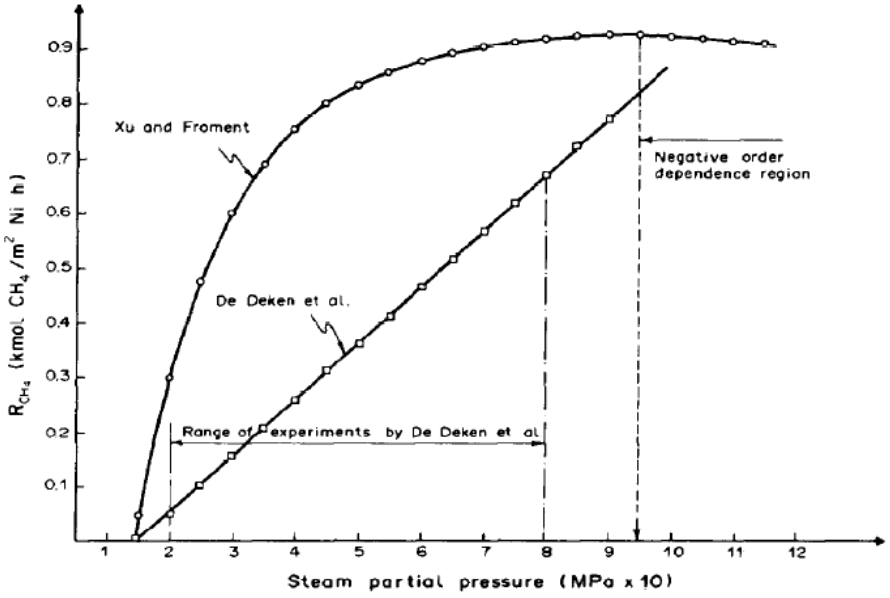

Figure 12 : Comparison of rate expressions by De Dekan et al. [64] and Xu and Froment [52], at 850K, P_{CH4}=0.2, P_{CO}=0.05, P_{CO2}=0.05, P_{H2}=0.2 (all in MPa) [63]

A comparison of this model with previously developed model by Temkin et al. [65] was presented where complex model developed by Temkin in. [65] converges to the model developed by Xu and Froment [52] under normal operating conditions of SMR process and for low hydrogen partial pressure [66]. Similar approach has been used by many authors to develop the rate of SMR reaction on different catalysts [40,55–58,66].

2.3 FLOW MODELING OF SMR

Different models have been developed for SMR to predict the extent of reaction under certain operating conditions and to serve for optimization purposes. The Intrinsic kinetic rates solely depend on the scheme of reaction and are independent of other flow factors such as diffusion, inertial and viscous resistance to the flow, heat transfer resistance etc. In actual case, the rates of reactions are different from the intrinsic reaction rates due to the diffusion limitations. The ratio of actual reaction rate to intrinsic reaction rate is called the effectiveness factor. Depending on the evaluation of the effectiveness factor, SMR models are classified into three types.

2.3.1 HOMOGENEOUS MODEL

In homogenous model, a predefined constant value of effectiveness factor is assumed [67–69]. Thus, observable or actual rates are directly obtained by multiplying the intrinsic rate with effectiveness factor. In this model, it is considered that whole reaction zone is filled with continuum of catalyst. Thus, the reaction is considered to happen everywhere in the reaction zone even in the empty spaces between the catalyst pellets. Reaction mixture and catalyst pellets are considered to have thermal homogeneity.

2.3.2 PSEUDO HOMOGENOUS MODEL

Pseudo homogenous models are same as that of homogenous model except that a profile of effectiveness factor along the direction of flow is taken into account instead of constant value. In these models, a correlation for effectiveness factor is used. Correlation usually depends on the shape of catalyst pellet. Thus, for one catalyst bed, profile of effectiveness factor remains same [70–73].

2.3.3 HETEROGENEOUS MODEL

Heterogeneous model is the most realistic one. In this model, actual catalyst pellets are simulated in the reaction zone. Thus, effectiveness factor is determined at every location in the reformer by solving species transport equations over the volume of catalyst pellet [60,74–80].

Heterogeneous models are very sensitive to diffusion limitations, thus, often misleading if the diffusion limitations are not handled carefully. These models are complex and require the solution of separate continuity equations over the volume of catalyst pellets. Pseudo homogenous models are catalyst bed specific and usually are insignificant while using reformers of small length. Homogenous models are simple and are good choice as long as the diffusion limitations are modeled precisely.

SMR reaction takes place over a wide range of gas hour space velocity. Therefore, both laminar and turbulent flows can be used to model the SMR reaction. Turbulence modeling of a chemical reaction is usually performed when reaction rates are controlled by mixing of reactants such as in combustion. In SMR, reaction rates are not controlled by mixing of reactants. Reaction rates totally depend on the local temperature, pressure

and relative molar ratios of species. Therefore, SMR is usually modeled using laminar flows. In most of the models, a general continuity equation representing the whole flow along with one momentum and one energy equation is solved. Estimation of pressure drop along the length of reactor is usually done by using Fanning friction factor [60,70,71,76–79] but separate pressure drop correlation are also used solely or in combination with complete momentum conservation equation [67,69]. In most of the one dimensional energy equations solved for various models, only heat losses and energy sink due to endothermic nature of reaction are taken into account [60,70,73,77–79]. Whereas in recently developed three dimensional models, heat generation by shear stresses and by expansion or contraction of fluid, heat diffusion due to mass diffusion caused by concentration gradient as well as temperature gradient along with convection are considered [67,74]. For the species in reaction mixture separate species transport equations are solved. Specie transport equations varies from simple one dimensional equation without diffusion [78,79] to complex three dimensional ones with mass and thermal diffusion [69,74,77]. Estimation of main fluid properties such as thermal conductivity, density, viscosity and specific heat varies largely from model to model. In simple one dimensional models, porosity of catalyst bed only affects the diffusion coefficients [77,79]. In three dimensional models, apart from affecting the diffusion, porosity affects the mass conservation by changing the velocity of flow. It also reduces the heat diffusion due to diffusion of species' flux and the volumetric rate of appearance or disappearance of species [69,74]. Mass diffusion coefficient is usually determined by taking the Knudsen and molecular diffusion into account [69,70,73,74,76–80]. The main problems faced by SMR are low methane conversion due to reversibility, coke formation,

catalyst deactivation, heat transfer issues and diffusion limitations [2,16,22,31–33,38,39,81–88]. There is a need to develop a SMR model that includes all of above mentioned phenomena so that extent of SMR reaction can be predicted with high accuracy.

2.4 ACCURACIES OF AVAILABLE SMR MODELS

A large number of models, dealing with kinetics as well as heat transfer phenomena, are available for SMR reaction [89–109]. Each of these models has certain accuracy. The accuracy depends on the kinetic and flow modeling of the reaction. When the choice of catalyst is made, the kinetics of the reaction becomes fixed. Kinetic models are available for almost every catalyst with reasonable accuracy. The flow modeling of SMR reaction faces some serious problems due to mass and heat transfer limitations. Therefore, the accuracy of the complete model mainly depends on the flow modeling of SMR reaction. The overall accuracy of the complete model is then estimated by the simulative studies to check the model under various operating conditions. The following issues necessitate the simulative study of SMR reaction:

- Complex kinetics due to the occurrence of parallel reactions
- Addition of hydrogen at the inlet feed
- Non-monotonic order of reaction rate with respect to the partial pressure of steam

The factors that mainly affect the accuracy of SMR reaction are:

- Diffusion of mass, energy and momentum attributed to temperature and concentration gradients
- Pressure drop due to porous catalytic medium
- Energy source as a result of endothermic nature of reaction

In simple one-dimensional models, it is difficult to incorporate such factors precisely. For instance, one-dimensional model by Murray et al. [46] has the maximum error around 26%. On the other hand, in three-dimensional CFD based SMR models, the above mentioned factors can be included with precise estimation of diffusion coefficients and material properties. This makes them more accurate as compared to one-dimensional models. For example, the three-dimensional model developed by Seo et al. [67] has the maximum error of 4%. This error can be attributed to inadequate modeling of the energy source due to chemical reaction. Zhai et al. [68] developed a three dimensional CFD based SMR model for micro reactors but, in this model, the energy source term was neglected. Therefore, the model has the maximum error of about 8%. Irani et al. [69] modeled a micro reactor SMR model using both surface and volume based reaction models. This model has about 2% error with surface based and about 9% error with volume based reaction model. While modeling volume based reaction, the pressure drop term was neglected so the error increased. In surface based reaction models, the source term is usually neglected which accumulates error. Chen et al. [110] developed a comprehensive three dimensional model with proper non-dimensionalization of parameters and achieved accuracy as high as 1.28%. SMR models available in the literature are compared in Table 5.

Table 5 : Percentage errors of different models available in the literature

References	**Dimensionality**	**Reference for Kinetic Models used**	**Types of Kinetic Model**	**% Error**
Murray et al. [46]	1 D	Murray et al. [46]	First order kinetic model	26%
Seo et al. [67]	3 D	Xu and Froment [52]	Kinetic Model based on rate limiting step	4%
Zhai et al. [68]	3 D	Deutschmann et al.		8%
Irani et al. [69]	3 D	Xu and Froment [52]		2% to 9%
Chen et al. [110]	3 D	Snoeck et al.[111,112]		1.28%

2.5 SOLAR COLLECTORS FOR SMR REACTION

The use of solar energy as heat source for SMR reaction raises some serious challenges. Methods for production of heat form solar energy are less efficient. Efficiency of the process strongly depends on the local weather. Large capital cost and long payback period are also the main discouraging factors [113]. Extensive research is needed to make the technology economical enough to be commercialized.

In almost all the solar heat generation systems, the key component is the solar collector. Solar collector is a device that intercepts a certain amount of solar energy falling on the earth and uses this energy to increase the internal energy of system under consideration. Solar collectors are divided into two main types of imaging and non-imaging collectors. Imaging solar collector are those which can make the image of their source. Non imaging solar collectors are those which are not able to make the image of their sources. Further classification of these collectors is as follows.

- Non imaging solar collectors
    - Flat plate collectors
    - Compound parabolic collectors
- Imaging solar collectors
    - Parabolic trough collectors
    - Parabolic dish collectors
    - Solar towers

Non imaging solar collectors are the ones that do not make the image of the source. That's why, the energy flux for these types of collectors is less, therefore, are used for low temperature applications. In the imaging solar collectors, an image of source is produced. Imaging collectors have high values of solar flux density. These types of collectors can give high temperatures and are used for high temperature applications. Imaging solar collectors have a reflecting surface and an absorber. Reflecting surface reflects as well as focus the flux density to the absorber by certain design ratio called concentration ratio. This is the ratio of area of reflector to the area of absorber and is given as

$$C_n = \frac{A_{ref}}{A_{abs}}$$

Where, C_n is the concentration ratio. A_{ref} is the area of reflector and A_{abs} is the area of absorber. Due to non-ideal behavior of reflector and absorber, temperature of absorber also depends on the reflectance and absorbance of the reflector and absorber respectively. Rabl [114] developed an equation for the maximum temperature achieved by a solar collector as below.

$$T_{abs} = T_s \left((1-\eta) \frac{\tau}{\varepsilon} \frac{C_n}{C_{ideal}} \right)^{1/4} \tag{2.1}$$

T_s is sun's surface temperature

T_{abs} is temperature of absorber

η is efficiency of heat removal by the process in present case it is SMR reaction

C_{ideal} is maximum concentration ratio

C_n is concentration of solar collector under consideration

This is maximum ideal value of temperature gained by a collector. It is clear that the temperature obtained by any collector depends on the concentration ratio. For flat plat collectors, the concentration ratio is one and the maximum achievable temperature is around 400K. It shows that the flat plat collector cannot be used for SMR reaction where the temperature requirements are in the range of 800K to 1000K. To obtain the temperature is this range, concentrating collectors should be considered. The actual values of temperature gained by a collector are far less than predicted by Eq.(2.1) and are shown in Table 6.

Table 6 : Comparison of temperatures obtained by different solar collectors [115]

Motion	**Collector Type**	**Absorber Type**	**Concentration ratio**	**Obtained temperature (°C)**
Stationary	Flat plate collector	Flat	1	30-80
	Evacuated Tube collector	Flat	1	50-200
	Compound Parabolic collector	Tubular	1-5	60-240

Single Axis tracking	Linear Fresnel reflector	Tubular	10-40	60-250
	Parabolic Trough collector	Tubular	15-45	60-300
	Cylindrical Trough collector	Tubular	10-50	60-300
Two axis tracking	Parabolic dish collector	Point	100-1000	100-500
	Heliostat Field collector	Point	100-1500	150-2000

This analysis shows that parabolic dish and solar tower are the collectors that can be used for SMR reaction.

2.6 SOLAR STEAM METHANE REFORMERS

Steam reformers can be heated by solar energy. As SMR process require the elevated temperatures to operate, the solar steam methane reformers are used in combination with solar concentrators. Small scale solar steam methane reformers use parabolic dish concentrators because of their ability to provide high temperatures. Compound parabolic concentrators are also used for steam methane reforming. Compound parabolic concentrators become important when effect of non-parallel nature of solar rays become

significant [116]. There are two types of solar reformers. One is directly irradiated and the other is indirectly irradiated. In directly irradiated solar steam methane reformers, the catalyst directly faces the concentrated solar radiations. A directly irradiated solar steam methane reformer is shown in Figure 13 [117].

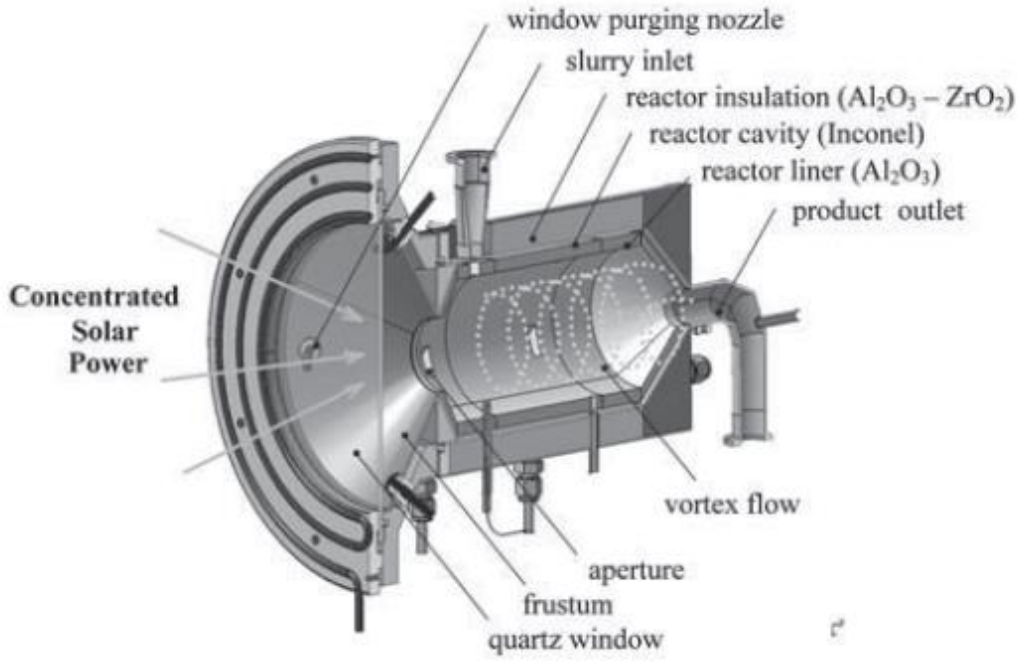

Figure 13 : Directly irradiated vortex flow reformer [117]

This particular type of reformer is vortex flow reformer. Reformer has a quartz window that receives solar radiations. The reformer has distant inlet and exhaust to minimize the heat losses. The flow area for reaction mixture is coated with catalyst that is directly irradiated with solar radiations. To prevent the thermal losses, reformer is also insulated. In other type of solar reformers, the concentrated solar energy is not made to fall directly on the catalyst. The solar energy heats a heat transferring fluid. This fluid

transfers the energy to chemical reaction. An indirectly irradiated solar reformer is shown in Figure 14 [117].

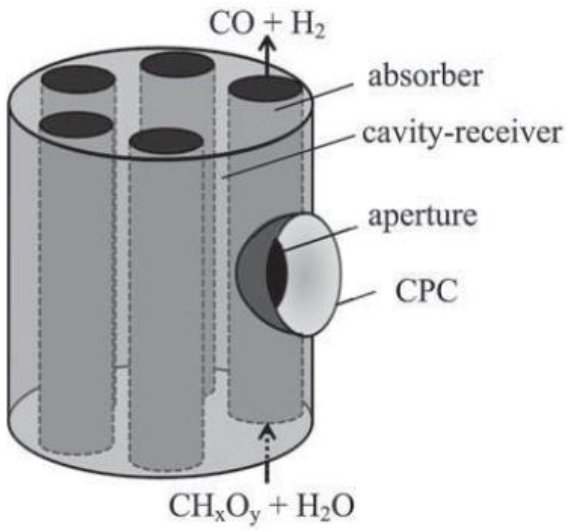

Figure 14 : Indirectly irradiated solar reformer [117]

In this reformer, catalyst is contained in tubes. The concentrated solar radiations are collected and concentrated by Compound Parabolic Collectors (CPC). This energy is transferred to the catalyst containing tubes by the mean of heat transferring fluid.

SMR reaction is very sensitive to the way the energy is supplied. The presence of hot spots and large amplitude of thermal cycling can degenerate the catalyst. Muir et al. [118] studied the SMR reaction integrated with solar dish. The flux density distribution and radially achieved temperature variation are shown in Figure 15 and Figure 16 respectively.

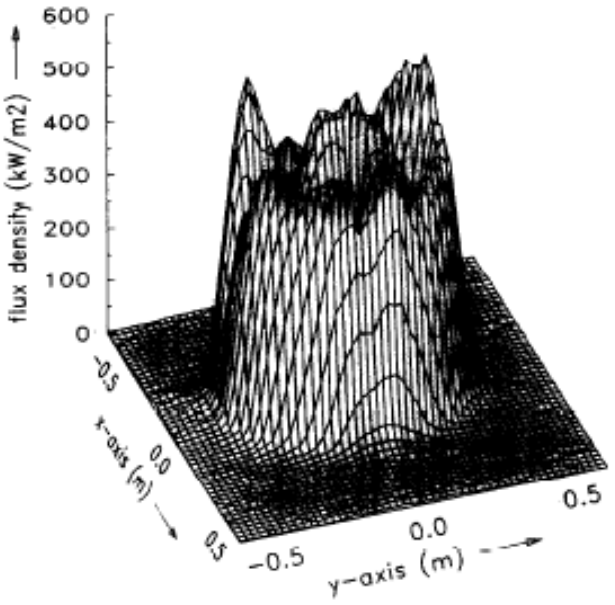

Figure 15: Solar flux density distribution [118]

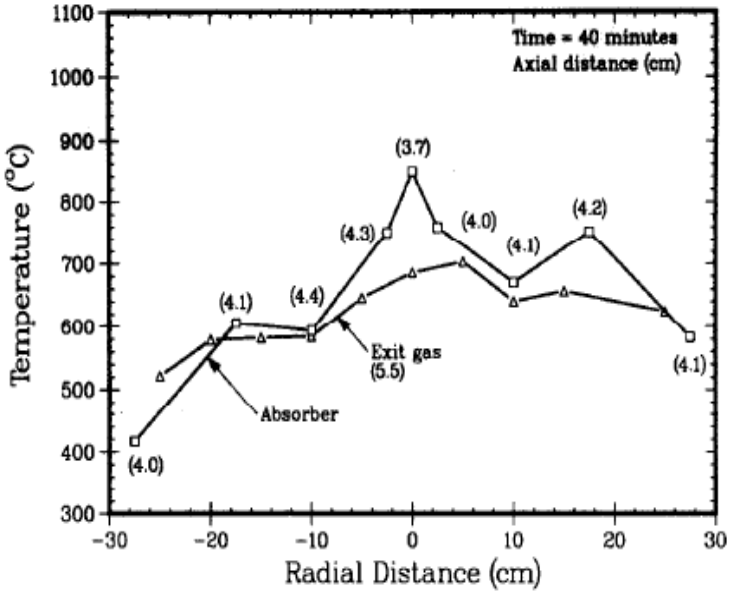

Figure 16 : Radial temperature distribution [118]

It can be seen from Figure 16 that the large variation is present in temperature distribution. This temperature cycling results in the severe cracking of catalyst as shown in Figure 17.

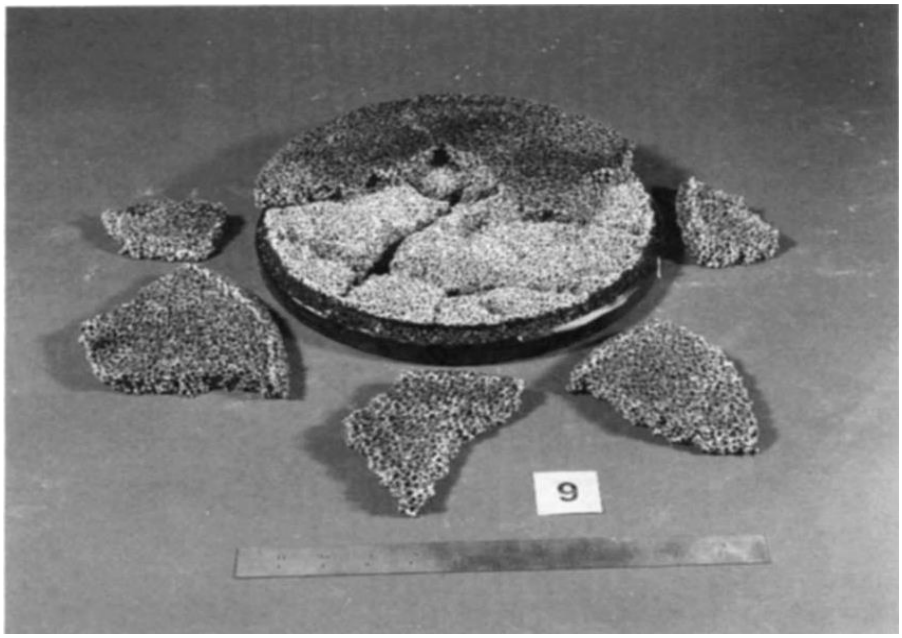

Figure 17 : Cracking of catalyst [118]

Thus, temperature distribution should be such that it has minimum effects on catalyst. Apart from affecting the catalyst, the specific energy distribution is also required for achieving the high conversion of SMR reaction. Anikeev et al. [119] tried to get the optimal temperature distribution over tubular reformer heated with solar parabolic dish as shown in Figure 18.

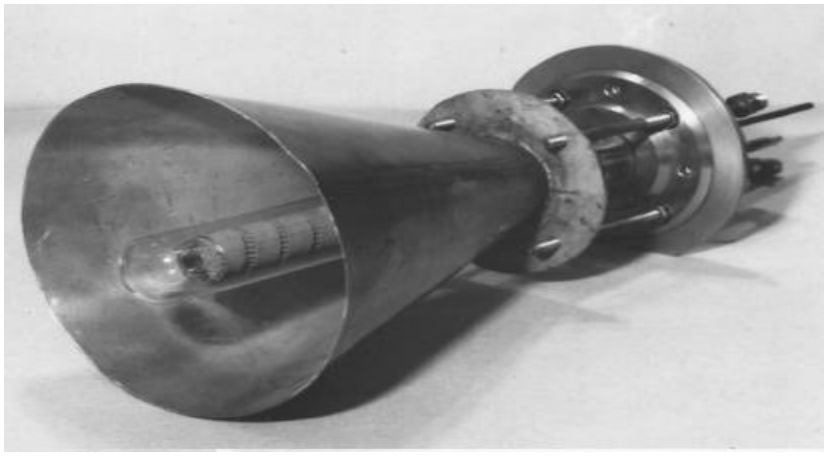

Figure 18 : Tubular reformer with solar parabolic dish [119]

The reformer is moved along the focal axis to get the temperature distribution that can give the maximum conversion. Figure 19 shows the five temperature distribution obtained for five different locations of reformer with respect to parabolic dish.

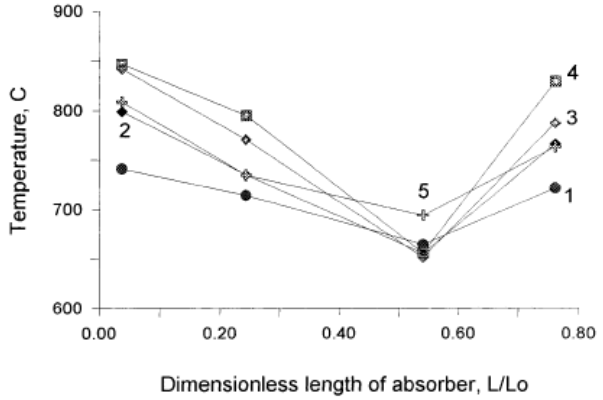

Figure 19 : Temperature distribution for five different location of reformer [119]

The distribution of temperature over the surface of reformer depends on the distribution of supplied heat flux. Pantoleontos et al. [60] optimized the SMR reaction and found a profile for supplied heat flux at the wall of tubular SMR as shown in Figure 20.

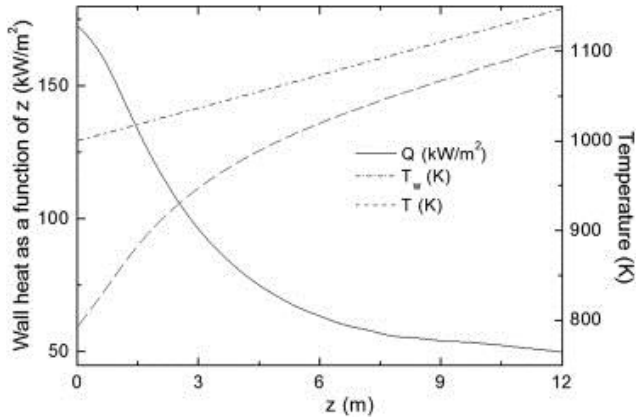

Figure 20 : Wall heat flux, bed temperature and wall temperature for optimal operation of SMR [60]

Thus, to efficiently integrate the SMR reaction with solar collector, specific distribution of supplied heat flux is required. Therefore, the distribution of heat flux over the surface of absorber and its effects must be reported if not handled as done by Zhigang Li et al. [120].

2.7 DESIGN OF SOLAR COLLECTOR

Solar parabolic dish is an imaging collector. The maximum energy concentration ratio is limited for this collector [115]. The extra restriction for a solar collector to be of imaging type was found to be irrelevant by Roland Winston [116]. He proposed a non-imaging concentrating solar collector that can give high concentration ratios than the imaging ones with a greater acceptance angle. After that, lot of work is reported by Rabl and Winston [114,121] to improve these collectors but still there is a question of flux distribution. Various attempts have been made to control the flux distribution over the surface of absorber. The shape of the absorbing surface is optimized to get uniform flux distribution by using the ray tracing technique but the shape is far away from the usual conduits used for heat transfer [122]. For a specific application of stiriling engine, the shape of absorber is also modified and a concave mirror like shape in the axisymmetric plane of the receiver is reported [123]. Splitting the aperture's cross sectional area by using small reflectors dealing with a smaller wave front is also conducted [124]. The collector has a complex geometry and reflecting surface is not continuous. Combinations of light path modification methods are also reported. In these methods, reflection and refraction are used together to control the energy absorbed by the absorber but the distribution of flux is not handled [125]. Some detecting mechanisms are also used to

change the position of the receiver with respect to energy being focused [126]. Some structures with a secondary reflector of parabolic shape are reported where the light reflected from first reflector is placed at the focus of the second but small parabola [127]. Moving the focal point along the focal axis of parabola is also reported [128]. The reflecting surface is imaging and can change its focus along the focal axis with change of sun's position. The use of cavity tubular receiver is also reported [129]. The solar radiations at the entrance of tubular cavity are made to fall at certain angle so that the light keeps on reflecting in the cavity until it is absorbed. The path of the rays is not studied which does not allow the understanding of the flux distribution along the length of absorber. A combination of Fresnel shapes reflector is also used to intercept a certain part of light wave front and to reflect it separately [130].

It can be seen from above survey that most of the present collectors do not handle the flux distribution precisely. Therefore, there is a need to develop a collector that can give flux distribution in a required pattern.

CHAPTER 3

APPROACH AND MEHODOLOGY

The objective of present work is to develop a computational fluid dynamics based homogenous steam methane reforming reaction model. Model is required to validate the available experimental data and previously published work with great accuracy. In the present work, a concentrating solar collector is also developed to provide the required flux distribution. The developed solar collector model is also integrated with steam methane reforming model in the later part of this work. The approach and methodology adopted to develop the steam methane reforming model and solar concentrator are discussed in this chapter.

3.1 APPROACH

3.1.1 DEVELOPMENT OF SMR MODEL

The approach towards development of SMR model includes following steps.

3.1.1.1 CHOICE OF KINETIC MODEL

The thorough literature survey presented in chapter 2 shows that the extent of SMR reaction is quantized by certain models called kinetic models. A large number of kinetic models are available in the literature. Most of the models are applicable only in the certain range of operating parameters and cannot be generalized. To develop a complete comprehensive model for SMR reaction, there is a need to look for a kinetic model that can operate over a wide range of operating conditions. The model should be able to predict all the previously observed trends in SMR. The model must also predict the results of other models in their operating ranges. Thus, the first step towards the development of comprehensive SMR model is to select the most accurate kinetic model available in the literature.

3.1.1.2 FLOW MODELING

The flow modeling of SMR reaction also has great importance. It can be seen in the literature survey that although there are some one dimensional models available in the literature, the true SMR phenomena can be accurately captured by two or three dimensional models. One of the most important phenomena that affect the SMR reaction is the diffusion. Diffusion of momentum and energy directly affect the velocity, pressure and temperature fields. The false development of velocity, pressure and temperature

fields gives false estimation of product's concentrations making the model less accurate. Therefore, a two dimensional axisymmetric model is developed to capture the precise estimation of product's concentrations.

3.1.1.3 MODELING OF CATALYST PELLETS

The presence of the catalyst in the steam methane reformer raises serious modeling challenges. The catalysts have pellets of different shapes. Each pellet has pore of different sizes and shapes. The SMR reaction takes place on the surface of these pellets as well as in the pores. The actual estimation of product's concentrations is achieved by modeling the catalyst pellets of exact size and shape. The actual pore structure's sizes and arrangement of the catalyst pellets are very difficult to determine. Therefore, it is very difficult to model the actual scenario of SMR reaction. This problem is handled by considering the reformer to be filled completely with a continuum of catalyst of reduced density. The SMR reaction is supposed to happen everywhere in the reformer. By using this approach, a generalized model for SMR reaction can be obtained.

3.1.1.4 PRESSURE APPROXIMATION

The porous nature of the catalyst pellets offers the inertial and viscous resistance to the flow. These resistances increase the pressure drop across the reformer. This pressure drop depends on the sizes and shapes of catalyst pellets. The true pressure drop across the reformer can only be obtained by modeling all the catalyst pellets and solving the flow for each of them. As stated earlier, there is very high uncertainty in determination of actual shapes and sizes of the catalyst pellets due to which catalyst is modeled as continuum of reduced density. Therefore, the estimation of pressure drop is obtained

using correlation. A semi empirical correlation developed by S. Ergun [131] is used. This correlation is applicable over wide range of Reynolds number and works for many types of porous beds.

3.1.1.5 DIFFUSION LIMITATIONS

The diffusion limitations, which is decrease in the appearance of product's concentrations due to lack of diffusion, are modeled using homogenous model. Homogenous model uses a constant value of effectiveness factor. This is a good approach as long as the pressure drop estimation across the reformer is accurate. By using this approach, small variations of concentrations around the catalyst pellets cannot be obtained.

3.1.1.6 TREATMENT OF DIFFUSION/CONVECTION OF MOMENTUM/ENERGY

Inertial and viscous resistances, offered by catalyst pellets, will reduce the velocity of the flow. However, decrease in cross sectional area of reformer, due to presence of catalyst pellets, will accelerate the flow to keep the mass flow rate constant. The thermal resistance will decrease the temperature of the reaction mixture. Therefore, the diffusion/convection of momentum and energy will decrease. The decrease in these quantities is modeled by multiplying them with porosity [55,69,74].

3.1.1.7 TREATMENT OF MASS AND ENERGY SOURCES

In the actual reformer, the reaction is taking place only on the surface of catalysts pellets and in the pores. With the approximation of continuum of the catalyst, the reaction will be taking place everywhere in the reaction mixture. Therefore, the mass and energy

sources produced as the result of the SMR reaction will be overestimated. These values must be decreased. The decreasing factor for these terms is one minus porosity. This factor (one minus porosity) when multiplied with volume, represents that volume of the reformer where the SMR reaction is actually happening.

3.1.1.8 DIFFUSION OF MASS

To account for diffusion of mass, a binary diffusion equation is solved, where the binary diffusion coefficients is calculated by Wilke Chang equation for dilute fluids [132]. The effective diffusion coefficient is obtained from Knudsen and molecular diffusion coefficients by using parallel pore model [62].

3.1.2 VALIDATION OF MODEL AND PARAMETRIC STUDIES

The model is validated with the experimental data reported by Xu and Froment [52]. For parametric studies, wide ranges of the operating parameters such as pressure, temperature, mass flow rate, steam to methane molar ratio and hydrogen to methane molar ratio are selected. The simulations are performed under these operating conditions. The effect of variation of these parameters on the methane conversion is reported.

3.1.3 DESIGN OF SOLAR COLLECTOR

Approach towards the design of solar collectors is of very basic nature. The rays tracing method is used in combination with law of reflection to develop the required solar collector. The dimensions of the SMR reformer, local solar flux density and the position of reformer with respect to the reflecting dish are the parameters that are taken as inputs. The local solar flux density is considered to be constant (no variation in space). The solar

collector is considered to operate under steady state conditions. It means that collector takes no time to respond to the change in solar flux density (change with respect to time). Solar radiations are considered to be parallel. Reflection of these radiations is considered to be specular and the collector is supposed to track the sun perfectly.

3.1.4 INTEGRATION OF SMR MODEL WITH DESIGNED SOLAR COLLECTOR

Having the results of simulation, the heat flux profile required to derive the reaction is extracted. This heat flux profile along with actual data of solar flux density is, then, used in design algorithm to develop solar collector.

3.2 WORK METHODOLOGY

3.2.1 SMR MODEL

The two dimensional axisymmetric conservation equations for mass, momentum, energy and species are established to include all the approximations mentioned in section 3.1.1. Finite volume method is used to solve these equations. For this purpose, commercially available CFD code ANSYS FLUENT 13.0 is used. UDF is written to incorporate the selected kinetic model in CFD code of ANSYS FLUENT 13.0.

3.2.2 DESIGN OF SOLAR COLLECTOR

Based on the assumption mentioned in section 3.1.3, design partial differential equations are developed for solar collector. These equations are solved numerically using MATHEMATICA software. The solution of these equations gives the data points for the

required solar collector surface. These equations can be solved to the required value of precision to get the smooth reflecting surface of solar collector.

CHAPTER 4

CFD MODELING OF STEAM METHANE REFORMER

In this chapter, a comprehensive two dimensional axisymmetric CFD based homogenous steam methane reforming model is developed. The assumptions made to develop the SMR model are discussed. The governing equations that describe SMR reaction under the assumptions made for the process are developed.

4.1 MODEL DESCRIPTION

To develop the SMR model, approaches discussed in the section 3.1 are used. In this section, these approaches are discussed briefly. Inside the reformer, instead of modeling the catalyst pellet, a continuum of catalyst of reduced density is modeled [67,69]. This approach is justified as long as catalyst particle size is small. This approach is also justified when interest is focused on changes in concentrations of species at length scale larger than the size of catalyst particle. In this case, a stretched distribution of concentrations of species is obtained. Modeling the catalyst bed as continuum requires special attention while solving temperature, pressure and velocity field throughout the

domain as there are no catalyst pellets to offer the inertial and viscous resistance to the flow. The effect of accelerating the coming flow due to difference in flow area and decreased diffusion/convection of momentum and energy cannot be obtained in the absence of catalyst pellets.

In actual reformers, porosity of catalyst bed is a decreasing factor for cross sectional area of the reformer to accelerate the fluid. In the present model, porosity is used as a decreasing factor for velocity to get the same mass flow rate through the reformer as the flow area is not being decreased due to absence of catalyst pellets. It decreases the convection and diffusion of momentum in such a way that per unit change in length at the scale larger than the scale of catalyst particle size, convection and diffusion are the same as expected in original reformer filled with catalyst pellets. Conductivity of reaction mixture is determined by mass weighted law. Volume averaged conductivity of reaction mixture and catalyst pellets is used for diffusion of energy. Density of reaction mixture is determined by volume averaged value of temperature and pressure dependent densities of individual species. Thermal conductivities are determined by mass weighted law.

The rate of chemical reaction expressed in ($kg/(m^3s)$) is corrected by multiplying it by one minus porosity that is actually the reducing factor for density of catalyst bed [55,69,74]. In some experiments, some diluents such are quartz or alumina are used. In this case, chemical reaction rate should be corrected such that reaction rate is always expressed per unit reformer volume. Molecular diffusion is obtained by solving Stephen-Maxwell equation and binary diffusion coefficients are calculated by Wilke Chang equation for dilute fluids [132]. Finally the effective diffusion coefficient was calculated by using parallel pore model.

4.2 CFD MODEL

The way the SMR process is modeled necessitates the solution of one continuity, momentum and energy equations. Where n-1 species transport equations along with one species conservation equation are solved. These equations are taken from the work of Seo et al. [67] and modified according to the approach discussed in chapter 3.

Continuity equation

$$\nabla.(\varepsilon\rho_f\vec{V}) = 0 \tag{4.1}$$

Momentum equation

$$\nabla.\left(\varepsilon\rho_f\vec{V}\vec{V}\right) = -\nabla\left(\varepsilon P\right) + \nabla\left(\varepsilon\vec{\tau}\right) - \frac{150}{d_p^2}\frac{(1-\varepsilon)^2}{\varepsilon^3}.\mu_f\vec{V} \tag{4.2}$$

In above equation, first term on left hand side is convection of momentum multiplied by porosity. First and second terms on right hand side are gradient of pressure and diffusion of momentum respectively. These terms are also multiplied by porosity to obtain actual physical velocity field inside the reformer. Last term in Eq. (4.2) is viscous loss due to porous nature of catalyst.

Energy equation

$$\nabla.(\rho_f\vec{V}E + \vec{V}P) = \nabla.(k_e\nabla T - \sum_i h_i j_i + (\vec{\tau}.\vec{V})) + (1-\varepsilon)\sum_i h_i\eta_i R_i \tag{4.3}$$

On the left hand side of above equation, first term represents convection of total fluid energy while second term represents heat generated by compression. First three terms on right side of above equation represent energy transfer due to conduction, species

diffusion and viscous dissipation respectively. Last term on right hand side is energy source due to chemical reaction. This term is multiplied with a factor (1-ε) to obtain the energy source from a volume where reaction actually happens.

Species transport equation

$$\nabla.\left(\rho_i \vec{V} Y_i\right) = -\nabla.J_i + \left(1-\varepsilon\right)\eta_i R_i \tag{4.4}$$

First term on left/right hand side of above equation is convection/diffusion of species. Second term on left hand side is mass source due to chemical reaction. This term is also multiplied with the factor (1-ε) to obtain the mass source from a volume where reaction actually happens.

$$R_i = \sum_{x=1}^{3} a_{ii} r_x - a_i r_x \tag{4.5}$$

In above equation, Ri is rate of appearance/disappearance of products/reactants [133]. r is rate of reaction 1, 2 and 3. x indicates reaction 1, 2 and 3. aii and ai are coefficients of specie i in products and reactants for reaction r respectively.

$$J_i = \rho_i D_{i,e} \nabla Y_i + D_{i,T} \frac{\nabla T}{T} \tag{4.6}$$

Diffusive flux, J_i, consists of mass and thermal fluxes shown respectively by first and second terms on right hand side of above equation [68].

$$\frac{1}{D_{e,i}} = \frac{1}{D_{n,i}} + \frac{1}{D_{m,i}} \tag{4.7}$$

The effective diffusion coefficient, $D_{e,i}$, is obtained from Knudsen, $D_{n,i}$, and molecular diffusion, $D_{m,i}$, coefficients by using parallel pore model [62].

Equation of state for reaction mixture is given as follows [67].

$$P = \rho_f RT \sum_i \frac{Y_i}{M_i} \tag{4.8}$$

Effective density of reaction mixture is calculated by using volume weighted mixing law and is shown as follows [133].

$$\rho_f = \frac{1}{\sum_i \frac{Y_i}{\rho_i}} \tag{4.9}$$

Specific heat capacity of species are calculated using fourth order polynomial and is shown as follows [133].

$$C_{pi} = \sum_{i=1}^{5} A_{C_p,i} T^{i-1} \tag{4.10}$$

Effective specific heat capacity of reaction mixture is calculated by using mass weighted mixing law as follows [133].

$$C_p = \sum_i Y_i C_{pi} \tag{4.11}$$

Viscosity of each specie is calculated by using power law as follows [133].

$$\mu_i = \mu_{i,o} \left(\frac{T}{T_o} \right)^n \tag{4.12}$$

Effective viscosity of reaction mixture is calculated using mass weighted mixing law and is given as follows [133].

$$\mu = \sum_i Y_i \mu_i \tag{4.13}$$

Temperature dependent thermal conductivity of each specie is calculated by following formula [133].

$$k_i = \frac{15R\mu_i}{4M_i}\left(\frac{5C_{pi}M_i}{R} + \frac{1}{3}\right) \tag{4.14}$$

Fluid mixture's thermal conductivity is calculated by mass weighted mixing law as follows [133].

$$k_f = \sum_i Y_i k_i \tag{4.15}$$

Effective thermal conductivity is calculated as follows [67].

$$k_e = \varepsilon k_f + (1-\varepsilon)k_s \tag{4.16}$$

The kinetic reaction rate for reactions 1, 2 and 3 are calculated as follows [52].

$$r_1 = \frac{k_{o,1}}{p_{H_2}^{2.5}} \frac{(p_{CH_4} p_{H_2O} - p_{CO} p_{H_2}^3 / K_{e,1})}{(DEN)^2} \tag{4.17}$$

$$r_2 = \frac{k_{o,2}}{p_{H_2}} \frac{(p_{CO} p_{H_2O} - p_{CO_2} p_{H_2} / K_{e,2})}{(DEN)^2} \tag{4.18}$$

$$r_3 = \frac{k_{o,3}}{p_{H_2}^{3.5}} \frac{(p_{CH_4} p_{H_2O}^2 - p_{CO_2} p_{H_2}^4 / K_{e,3})}{(DEN)^2} \tag{4.19}$$

Where the denominator (*DEN*) is given as

$$(DEN) = 1 + K_{CH_4} p_{CH_4} + K_{CO} p_{CO} + K_{H_2} p_{H_2} + p_{H_2O} K_{H_2O} / p_{H_2} \tag{4.20}$$

Equilibrium constants ($K_{e,1}$, $K_{e,2}$ and $K_{e,3}$) are calculated as follows [74].

$$K_{e,1} = 10^{13.076 - 11650/T} \tag{4.21}$$

$$K_{e,2} = 10^{-1.764 + 1910/T} \tag{4.22}$$

$$K_{e,3} = 10^{11.312 - 9740/T} \tag{4.23}$$

Eq. (4.17), Eq. (4.18), Eq. (4.19) and Eq. (4.20) are used to develop User Defined Function (UDF). This UDF calculates reaction rates which are used in Eq. (4.5) to calculate the rate of appearance or disappearance of species.

4.2.1 PARAMETERS FOR KINETIC MODEL OF SMR

Rate constants for Arrhenius equation $k_{o,i} = A_i \exp(\frac{-E_i}{RT})$

Table 7 : Rate constant for Arrhenius equation [52]

Activation Energy, E_i ($kJmol^{-1}$)	**E_1**	**E_2**	**E_3**
	240.1	67.13	243.9

Pre-Exponential factor, A_i (dimension of k_i)	A_1, ($kmolbar^{0.5}/kg_{cat}\ h$)	A_2, ($kmol/bar\ kg_{cat}\ h$)	A_3, ($kmolbar^{0.5}/kg_{cat}\ h$)
	4.225×10^{15}	1.955×10^{6}	1.020×10^{15}

Constants for Van't Hoff equation $K_i = B_i \exp(\frac{-H_i}{RT})$

Table 8 : Constant for Van't Hoff equation [52]

Absorption Enthalpy Change, H_i ($kJmol^{-1}$)	$\mathbf{H_{H2O}}$	$\mathbf{H_{CH4}}$	$\mathbf{H_{CO}}$	$\mathbf{H_{H2}}$
	88.68	-38.28	-70.61	-82.90
Pre-Exponential factor, B_i (dimension of K_i)	B_{H2O}	B_{CH4},(bar^{-1})	B_{CO},(bar^{-1})	B_{H2},(bar^{-1})
	1.77×10^{5}	6.65×10^{-4}	8.23×10^{-5}	6.12×10^{-9}

4.3 LIST OF USER DEFINED FUNCTIONS

To solve the developed SMR model, following user defined functions are written

- UDF to calculate reaction rates
- UDF to calculate diffusion coefficients of species
- UDF to calculate density of methane

- UDF to calculate density of steam
- UDF to calculate density of hydrogen
- UDF to calculate density of carbon monoxide
- UDF to calculate density of carbon dioxide

4.4 SOLUTION PROCEDURE

The developed mathematical model is solved numerically by finite volume method. For this purpose, commercially available CFD code provided by ANSYS FLUENT 13.0 is used. As the code ANSYS FLUENT 13.0 does not have the built-in kinetic models, a separate User Defined Function (UDF) is written to incorporate the kinetic model in the code. This UDF calculates the intrinsic reaction rates and then modifies them by the effectiveness factor. These rates, provided by the user defined function, are used as the mass source in species transport equations. Similarly, to calculate the diffusion of mass, a separate UDF is written. This UDF calculates the diffusion coefficient for each species. These diffusion coefficients are used in species transport equations to calculate the diffusivity of mass. UDFs are also written to edit the densities of the species.

A pressure-correction based solver is used to solve these equations. Firstly, momentum equations are solved separately by taking each velocity component as a scalar [134]. After that, the continuity and pressure correction equation based on SIMPLE algorithm, is solved to correct the velocity and pressure field [133]. Then, the energy equation is solved. After that, certain data such as pressure, temperature and mass fraction of species are extracted and used to edit the kinetic reaction rate using the

developed UDF. Diffusion coefficients for each species are also edited using UDF. This data is, then, used in the species transport equation to provide the concentration profiles. UDF written for properties of species are used before the solution of momentum equations to edit the material properties. Finally, absolute convergence criterion of 10^{-7} is applied for each flow variable. The overall flow chat of the process is shown in Figure 21.

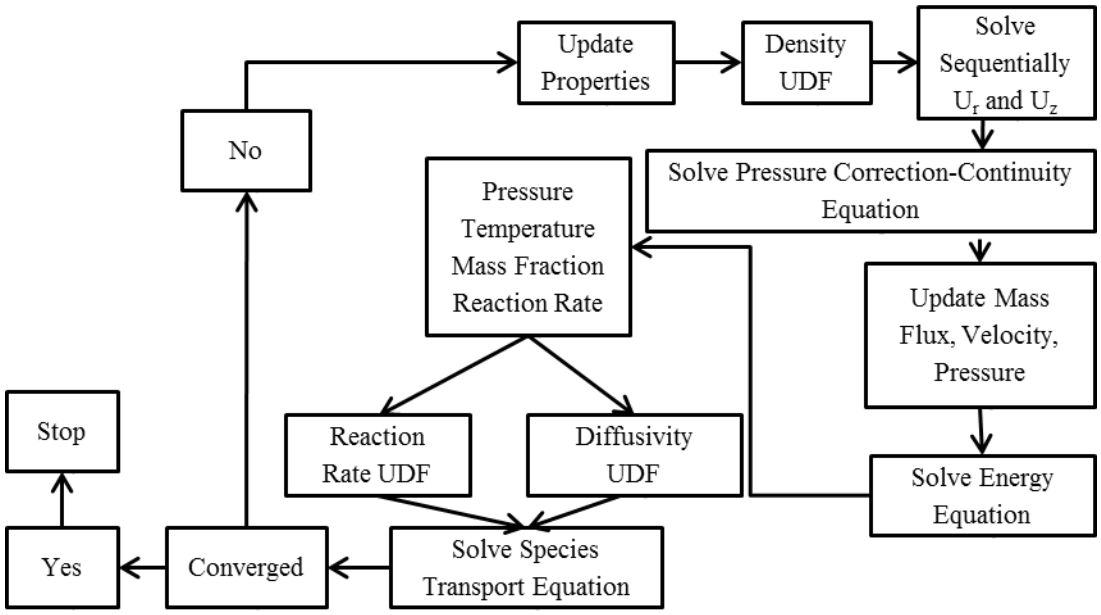

Figure 21 : Flow chart for the solution method of governing equations

CHAPTER 5

VALIDATION AND PARAMETRIC STUDIES

In this chapter, solution of the model developed in the previous chapter is presented. Mesh independence study is conducted. Model is validated with experimental data. Effect of temperature, pressure and relative molar ratios of inlet feed on methane conversion is studied.

To solve the flow model of SMR developed in Chapter 4, a tubular domain is selected. The selected domain is shown in Figure 22. Constant value of porosity allows modeling of reformer as two dimensional axisymmetric domain. Mass flow rate boundary condition is used at the inlet to make the value independent of the pressure and temperature developed at the inlet of the reformer. Wall of the reformer is isothermally heated with zero wall thickness and the exit pressure of reformer is maintained at constant value.

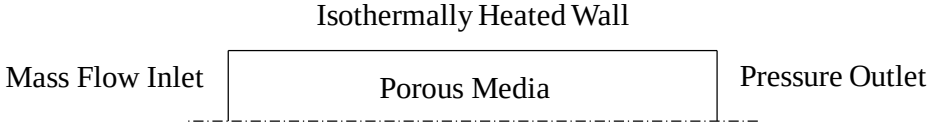

Figure 22 : Axi-symmetric solution domain

5.1 MESH INDEPENDENCE

To check the independence of the solution on the grid, a grid independence study is conducted and a convergence criterion of flow field variables of 10^{-7} is applied. In this regard, five meshes are developed. Details of meshes containing the number of nodes and elements are shown in Table 9.

Table 9 **:** Details of meshes and respective fractional methane conversion

Mesh no.	**No. of elements**	**No. of nodes**	**Fractional methane conversion**
1	200	246	0.153
2	600	671	0.144
3	1200	1296	0.145
4	2000	2121	0.145
5	3000	3146	0.145

The fractional methane conversion is selected as a judging variable to decide that either the solution is independent of the grid or it needs further refinement. It can be seen from Figure 23 that initially a very high value of fractional methane conversion is achieved for very course mesh but as the mesh is refined the relative difference in the

fractional methane conversion decreases and finally vanishes for the mesh containing up to 3000 elements. Thus, the grid is not refined further to save the simulation time. Therefore, mesh no. 5 with 3000 elements and 3146 nodes have been used to generate all the results.

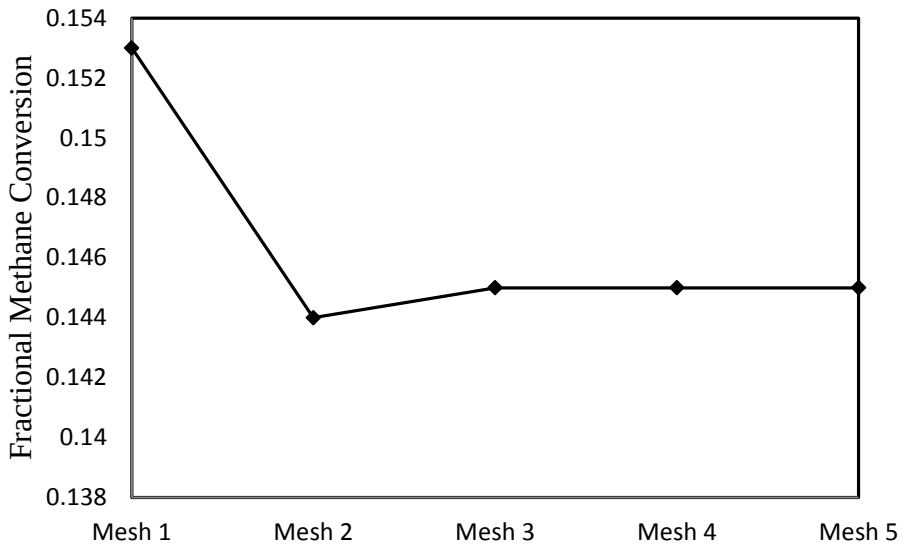

Figure 23 : Fractional methane conversion variation with the mesh size

5.2 MODEL VALIDATION

To check the validity of the model, simulations are carried out at the operating conditions reported by Xu and Fromen [52]. These operating conditions include the wall temperature of 848 K, 823 K, 798 K and 773 K, exit pressure of 10 bar with F_{H2O}/F_{CH4} value of 3 and H_2/CH_4 value of 1.25. Variation of fractional methane conversion with W_{cat}/F_{CH4} obtained from present work is compared with the one reported by Xu and Fromen [52]. Fractional methane conversion is obtained from the carbon balance and is defined as follows:

$$\text{Fractional Methane conversion} = \frac{n_{CO} + n_{CO_2}}{n_{CO} + n_{CO_2} + n_{CH_4}} \tag{5.1}$$

Where n_i is the mole fraction of specie i. W_{cat} is the mass of catalyst that is present inside the reformer. F_{CH4} is the initial molar flow rate of methane. For present study, dimensions of reformer are kept constant. Thus, mass of catalyst inside the reformer remains constant. The factor W_{cat}/F_{CH4} is varied by varying the molar flow rate of methane, F_{CH4}.

To quantize the quality of fit between simulated methane conversion and the one reported by Xu and Fromen [52], a correlation factor is used which is defined as follows.

$$\text{Correlation factor} = \frac{\sum (x - \bar{x})(y - \bar{y})}{\sqrt{\sum (x - \bar{x})^2 \sum (y - \bar{y})^2}} \tag{5.2}$$

This correlation factor is a measure of fit of a line between experimental methane conversion, represented by *x*, and methane conversion obtained from simulation which is represented by *y*. Values of 0.9929, 0.9919, 0.9954 and 0.9975 are calculated for operating temperatures of 848 K, 823 K, 798 K and 773 K respectively. A value very close to one indicates a high quality validation of developed model against the experimental data as shown in Figure 24. Thus, the developed model can be effectively used for further studies.

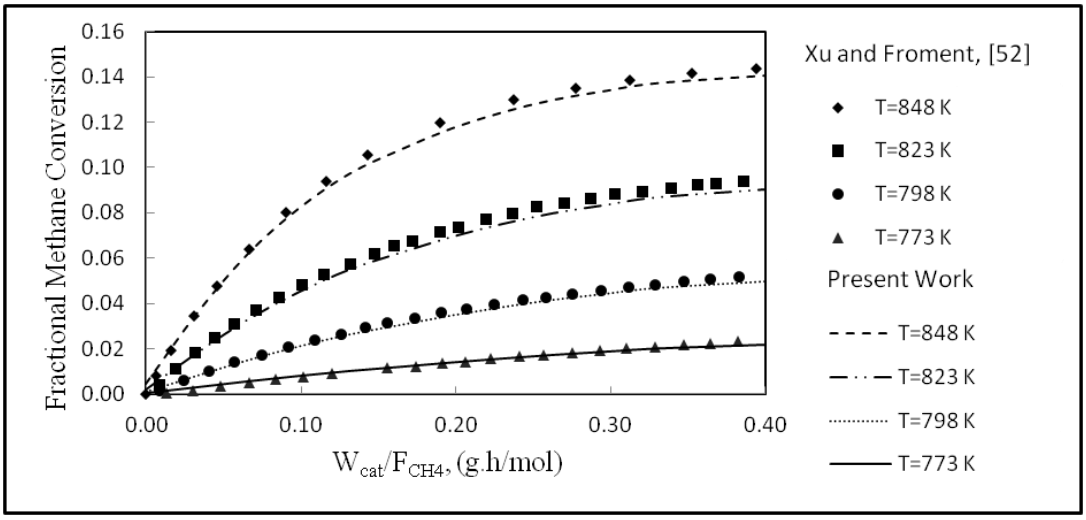

Figure 24 : Variation of fractional methane conversion Vs W_{cat}/F_{CH4} at F_{H2O}/F_{CH4}=3, F_{H2}/F_{CH4}=1.25 and P=10 bar

5.3 TEMPERATURE DISTRIBUTION

Temperature in catalyst bed of SMR reformers has its unique distribution. The temperature, first, decreases at the start of reformer then increases in the later part. As the reactants enter the reformer, only reaction 1 and 3 can take place because there is no CO and H_2 for the reaction 2 to happen. Both reaction 1 and 3 are endothermic in nature, therefore, temperature decreases. As some of the reactants for reaction 2 forms, it takes place quickly and raises the temperature sharply as shown in Figure 25 [135].

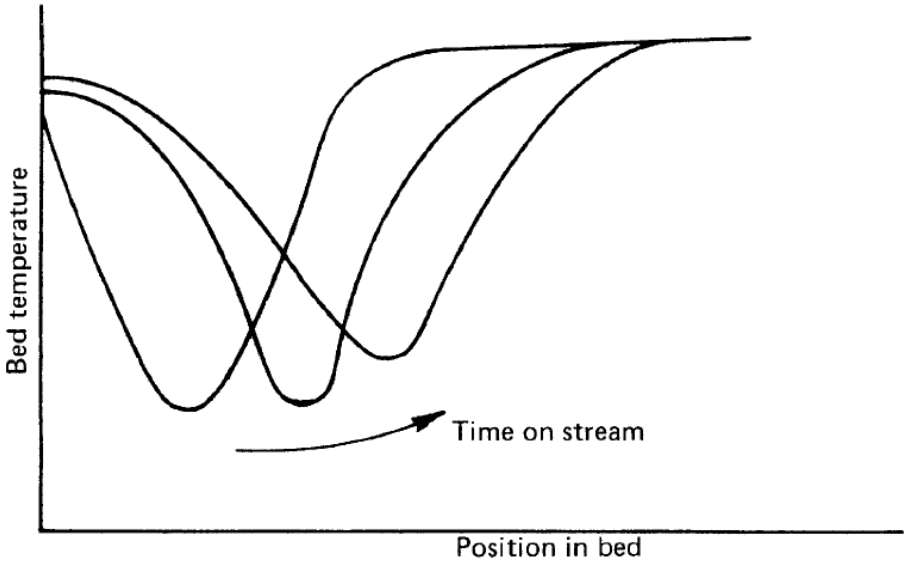

Figure 25 : Usual temperature distribution inside SMR reformer [135]

This behavior of the temperature distribution is also used as a measure of the catalyst quality. Greater the decrease in the temperature better is the catalyst. As the catalyst ages, less decrease in the temperature takes place and reaction 2 takes large time to recover the temperature [135]. The present SMR model can capture this temperature distribution effectively. Figure 26 shows the variation of reaction mixture's temperature along the axis of reformer. It can be seen that temperature decreases at the start of reformer but it starts increasing afterwards. Temperature distribution over the whole reformer's domain is also shown in Figure 27.

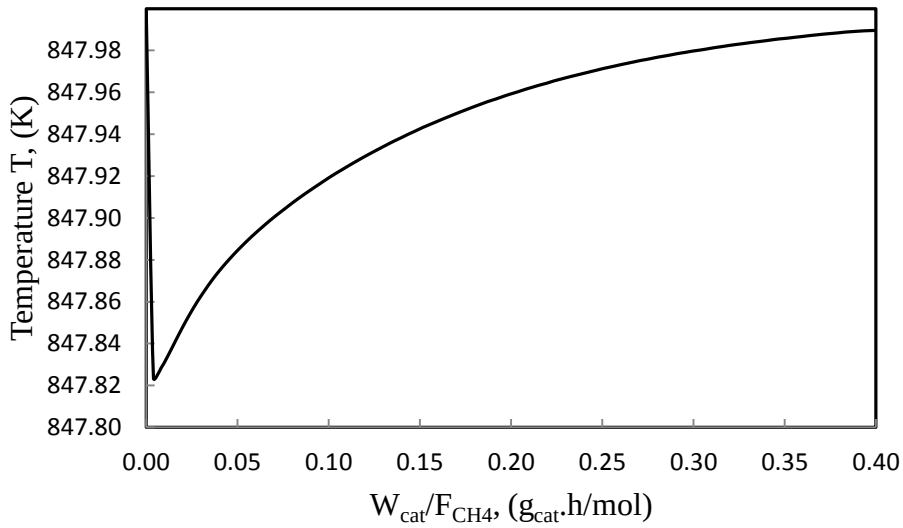

Figure 26 : Tempeature distribution along the axis of reformer

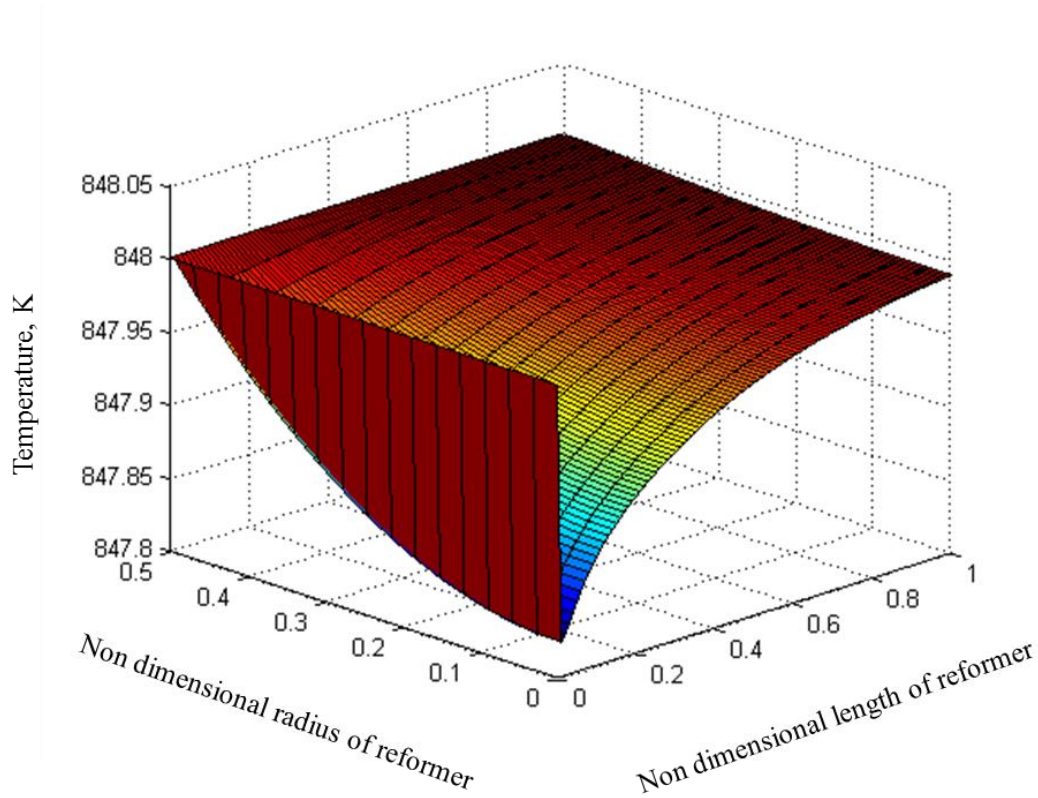

Figure 27 : Contour of temperature distribution inside SMR reformer

To capture this phenomenon, the inlet feed is supplied at the same temperature at which wall of reformer is maintained. This effect is also explained by the variation of rates of reaction 1, 2 and 3 in the later part of this chapter.

5.4 EFFECT OF TEMPERATURE ON SMR

Steam methane reforming reaction is endothermic and proceeds with increase in entropy. Thus, increase in temperature makes the reaction more favorable, therefore, having more conversion of reactants to products. Figure 28 shows the variation of fractional methane conversion with W_{cat}/F_{CH4} for various wall temperatures. It can be seen from Figure 28 that methane conversion increases as the temperature increases. It can be also seen that, at maximum achieved value of W_{cat}/F_{CH4}, the gradient of methane conversion with respect to W_{cat}/F_{CH4} is almost zero at 1000 K to 1200 K. This indicates that the mixture has reached equilibrium. While at low temperature of 800 K to 1000 K, a non-zero value of gradient indicates that mixture is far from equilibrium.

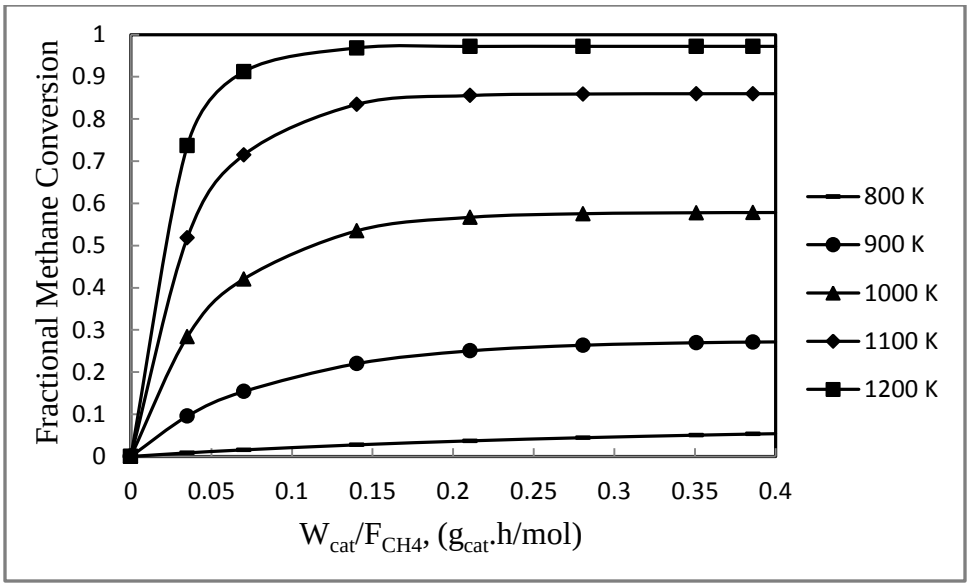

Figure 28 : Fractional methane conversion variation with W_{cat}/F_{CH4} at different temperature for F_{H2O}/F_{CH4}=3, F_{H2}/F_{CH4}=1.25 and P=10 bar

Figure 29 presents a comparison of simulated and equilibrium methane conversions at W_{cat}/F_{CH4} value of 0.4. Equilibrium conversion is calculated by thermodynamic equilibrium over SMR reaction. Whereas, simulated conversion is obtained from present work. It is clear that, at low temperature, conversion is lower than the equilibrium conversion value. However, the reaction approaches the equilibrium conversion values at high temperature. Thus, it can be concluded that the reaction is kinetically limited at low temperature but thermodynamically limited at high temperature.

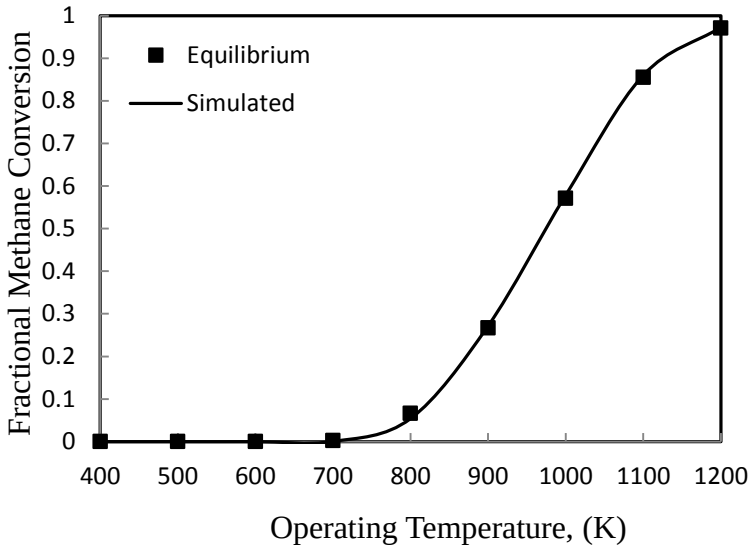

Figure 29 : Fractional methane conversion Vs operating temperature at F_{H2O}/F_{CH4}=3, F_{H2}/F_{CH4}=1.25 and P=10 bar

5.5 PRESSURE DISTRIBUTION

Pressure drop due to porous nature of catalyst is estimated using correlation. Therefore, the pressure field does not highlight the minor pressure variations at the scale smaller than the size of catalyst particle. According to the used correlation, the pressure field depends on the inlet feed velocity, size of catalyst particle and porosity of the catalyst bed. A catalyst bed with high porosity and large catalyst particles give low pressure gradient across the reformer. Similarly, the high value of inlet feed velocity gives high pressure gradient across the reformer. For the present study, the variation of pressure drop is shown in Figure 30. In the present study, a reformer of small length (0.114 m) is used; therefore, over all pressure drop is small.

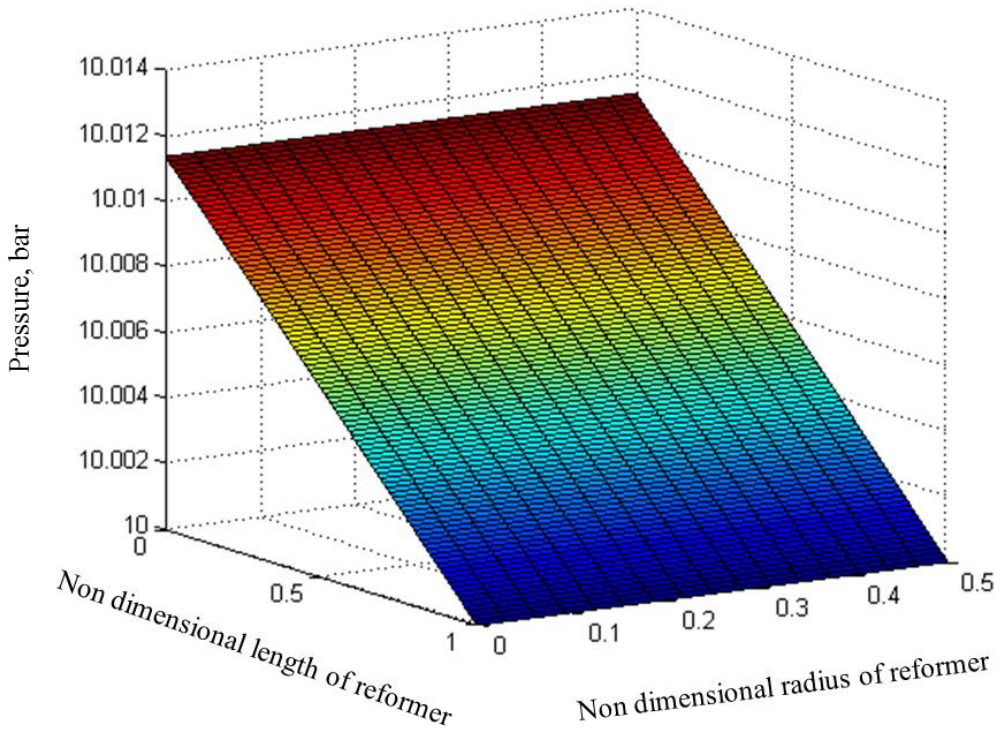

Figure 30 : Pressure distribution inside the reformer

5.6 EFFECT OF PRESSURE ON SMR

As stated earlier, steam methane reaction is favored by expansion, thus, decreasing the pressure results in an increase in fractional methane conversion as shown by Figure 31. A comparison of fractional methane conversion, obtained from simulation, with equilibrium fractional methane conversion is also presented in Figure 31.

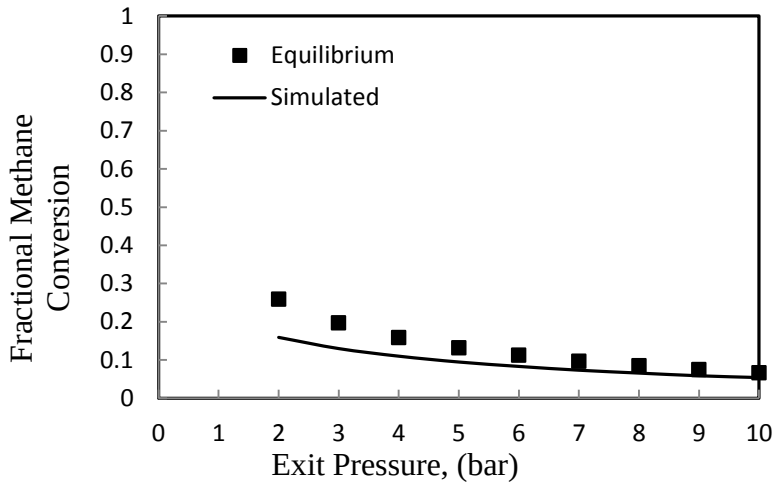

Figure 31 : Fractional methane conversion Vs exit pressure for F_{H2O}/F_{CH4}=3, F_{H2}/F_{CH4}=1.25 and T=800K

It can be seen that as pressure increases difference between equilibrium and simulated methane conversion decreases. Same behavior can also be seen if gradients of fractional methane conversion with W_{cat}/F_{CH4} are compared at different pressures, it is clear that the gradient deceases as the pressure increases, indicating that reaction mixture is closer to equilibrium at high pressure but far from equilibrium at low pressure as shown in Figure 32.

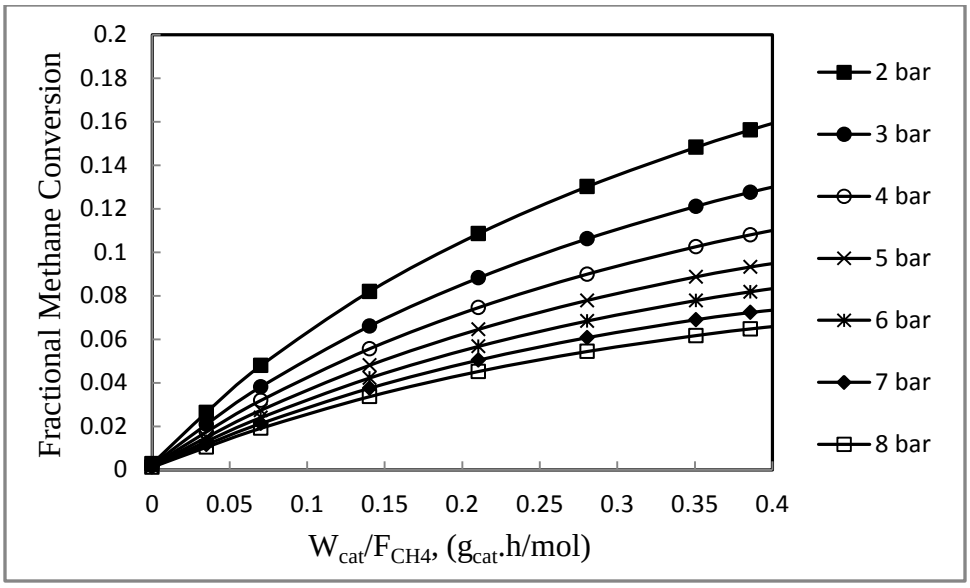

Figure 32 : Fractional methane conversion Vs W_{cat}/F_{CH4} at different operating pressure for F_{H2O}/F_{CH4}=3, F_{H2}/F_{CH4}=1.25 and T=800 K

To elaborate more on this effect, a comparison of approach towards equilibrium at the pressure of 2 bar and 10 bar is conducted. Approach towards equilibrium is defined for each reaction of SMR separately by following parameters.

$$\gamma_1 = 1 - \frac{P^2 n_{CO} n_{H_2}^2}{K_1 n_{CH_4} n_{H_2O}}$$

$$\gamma_2 = 1 - \frac{n_{CO} n_{H_2O}}{K_2 n_{CO_2} n_{H_2}}$$

$$\gamma_3 = 1 - \frac{P^2 n_{CO_2} n_{H_2}^4}{K_3 n_{CH_4} n_{H_2O}^2}$$

Value of zero for any of above parameters (γ_1, γ_2 *and* γ_3) indicates that respective reaction is at equilibrium. For whole SMR process to be at equilibrium, all of these

parameters should be zero. When these parameters are studied at pressure of 2 and 10 bar, SMR is found to be more close to equilibrium at high pressure of 10 bar than at 2 bar as shown in Figure 33.

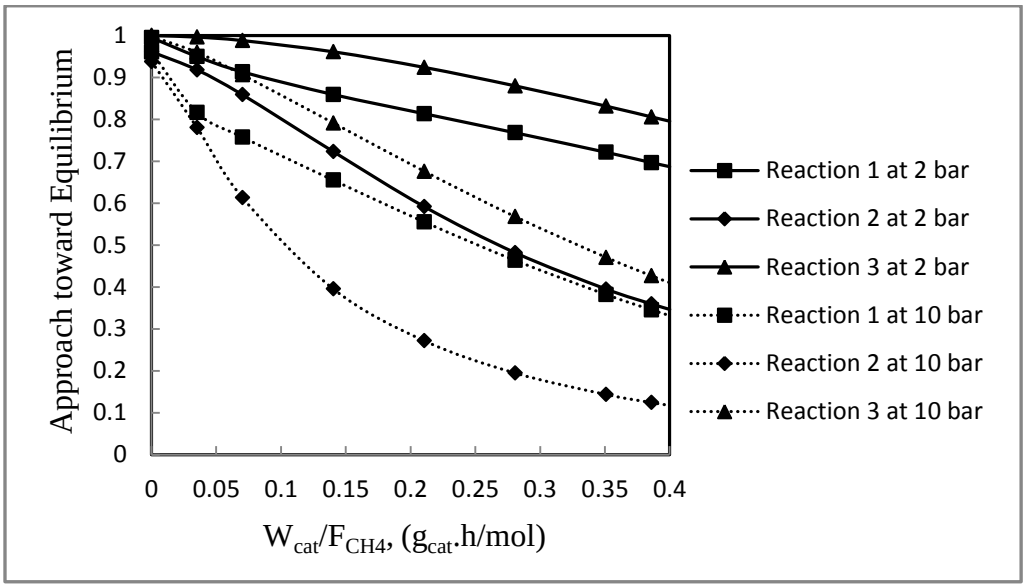

Figure 33 : Fractional distance from equilibrium Vs W_{cat}/F_{CH4} at 2 bar and 10 bar for F_{H2O}/F_{CH4}=3, F_{H2}/F_{CH4}=1.25 and T=800 K

Thus, more contact time or longer reformer is needed to reach equilibrium conversion at low pressure. Moreover, a threshold minimum value of approach towards equilibrium can be used as an optimization limit so that process can always be thermodynamically limited. Ideally, this threshold value should be zero. To further elaborate on the effect of pressure on the mole fraction of individual species, Figure 34 shows the increase in mole fraction of CO, CO_2 and hydrogen and decrease the mole fraction of CH_4 and H_2O as pressure is decreased from 10 bar to 2 bar.

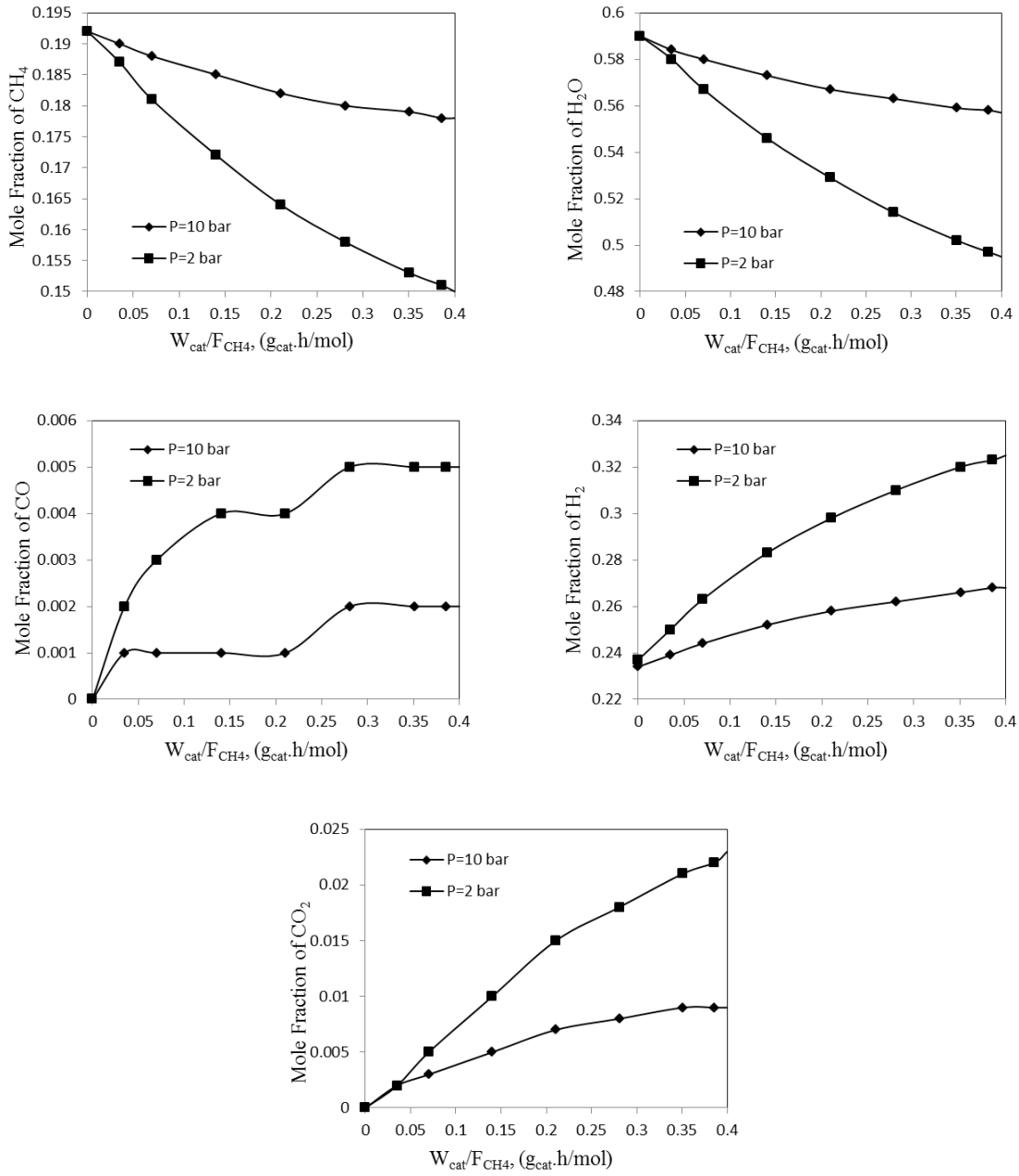

Figure 34 : Comparison of species mole fraction along the reformer length at 2 bar and 10 bar for F_{H2O}/F_{CH4}=3, F_{H2}/F_{CH4}=1.25 and T=800 K

5.7 EFFECT OF MASS FLOW RATE

Increasing the mass flow rate of gas reduces the contact time over constant length of the rector. Eventually, conversion of the reactants decrease but the way the mass flow rate is changed also matters. Changing the mass flow rate by changing the flow velocity of the reacting mixture can produce different methane conversion curve with contact time than those result by changing the pressure of the reformer. Change in flow velocity changes the mass flow rate directly. On the other hand, change in mass flow rate due to change in operating pressure is complicated. Steam methane reformers are characterized by their exit pressures. Change in exit pressure changes the pressure of inlet feed which changes its density. This change in density changes the mass flow rate. If the effect of pressure on methane conversion is studied separately as in the present study, mass flow rate should only be varied by changing inlet feed velocity. Thus, instead of mass flow rate, the variation of conversion with respect to the inlet feed velocity can be studied directly when effect of pressure is studied separately as shown in Figure 35.

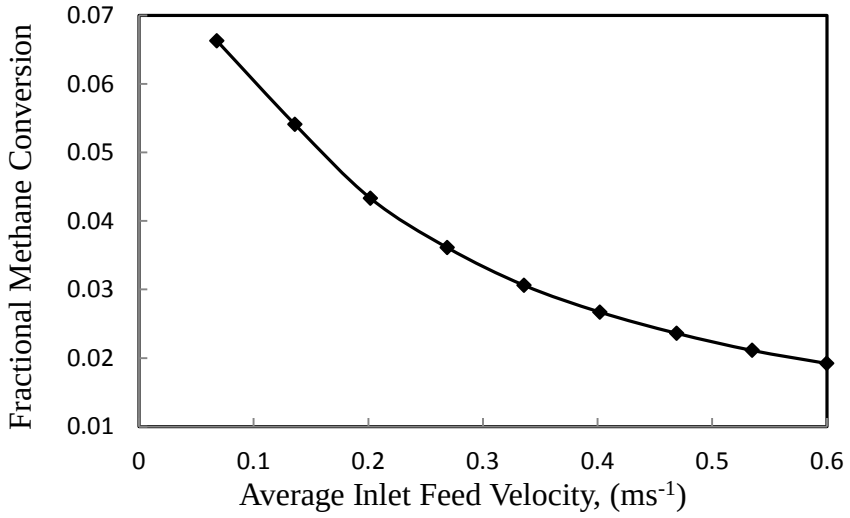

Figure 35 : Fractional methane conversion Vs average inlet feed velocity for F_{H2O}/F_{CH4}=3, F_{H2}/F_{CH4}=1.25, T=800 K and P=10 bar

The general trends of the steam methane reforming reaction rates are important. The rate of reaction 1 and 3 are very high at the start of the reformer. This is due to the presences of excess of reactants for both of these reactions. Rates of reaction 1 and 3 decrease gently along the reformer as shown in Figure 36.

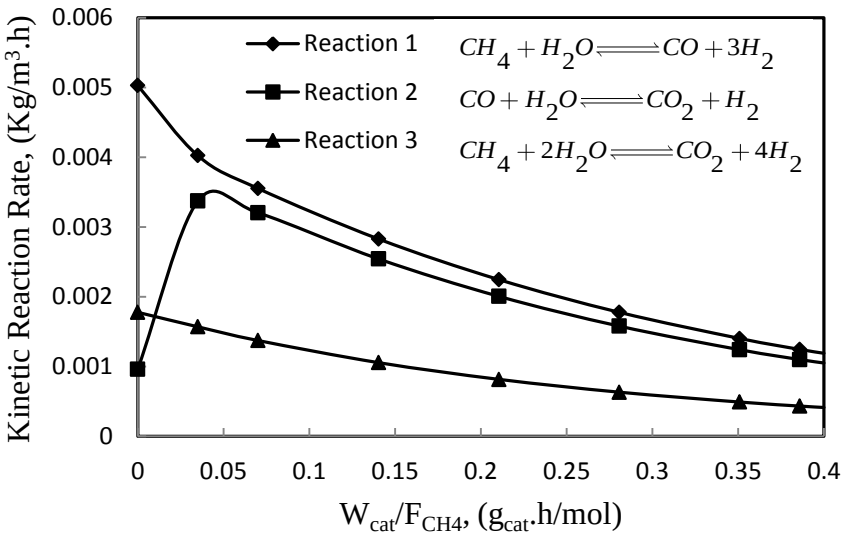

Figure 36 : Kinetic reaction rate Vs W_{cat}/F_{CH4} for F_{H2O}/F_{CH4}=3, F_{H2}/F_{CH4}=1.25, T=800 K and P=10 bar

The rate of reaction 2 is close to zero at the start of the reformer due to absence of CO in reaction mixture. As reactions 1 proceeds producing CO, rate of reaction 2 increases sharply as shown in Figure 36. At the start of reformer, excess of steam and low concentrations of CO_2 in reaction mixture also cause the rate of reaction 2 to increase sharply. When considerable amounts of CO_2 and H_2 (Products for reaction 2) are produced in reaction mixture, the rate of reaction 2 decreases.

5.8 EFFECT OF RELATIVE MOLAR RATIOS OF SPECIES

To study the effect of reacting species at the inlet, three ratios F_{H2O}/F_{CH4}, F_{H2}/F_{CH4} and F_{MIX}/F_{CH4} have been defined as below.

$$F_{CH_4} + F_{H_2O} + F_{H_2} = F_{MIX}$$

$$\frac{F_{CH_4}}{F_{CH_4}} + \frac{F_{H_2O}}{F_{CH_4}} + \frac{F_{H_2}}{F_{CH_4}} = \frac{F_{MIX}}{F_{CH_4}}$$

$$1 + \frac{F_{H_2O}}{F_{CH_4}} + \frac{F_{H_2}}{F_{CH_4}} = \frac{F_{MIX}}{F_{CH_4}}$$

F_{H2O}/F_{CH4} and F_{H2}/F_{CH4} are molar ratios of Steam to methane and hydrogen to methane respectively. F_{MIX}/F_{CH4} is inverse of mole fraction of methane. F_{H2O}/F_{CH4} and F_{H2}/F_{CH4} ratios are varied from 1 to 4 and ratio is F_{MIX}/F_{CH4} varied from 6 to 12. Figure 37 and Figure 38 show the variation of methane conversion with respect to F_{H2O}/F_{CH4} ratio. It is clear that methane conversion increases with increase in F_{H2O}/F_{CH4} ratio but the value of increment depends on either F_{H2O}/F_{CH4} ratio is increased on the expense of F_{H2}/F_{CH4} ratio or F_{MIX}/F_{CH4} ratio. If F_{H2O}/F_{CH4} ratio is increased by keeping the F_{H2}/F_{CH4} ratio constant as in Figure 37, the mole fractions of CH_4 and hydrogen decrease in the inlet feed and mole fraction of H_2O increases. Thus, the methane conversion is always increasing but increase is less because along with hydrogen, methane is also decreasing.

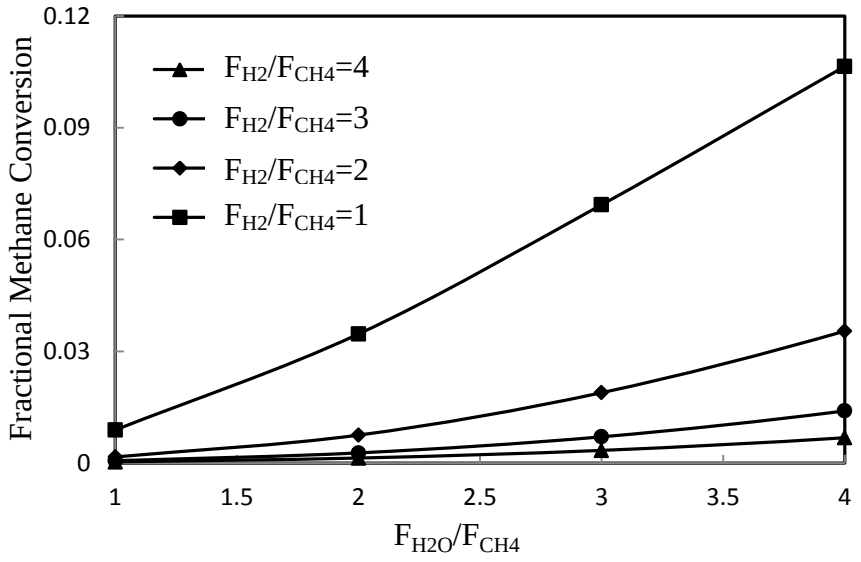

Figure 37 : Fractional methane conversion Vs F_{H2O}/F_{CH4} ratio at T=800 K and P=10 bar

On the other hand if F_{MIX}/F_{CH4} ratio is kept constant as in Figure 38, mole fraction of the methane remains constant.

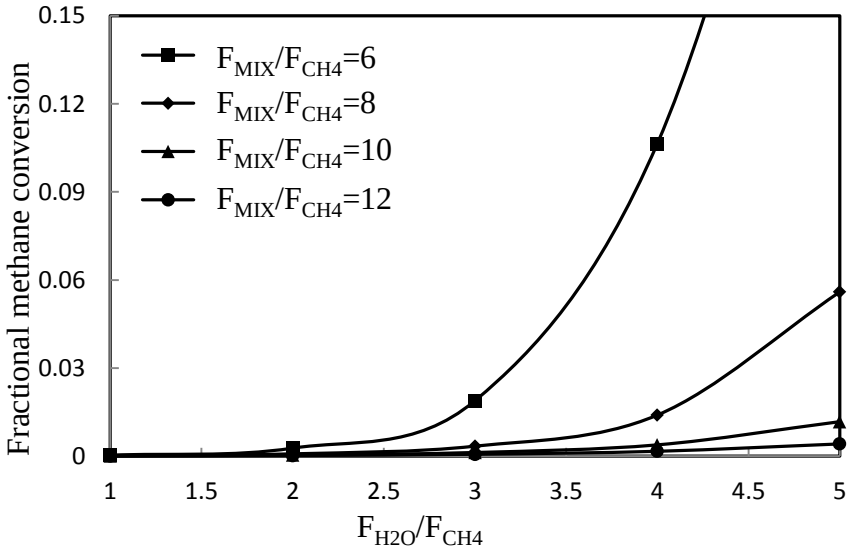

Figure 38 : Fractional methane conversion Vs F_{H2O}/F_{CH4} Ratio at T=800 K and P=10 bar

Increasing the F_{H2O}/F_{CH4} ratio decreases the hydrogen mole fraction that in turn is going to move all the reaction in forward direction. Thus methane conversion increases sharply as compared to the precious case.

Moreover, the variation of methane conversion for constant value of F_{H2O}/F_{CH4} ratio is also studied that is varying the F_{H2}/F_{CH4} ratio with F_{MAX}/F_{CH4} ratio. It is clear from Figure 39 that for the constant value of F_{H2O}/F_{CH4} ratio, increase in F_{H2}/F_{CH4} ratio requires a decrease in mole fraction of CH_4 and H_2O. Thus, mole fraction of H_2 increases. This makes the reaction to proceed in reverse direction. Similarly, if some inert gases are used along with feed, the effect of change in mole fraction of these gases on methane conversion depends on the way their mole fraction is decreased.

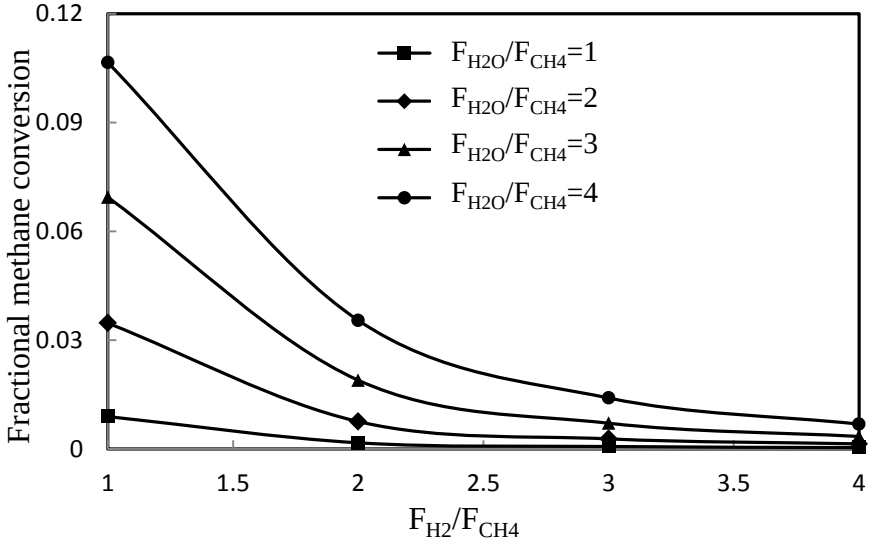

Figure 39 : Fractional methane conversion Vs F_{H2}/F_{CH4} Ratio at T=800K and P=10 bar

5.9 CONCLUSION

The validation of the model with experimental data proved that modeling the continuum of catalyst inside the reformer instead of catalyst pellets is a valid assumption and can provide highly accurate results. Moreover, by using the porosity as a decreasing factor for the source term in species transport equations along with the other term in momentum and energy equations, actual trends of fractional methane conversion with different operating parameters can be obtained. Validity up to 99.75% of developed model with experimental data is obtained which showed that the model can be used for parametric analysis of SMR reaction.

Parametric studies have shown that longer reformers are required at low pressure to attain the thermodynamically limited conversion. It is also recognized that approach towards equilibrium with some minimum threshold value can be used as an optimization limit to get thermodynamically limited conversion. The influence of ratios of reacting species at the inlet is also highlighted and it is shown that not only increasing the F_{H2O}/F_{CH4} ratio enhances the methane conversion but the way this ratio is increased also affect the conversion to a considerable extent. The methane conversion varies sharply if F_{H2O}/F_{CH4} ratio is varied on expense of F_{H2}/F_{CH4} ratio. On the other hand, the change in methane conversion is not sharp enough if F_{H2O}/F_{CH4} is varied on the expense F_{MIX}/F_{CH4} ratio.

CHAPTER 6

DESIGN OF SOLAR COLLECTOR FOR SMR

In this chapter, a general methodology for the development of a concentrating solar collector is presented. Some basic laws of optics are discussed. Limitations and assumptions of the developed method are also highlighted.

6.1 REFLECTION, TRANSMISSION AND ABSORBANCE

Light travels in a straight path. When it falls on a surface, it undergoes the three phenomena of reflection, transmission and absorbance. In most of the light intercepting surfaces, one of these phenomena is preferred than the others and surfaces got their name accordingly. For example, a surface reflecting a large portion of incident radiation while transmitting and absorbing a small portion is called reflector. Similarly, a surface absorbing a large portion of incident radiations while reflecting and transmitting a small portion is called absorber and transmitter is the surface that transmits a large portion of incident radiations. The phenomena of reflection, absorbance and transmission are

quantized by reflectance, absorbance and transmittance respectively which are defined as follows

6.1.1 REFLECTANCE

It is the ratio of the energy reflected by a surface to the total energy incident on the surface and denoted by ρ.

6.1.2 TRANSMITTANCE

It is the ratio of energy transmitted through a surface to the total energy incident on the surface and denoted by τ.

6.1.3 ABSORBANCE

It is the ratio of energy absorbed by the surface to the total energy incident on the surface and denoted by α.

These are non-dimensional ratios and material properties. These values also depend on the incident angle of light rays. The relationship between these properties can be found by law of conservation of energy as follows.

Energy incident = Energy reflected + Energy absorbed + Energy transmitted

or

$$1 = \frac{\text{Energy reflected}}{\text{Energy incident}} + \frac{\text{Energy absorbed}}{\text{Energy incident}} + \frac{\text{Energy transmitted}}{\text{Energy incident}}$$

or

1=Reflectance + Absorbance + Transmittance

$1=\rho + \alpha + \tau$

There is another property called emittance which is the ratio of energy emitted by a surface to the total energy incident on the surface. It is denoted by ϵ. For a surface in thermal equilibrium, no energy is stored. Therefore,

Energy absorbed = Energy emitted

Dividing by the total energy incident on the surface

$$\frac{\text{Energy absorbed}}{\text{Energy incident}} = \frac{\text{Energy emitted}}{\text{Energy incident}}$$

or

Absorbance = Emittance

or

$\alpha = \epsilon$

For reflectors, the value of ρ is greater than α and τ. Similarly, for absorber α and for transmitters τ is greater than the other two properties.

6.2 SPECULAR REFLECTION

When the light falls on a reflector at an angle, it reflects back with a certain angle. The angle between the incident light ray and reflecting surface is called the angle of incidence. Similarly, the angle between the reflected light ray and reflecting surface is called angle of reflection. If the angle of incidence and angle of reflection are equal, the reflection is called specular reflection. The corresponding surface is called a specular surface. For every angle, there is always a reference ray and tilted ray. In the present case, the reference ray for angle of incidence and angle of reflection is the reflector itself. If the angles of incident and reflected rays are measured from a reference other than the reflector, an angular relationship can be found between the angles of incident and reflected rays by securing the condition of specular reflection as shown in the Figure 40.

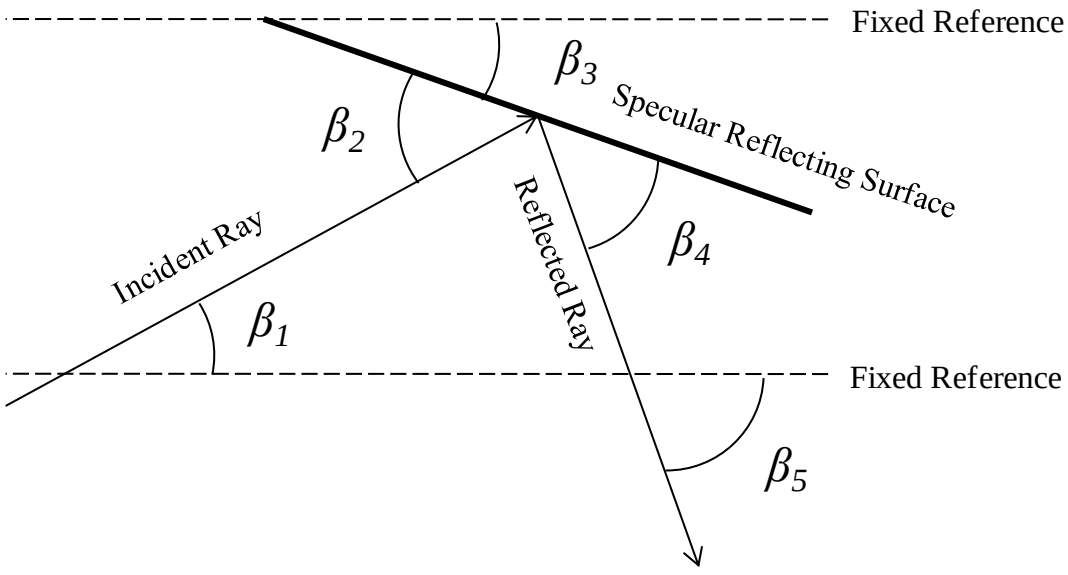

Figure 40 : Specular reflection

$$\beta_5 = \beta_3 + \beta_4 \tag{6.1}$$

$$\beta_2 = \beta_4 \tag{6.2}$$

$$\beta_2 = \beta_3 + \beta_1 \tag{6.3}$$

β_1 is angle of incident ray w.r.t. a fixed reference

β_2 is angle of incident ray with reference to reflector

β_3 is angle of reflector w.r.t. a fixed reference

β_4 is angle of reflected ray with reference to reflector

β_5 is angle of reflected ray from fixed reference

According to Eq.(6.1), the angle of reflected ray w.r.t. a fixed reference is equal to the sum of the angle on reflection of reflected ray and the angle of reflector with fixed reference. Eq.(6.2) is just the condition of specular reflection with equal angle of incidence and angle of reflection. Eq.(6.3) states that the angle of incidence of a light ray is equal to the sum of angles of incident ray and the reflector with the fixed reference.

Using Eq.(6.2) and Eq.(6.3) in Eq.(6.1) to eliminate the β_2 and β_4, we get

$$\beta_5 = 2\beta_3 + \beta_1 \tag{6.4}$$

Eq.(6.4) has three variables namely angle of incident ray, angle of reflected ray and angle of reflector w.r.t. a fixed reference. Any of these three angles can be found by knowing the other two angles.

6.3 PARALLEL AND NON PARALLEL SOLAR RADIATIONS

A light source emits the light in all directions. These light rays keep on traveling in all directions until they are intercepted by a surface placed in their path. Consider a light source emitting the light rays in all direction and an intercepting surface placed at a distance *d* from the light source is intercepting the light rays as shown in Figure 41.

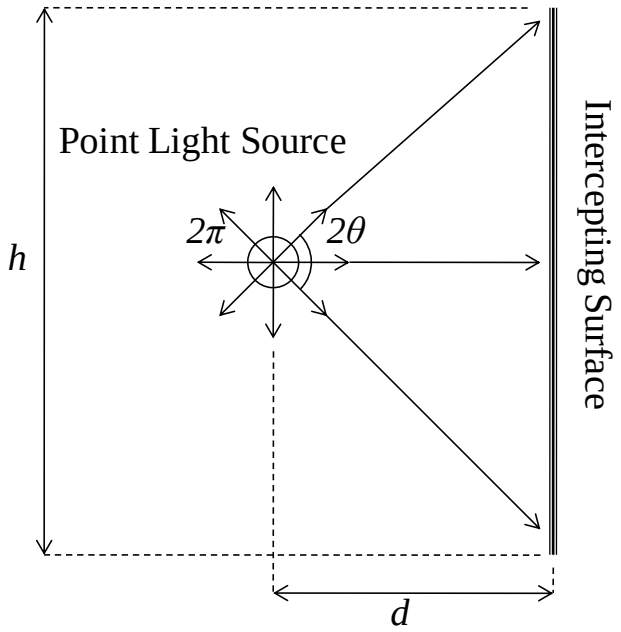

Figure 41 : Point light source and straight intercepting surface

The light source is emitting the light in all direction over the angular range of 2π. The intercepting surface is intercepting a certain portion of emitted light rays over the angular range of 2θ. The angular range of intercepted light portion depends on the distance between the source and intercepting surface as well as the height of intercepting surface as follows.

$$Tan(\theta) = \frac{h}{2d}$$

If the height of intercepting surface decreases or the distance between the source and intercepting surface increases, θ decreases. Thus, for a very small surface placed at a very large distance from the point source, the angular range of intercepted portion of light rays is very very small. This angular range is the angle between the two extreme light rays received by the intercepting surface. If the angle between the two light rays is very very small, these light rays can be considered parallel. Thus, it is the height of the intercepting surface and the distance between the source and the intercepting surface or simply the angular receiving range of the intercepting surface that decide that whether the light rays can be considered parallel or not.

The light rays emitted by a light source contain certain amount of energy. This energy travels in the direction of light rays. When a surface intercepts the light rays, it harness the energy contained by the light rays. If the point source shown in the Figure 40 is emitting the energy E_1 in all direction over the angular range of 2π radians, the intercepting surface is receiving the energy over the angular range of 2θ. Thus, the energy received by the intercepting surface is

$$E_2 = E_1 \frac{\theta}{\pi} \tag{6.5}$$

Energy received by the intercepting surface will decrease by the factor $\frac{\theta}{\pi}$. As the intercepting surface moves away from the source, the angle θ will decrease. The energy

received by the intercepting surface will also decrease. As the area of the intercepting surface remains constant, the energy flux decreases with decrease of angle θ. If A is the area of intercepting surface then the energy flux B over the surface is given as

$$B = \frac{E_1 \theta}{A\pi} \tag{6.6}$$

The actual light sources are not just a one point but they are the combination of infinite points. Each point on light source emits light rays in all directions. Consider a line light source of length l. It is emitting the light rays that are intercepted by a surface of height h placed at a distance d from in line light source as shown in Figure 42.

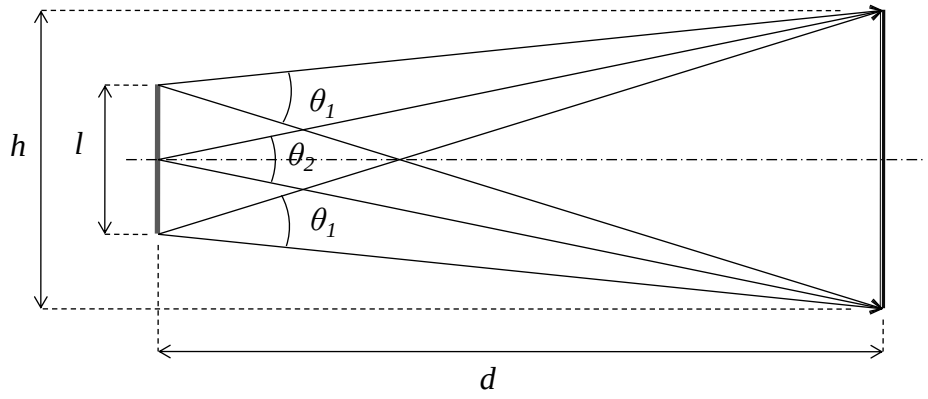

Figure 42 : Line light source and intercepting surface with inline centers

Each point on the line source is emitting the light rays in all directions and intercepting surface is receiving the light rays from each point. Three representative point sources are taken on the line light source emitting the light toward the intercepting surface. Figure 42 shows three point sources emitting the light rays towards intercepting surface.

The portion of the light rays received by intercepting surface from each point on line source will lie in the angular range of θ_1 and θ_2. The angles θ_1 and θ_2 are given as

$$\theta_1 = Tan^{-1}\left(\frac{h-l}{2d}\right) + Tan^{-1}\left(\frac{h+l}{2d}\right)$$

$$\theta_2 = 2Tan^{-1}\left(\frac{h}{2d}\right)$$

It can be seen from above equations that if the height of line source decreases and the distance between the source and the intercepting surface increases, the angular range will decrease. Thus, for a small light source place at very large distance from the intercepting surface the angular range will be very small. Therefore, the light rays coming from every point on the surface of the source can be considered parallel.

For line source and intercepting surface with centers not in line, the intercepting surface will receive energy at different angles from both ends of line source as shown in Figure 43.

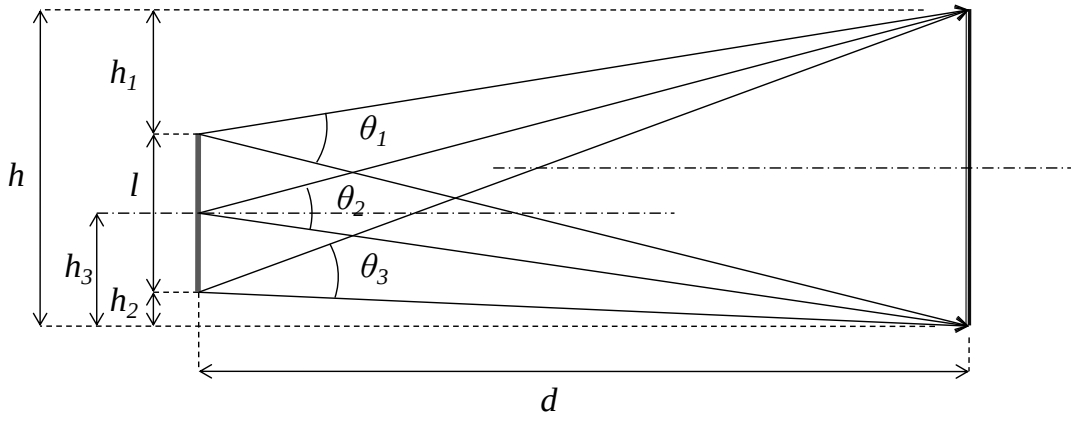

Figure 43 : Line light source and intercepting surface with centers not in line

Angles θ_1, θ_2 and θ_3 are given as follows

$$\theta_1 = Tan^{-1}\left(\frac{h_1}{d}\right) + Tan^{-1}\left(\frac{h-h_1}{d}\right)$$

$$\theta_2 = Tan^{-1}\left(\frac{h_2}{d}\right) + Tan^{-1}\left(\frac{h-h_2}{d}\right)$$

$$\theta_3 = Tan^{-1}\left(\frac{h_3}{d}\right) + Tan^{-1}\left(\frac{h-h_3}{d}\right)$$

It is clear from these relations that greater the distance between source and intercepting surface, smaller will be the angles. Similarly, smaller the height of intercepting surface, smaller will be the angles. Therefore, for a very small intercepting surface placed at very large distance from source, intercepting light rays will have very small angles with each other. Thus, these light rays can be considered parallel.

If the length of the line source is very small and the distance d is very large, the line source can be considered as a point source. In this case, the energy and the flux received by the intercepting surface can be given by the Eq.(6.5) and Eq.(6.6) respectively with θ be the angle subtended by the intercepting surface on the source.

6.4 CONCENTRATION OF LIGHT

Consider the light rays coming from a distant source such that the light rays are parallel. Let these light rays fall on a surface that modifies the rays such that it made them fall on a surface smaller than itself. These light rays are said to be concentrated. Consider

the parallel light rays are falling on surface 1 of area A_1. This surface modifies the path of light rays such that all the rays fall on surface 2 of area A_2. If the area A_1 is larger than the area A_2, the light rays are said to be concentrated as shown in Figure 44. The flux of the light rays, which is the number of light rays per unit area, increase as the result of concentration.

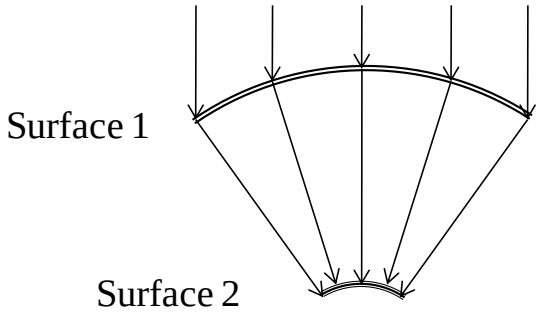

Figure 44 : Concentration of parallel light rays

In this case, all the energy received by the surface 1 is transferred to surface 2. Let the surface 1 is receiving the energy E. Let the B_1 is the flux through the surface 1 and B_2 is the flux through the surface 2 then

$$B_1 A_1 = B_2 A_2$$

or

$$\frac{A_1}{A_2} = \frac{B_2}{B_1}$$

where

$$C_n = \frac{B_2}{B_1}$$

As the area of the surface 1 is greater than the area of surface 2, the energy flux through the surface 2 will be greater than the flux through surface 1. The ratio of the flux through the surface 2 to the flux through the surface 1 is called the concentration ratio.

Surface 1 can make the light undergo the reflection or refraction. In case of refraction, the light rays will be coming from one side of surface 1 and leaving from the other. Therefore, Figure 44 is more like refraction media. In case of reflection, the light rays will be coming and leaving the surface on the same side. Surface 1 cannot be a straight line if it is of reflection type. It is because of the fact that a straight reflecting surface will reflect all the rays at the same angle of reflection. Thus, the flux of light rays will be the same.

Consider parallel light rays coming from a distant point source. Let ray 1 and ray 2 are the two extreme rays coming from the source. All the rays emitted by the source are in between the two rays 1 and 2. Let these rays fall on a reflecting surface and reflect at an angel of θ as shown in Figure 45. Let these light rays fall on an intercepting surface of certain length. The length of the intercepting surface is such that it is equal to the smallest distance between the two rays. The flux of these reflected light rays over this intercepting surface would be the same as it on the surface of source. Thus, no concentration will be achieved.

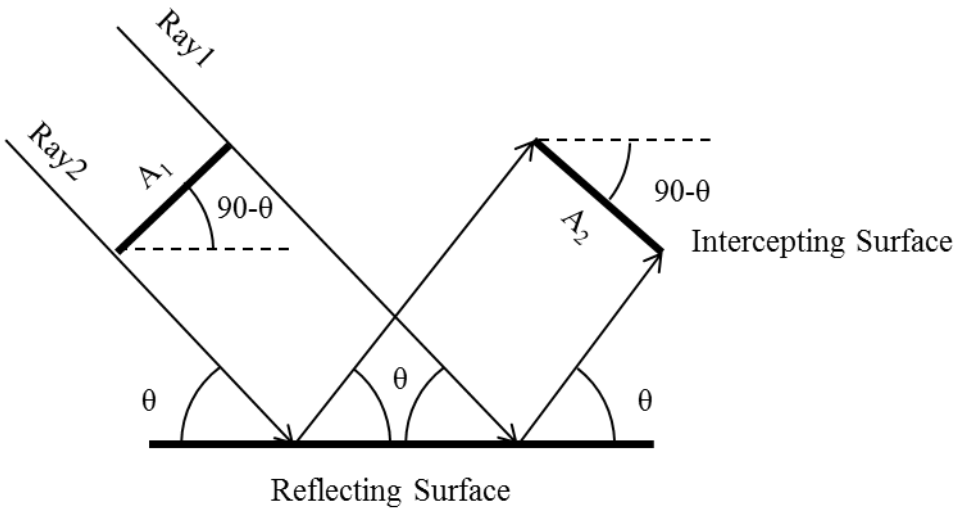

Figure 45 : Reflection of parallel rays

Let E be the energy emitted by the light source. A_1 and A_2 are the areas perpendicular to the incident and reflected rays respectively. The flux of the incident rays B_1 will be

$$B_1 = \frac{E}{A_1}$$

And the flux of the reflected rays will be

$$B_2 = \frac{E}{A_2}$$

In the present case, $A_1=A_2$ giving no concentration. For concentration to take place $A_1>A_2$.

The area A_2 can be decreased by moving the ray 2 closer to the ray 1 by keeping the area A_1 constant. This can be achieved by changing the shape of reflecting surface. To

understand it, let's split the intercepting surface into small parts so that each part is reflecting a separate light ray. Let's consider two light rays 1 and 2 are being reflected from two separate surfaces (RS_1 and RS_{21}) having independent angular rotation. These light rays are being intercepted by an intercepting surface (IS) as shown in Figure 46.

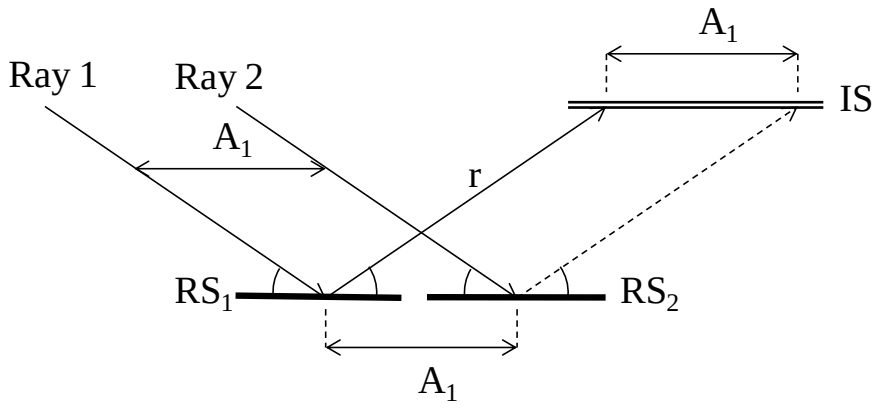

Figure 46 : No concentration of light rays reflected from two separate reflecting surfaces

Let the two reflecting surfaces do not have any angular rotation with respect to each other. In this case, the area A_1 will remain constant though out the path of rays and no concentration will be obtained.

If the surface RS_2 is given an angular rotation with respect to surface RS_1, then ray 2 will strike at different location over intercepting surface. To strike the ray 2 close to ray 1, surface RS_2 should be rotated towards surface RS_1 as shown in Figure 47.

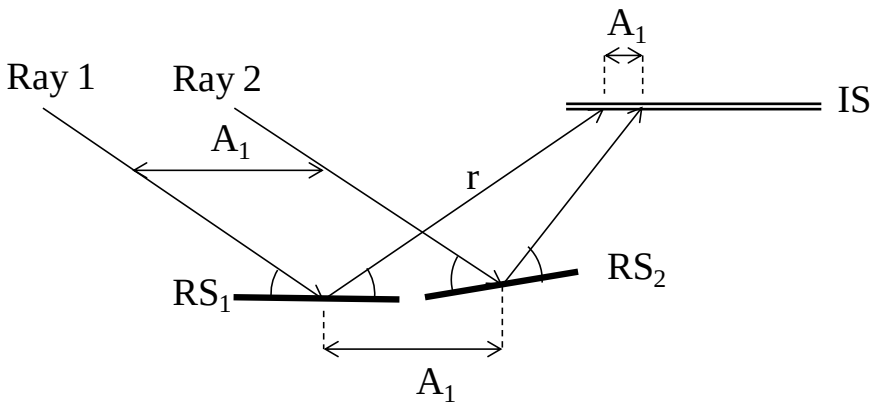

Figure 47 : Concentration of light rays reflected from two separate reflecting surfaces

The area A_1 is greater than area A_2. The light rays are concentrated by a ratio of A_2/A_1 which is called concentration ratio.

It is concluded from this section that if the light rays are required to be concentrated on a surface of specific shape, it can be achieved by changing the shape of reflecting surface.

6.5 SOLAR RADIATIONS

The sun emits a large amount of energy in all direction. A portion of this energy is also intercepted by the earth. According to a study, earth is receiving 10^{14} kJ of energy each second from the sun. The sun subtend a very small angle of 32′ at the center of earth despite of its large diameter that is 1.39 $10\times^{9}$ m [136]. This is due to the fact that the average distance between the sun and earth is also very large. The geometric relationship between sun and earth is shown in Figure 48.

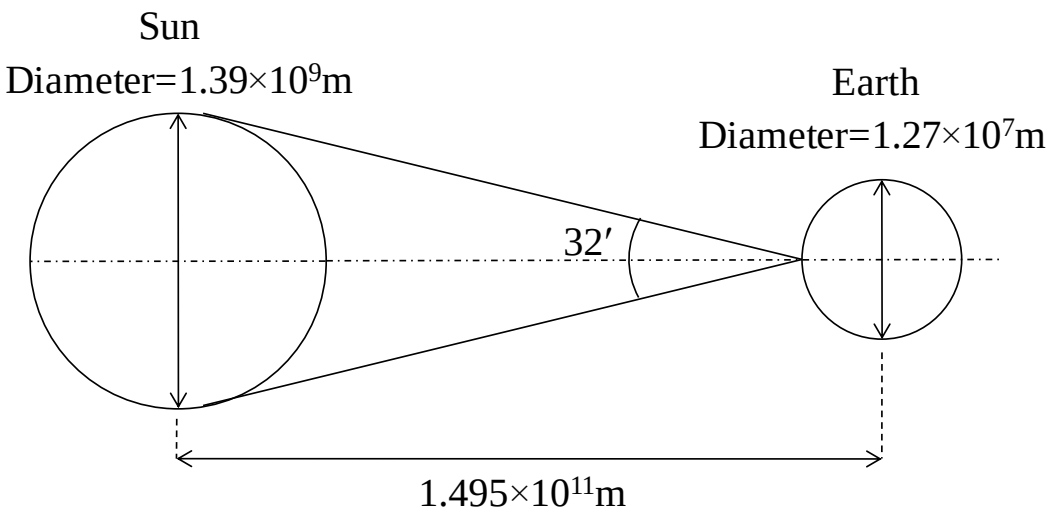

Figure 48 : Geometric relationship of earth and sun [136]

Therefore, the solar radiations received by the earth can be considered parallel. The solar flux reaching the earth outside the earth's environment is nearly constant and is called the solar constant. It value is 1367W/m^2[136].

6.6 SOLAR COLLECTOR

Solar concentrator is a device that intercepts a certain portion of solar radiations and modifies their path to concentrate them on a certain receiving surface. Most of the solar concentrators used a reflecting surface to modify the path of solar radiations. The reflecting surfaces always have a concave shape. It can be a two dimensional concave as in the case of parabolic trough collector or three dimensional as in the case of parabolic dish.

Each solar concentrator has a surface that receives the solar radiations. This surface is called absorber. The shape of absorber varies from collector to collector. It depends on the application for which the collector is being used. For example, tubular absorbers are used for the flow purposes. There are also the collectors with disc type absorber.

First and foremost design requirement for a solar collector is that it should concentrate all the solar radiations intercepted by the reflecting surface to the absorber. In most of the absorbers, some chemical or thermal processes are taking place so specific shapes of the absorbers are required. Therefore, in most of the applications, the shape of the absorber is fixed. Sometimes, the process taking place in the absorber also needs the energy with a specific distribution. Thus, the shape of reflecting surface is changed to concentrate all the energy to an absorber of specific shape and also to get a concentration of specific distribution.

CHAPTER 7

MATHEMATICAL FORMULATION FOR SOLAR COLLECOTR

In this chapter, mathematical formulation to develop a solar collector is presented. Assumptions, made for developing mathematical formulation, are also stated. Finally, a case study is presented in which a solar collector is required to achieve a specific flux distribution for optimum operation of SMR process.

7.1 ASSUMPTIONS

To develop the profile of solar collector, following assumptions are made

1) The collector is supposed to track the sun with 100%

2) Solar flux incident on the aperture surface is taken to be constant (no variation in space)

3) System is in steady state case which means that the system takes no time to respond to the variation of solar flux (variation with respect to time)

4) Solar radiations are taken to be parallel

5) Specular reflection is taken into account

6) Absorbance of the reflecting surface is neglected but a constant value independent of the incident angle can be taken into account so that it can only act as a reducing factor without affecting the distribution

7) It is also assumed that energy carried by each solar ray does not change as it travels from reflector to absorber.

7.2 MATHEMATICAL FORMULATION

Let's consider a tubular absorber of length L and outer radius r_{ab}. Let the solar flux falling on the aperture of collector is B. after reflection from desired solar surface, solar radiations shall fall on the absorber. Let the length of reflected ray, which falls on the absorber at the distance x, is r and it becomes $r+dr$ at the length of $x+dx$ of absorber as shown in Figure 49.

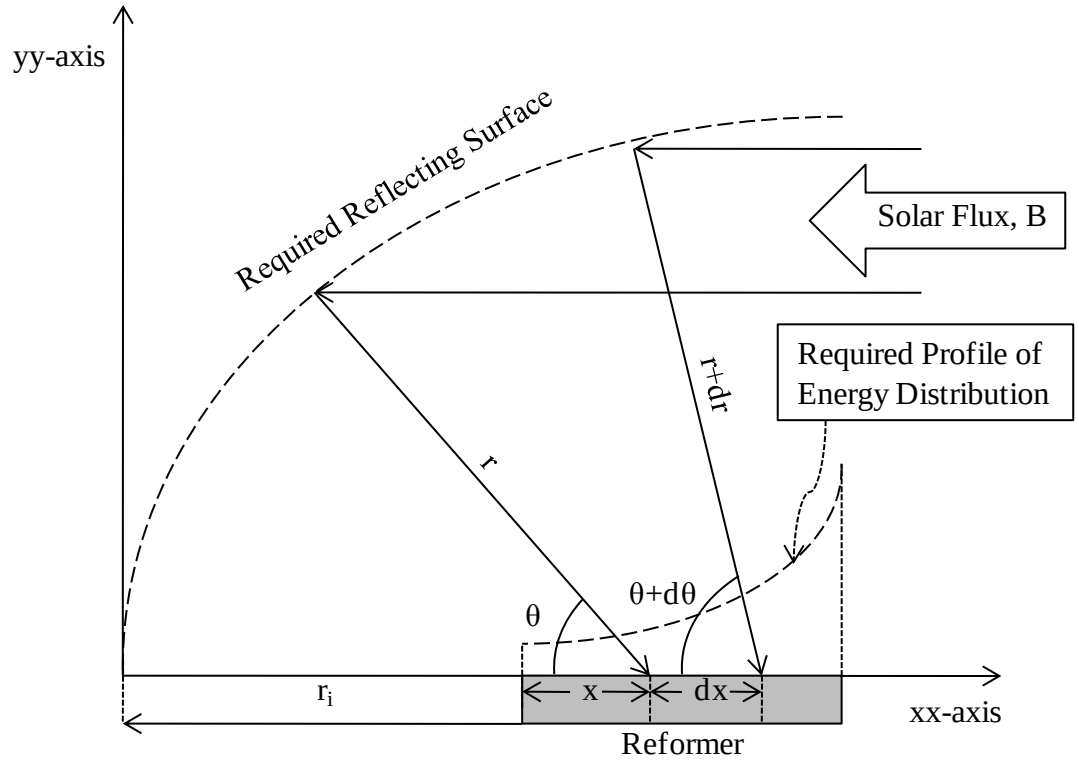

Figure 49 : Relationship of local and global co-ordinates

In this case, the energy received by small length of absorber '*dx*' shall be the energy coming from the projected area of reflector between the intercepting points of rays with lengths *r* and *r*+*dr*. Thus, energy falling on the small length of absorber '*dx*' is

$$E_{dx} = \pi B\left(\left(r+dr\right)^2 Sin^2\left(\theta+d\theta\right) - r^2 Sin^2\theta\right)$$

$$E_{dx} = \pi B\left(\left(r^2+dr^2+2rdr\right) Sin^2\left(\theta+d\theta\right) - r^2 Sin^2\theta\right)$$

Neglecting the dr^2 as it is very small

$$E_{dx} = \pi B\left(\left(r^2+2rdr\right) Sin^2\left(\theta+d\theta\right) - r^2 Sin^2\theta\right)$$

$$E_{dx} = \pi B\left(r^2 Sin^2\left(\theta + d\theta\right) - r^2 Sin^2\theta\right) + 2\pi Brdr Sin^2\left(\theta + d\theta\right)$$

By adding and subtracting the term $2\pi BrSin^2(\theta)dr$

$$E_{dx} = \pi B\left(r^2 Sin^2\left(\theta + d\theta\right) - r^2 Sin^2\theta\right) + 2\pi Brdr Sin^2\left(\theta + d\theta\right) - 2\pi BrSin^2\theta dr + 2\pi BrSin^2\theta dr$$

$$E_{dx} = \pi Br^2\left(Sin^2\left(\theta + d\theta\right) - Sin^2\theta\right) + 2\pi Brdr\left(Sin^2\left(\theta + d\theta\right) - Sin^2\theta\right) + 2\pi BrSin^2\theta dr$$

Putting $\dfrac{Sin^2\left(\theta + d\theta\right) - Sin^2\theta}{d\theta} = 2Sin\theta Cos\theta$

$$E_{dx} = \pi Br^2\left(2Sin\theta Cos\theta d\theta\right) + 2\pi Brdr\left(2Sin\theta Cos\theta d\theta\right) + 2\pi BrSin^2\theta dr$$

$$E_{dx} = 2\pi Br^2 Sin\theta Cos\theta d\theta + 4\pi BrSin\theta Cos\theta drd\theta + 2\pi BrSin^2\theta dr$$

Neglecting the term $4\pi BrSin\theta Cos\theta drd\theta$ as it is very small

$$E_{dx} = 2\pi Br^2 Sin\theta Cos\theta d\theta + 2\pi BrSin^2\theta dr \tag{7.1}$$

Let a specific profile of heat flux 'B_x' be required over the surface of reformer then the energy absorbed by the small length of reformer 'dx' will be

$$E_{dx} = 2\pi r_{ab} B_x dx \tag{7.2}$$

Equating the Eq.(7.1) and Eq.(7.2) then rearranging, Eq. (7.3) is obtained as follows

$$r_{ab} B_x = Br^2 Sin\theta Cos\theta \frac{d\theta}{dx} + Br\frac{dr}{dx} Sin^2\theta \tag{7.3}$$

To develop the desired solar collector, two coordinate systems are used which are

- Global co-ordinates *xx*-*yy* axes
- Local co-ordinates (*r*-θ axes) that move along the length of absorber

The equations of transformation between these co-ordinates systems are as follows

$$xx = x - rCos(\theta) \tag{7.4}$$

$$yy = rSin(\theta) \tag{7.5}$$

Differentiating Eq.(7.4) and Eq.(7.5) with respect to *r* and then dividing to get *dyy/dxx*

$$\frac{dxx}{dr} = \frac{dx}{dr} - Cos(\theta) + rSin(\theta)\frac{d\theta}{dr}$$

$$\frac{dyy}{dr} = Sin(\theta) + rCos(\theta)\frac{d\theta}{dr}$$

$$\frac{dyy}{dxx} = \frac{Sin(\theta) + rCos(\theta)\frac{d\theta}{dr}}{\frac{dx}{dr} - Cos(\theta) + rSin(\theta)\frac{d\theta}{dr}} \tag{7.6}$$

The relationship between the slope of the reflecting surface and angle of reflected ray with the absorber surface is given by the Eq.(7.6) and shown in Figure 50.

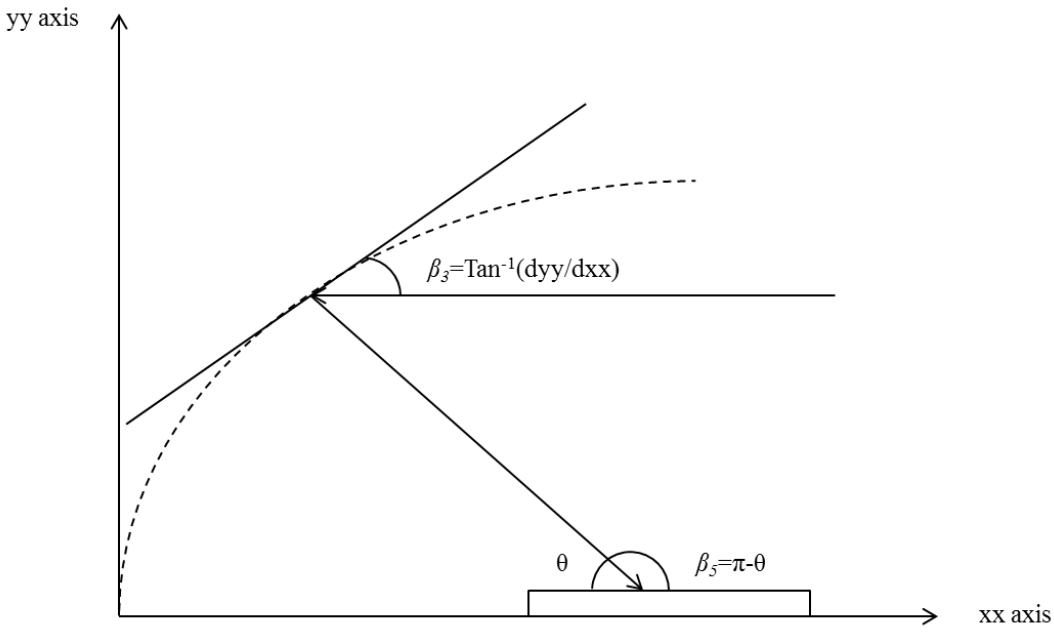

Figure 50 : Angular relationship of intercepting and reflected ray

$$\beta_5 = 2\beta_3 + \beta_1$$

In the present case

$\beta_1 = 0$

$\beta_5 = \pi - \theta$

and

$$\beta_3 = Tan^{-1}\left(\frac{dyy}{dxx}\right)$$

Thus, the following relation can be achieved

$$\pi - \theta = 2Tan^{-1}\frac{dyy}{dxx}$$

Rearranging

$$\frac{dyy}{dxx} = Tan(90 - \theta/2)$$

$$\frac{dyy}{dxx} = Cot(\theta/2) \tag{7.7}$$

Equating Eq.(7.6) and Eq.(7.7), we get

$$\frac{Sin(\theta) + rCos(\theta)\frac{d\theta}{dr}}{\frac{dx}{dr} - Cos(\theta) + rSin(\theta)\frac{d\theta}{dr}} = Cot(\theta/2) \tag{7.8}$$

Thus, Eq.(7.3) and Eq.(7.8) define the system and are solved to get final reflecting surface.

The Eq.(7.3) and Eq.(7.8) require following inputs

- Local solar flux
- The required flux profile
- Length of the absorber
- Radius of absorber
- Initial radius of the reflecting surface

Local solar flux density depends on the geographical location and weather. It should be selected accordingly to get accurate results. On the other hand, the polynomial of the required heat flux distribution, radius and length of the absorber depend solely on one's own choice. Collector can be used for heating the absorber of any length. Similarly, any distribution of required flux can be achieved. Moreover, it is worth mentioning that the value of initial radius for reflecting surface (r_i in Figure 49, which is also the relative location of the absorber with respect to the reflector surface) decides the overall space occupied by the collector. The small value of the initial radius makes the collector to occupy the less space but the reflecting surface will have more curvature. On the other hand, large value of initial radius makes the collector to occupy more space but the reflecting surface will have less curvature. By changing the value of initial radius, the relative position of the absorber will also change with respect to the reflecting surface. By increasing the value of initial radius, the absorber will come out of the reflector which would increase the overall space occupied by the reflector-absorber module as shown in Figure 51.

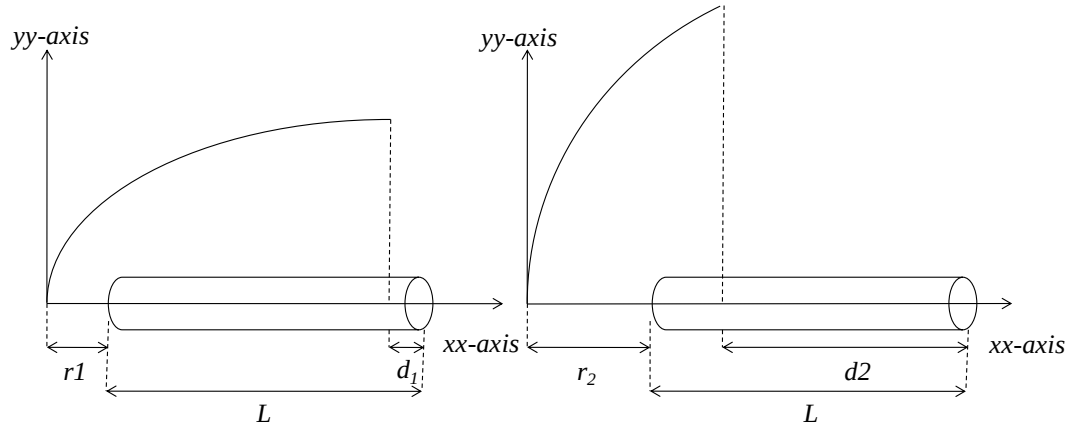

Figure 51 : Influence of initial radius on the space occupied by collector

The $r_1$and r_2 are the small/large initial radii (r_i). The d_1 and d_2 are the partial lengths of the absorber that are out of the aperture of the collector for the small/large initial radius (r_i), respectively. However, the reflecting surface with greater initial radius will have less curvature. Figure 51 is not drawn up to scale. Thus, the choice of initial radius of collector totally depends on one's space limitations. The reflecting surface will have a hole at the apex of the collector. It is due to the fact that when the point of intersection of solar radiations with the reflecting surface become in line with absorber's surface, no energy is absorbed. Thus, this hole can be left open as an air vent for cleaning/installation purposes. It can also be closed to give strength to the structure.

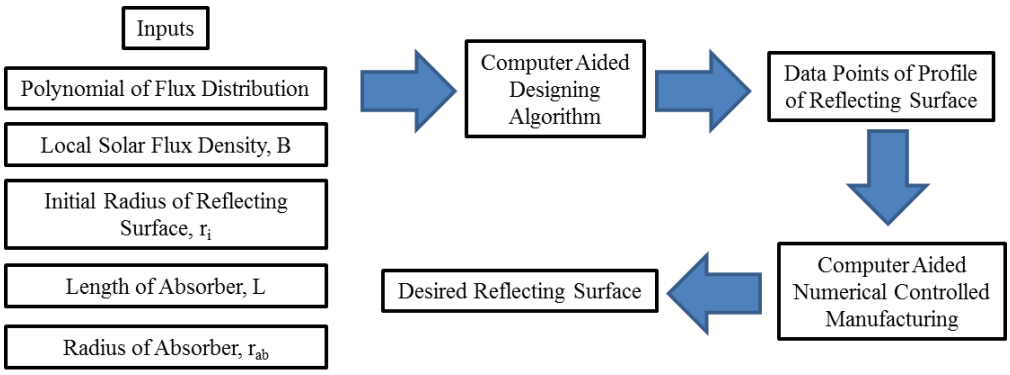

Figure 52 : Flow chart of the process

7.3 CASE STUDY: OPTIMAL HEAT PROFILE FOR SMR

Pantoleontos et al. [60] reported the optimal heat flux profile for steam methane reforming (SMR) reaction which can approximated by a third order polynomial as

$$B_x = 0.1281x^3 - .871x^2 + 2.806x + 49.7$$

This flux distribution is used to develop a solar collector with following user defined inputs

Radius of tubular absorber, r_{ab}=*.00865 m*

Length of tubular absorber, *L=12 m*

Initial radius, r_i*=0.04 m*

Solar flux, $B=1KW/m^2$

r_{ab}, *B* and r_i are the constants used in Eq. (7.3). *L* is used as upper boundary condition for *x*. By solving the Eq. (7.3) and Eq. (7.8) numerically, required reflecting surface is obtained. The two dimensional axisymmetric curve for developed solar collector is shown below.

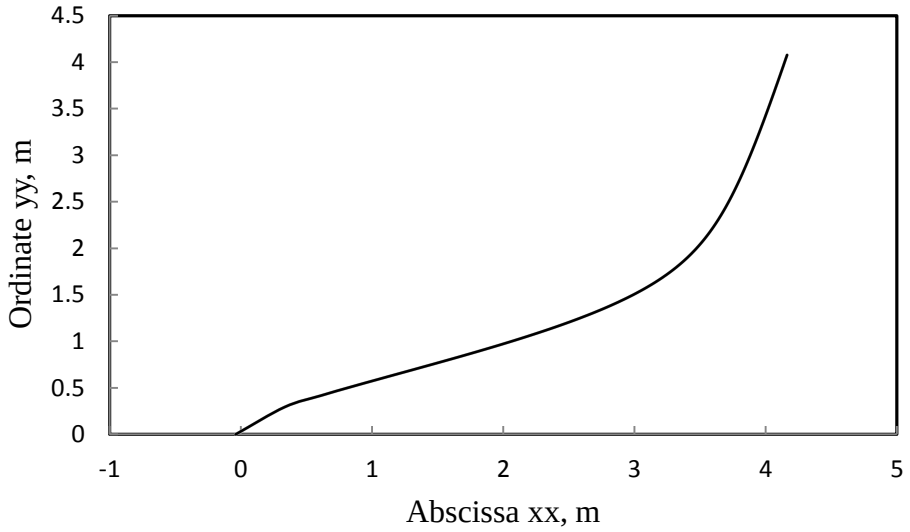

Figure 53 : Final curve of reflecting surface for optimal heat flux profile for SMR

To elaborate more, front side and isometric views of final collector are given below.

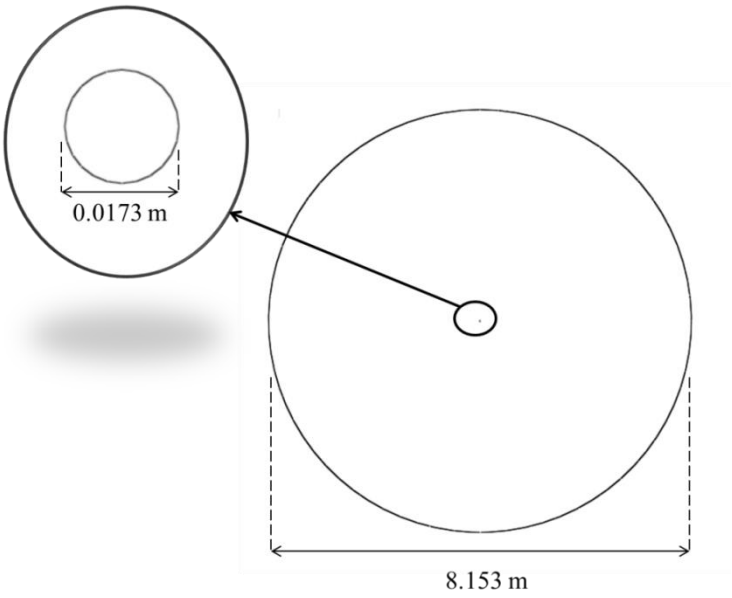

Figure 54 : Front view of developed solar collector

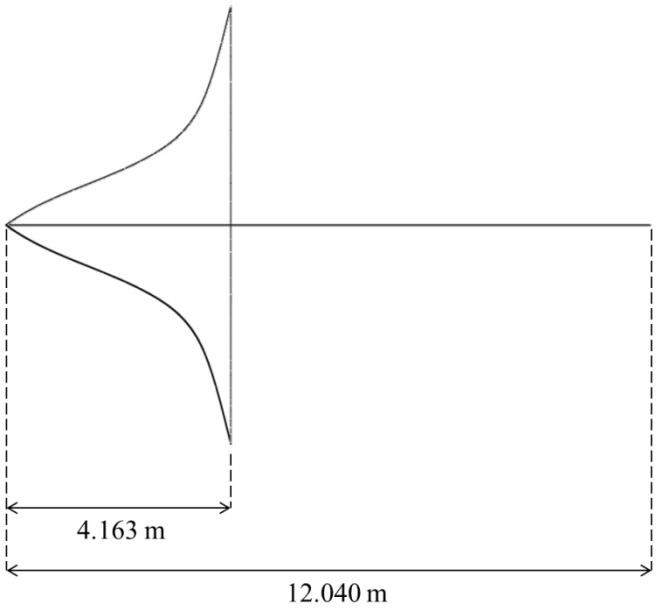

Figure 55 : Side view of developed solar collector

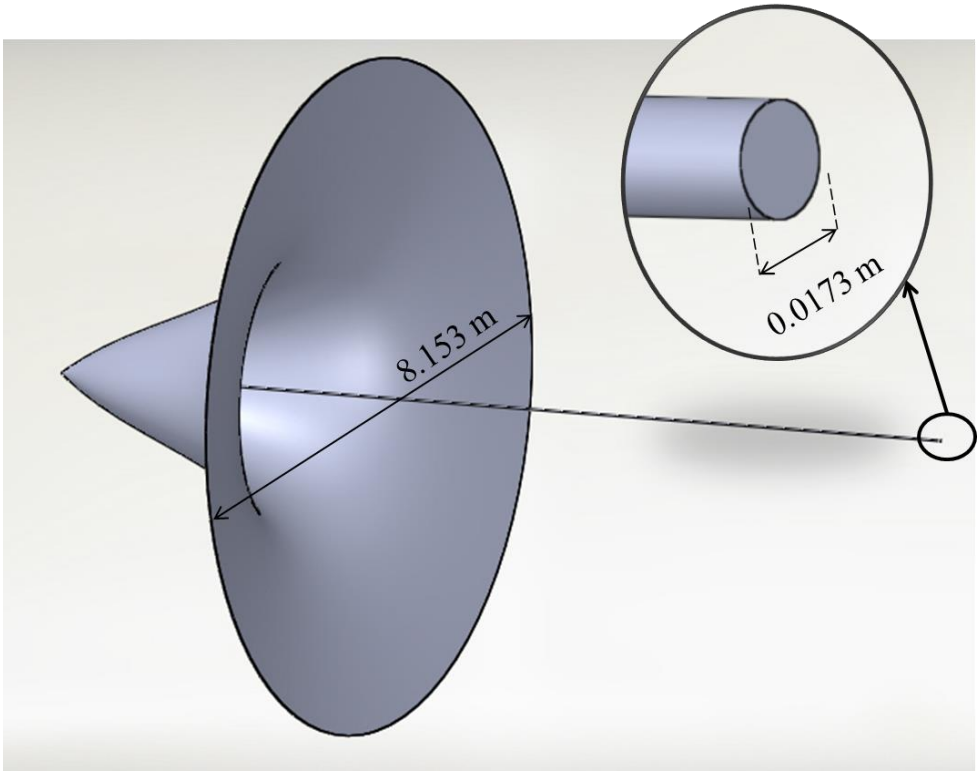

Figure 56 : Isometric view of developed solar collector

A comparison is made between required and achieved flux at the absorber surface. For the present case study, required flux is the one reported by Pantoleontos et al. [60]. Achieved flux is the flux transferred by the collector at the absorber surface and is calculated as follows

$$\pi B\left(y_2^2 - y_1^2\right) = 2\pi r_{ab} B_x \left(x_2 - x_1\right)$$

B_x is the achieved flux over the small length (x_2-x_1) of absorber. Figure 57 shows the comparison of required and achieved flux over the surface of absorber.

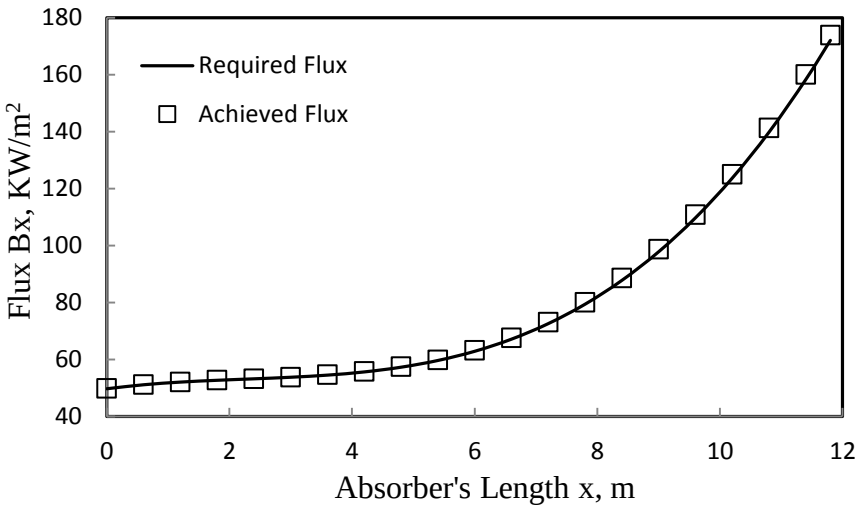

Figure 57 : Comparison of required and achieved flux

It can be seen that a great agreement is found between the required and achieved flux. To quantize the agreement achieved, a correlation factor is calculated between achieved and required flux. This correlation factor is a measure of fit of a straight line between required and achieved flux and is given as follows.

$$\text{Correlation factor} = \frac{\sum (x-\bar{x})(y-\bar{y})}{\sqrt{\sum (x-\bar{x})^2 \sum (y-\bar{y})^2}}$$

In above relation, x and y are the required and achieved flux respectively. A value of 1 indicates the perfect agreement between two series being compared. For the present comparison, a correlation factor of 0.999998 is achieved.

Apart from achieving the required flux distribution, present collector is also capable of achieving more than one reflecting surfaces of different sizes and shapes. This is achieved by introducing a free variable r_i. By changing the value of r_i, reflecting surface

of various shapes and sizes can be obtained. Present case is solved for r_i values of 0.1, 0.5, 1 and 2 m. Figure 58 shows that reflecting surface gained various shapes to achieve same distribution of flux.

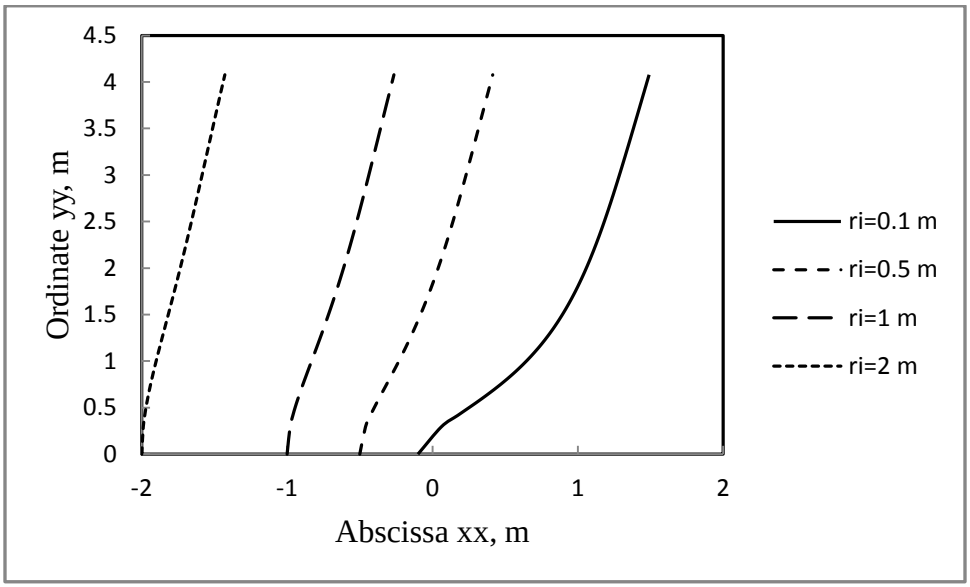

Figure 58 : Reflecting surfaces with various values of r_i

It can also be seen that as the value of r_i changes, the surface area of reflecting surfaces changes. Figure 59 shows the variation of surface areas of reflecting surfaces with various values of r_i.

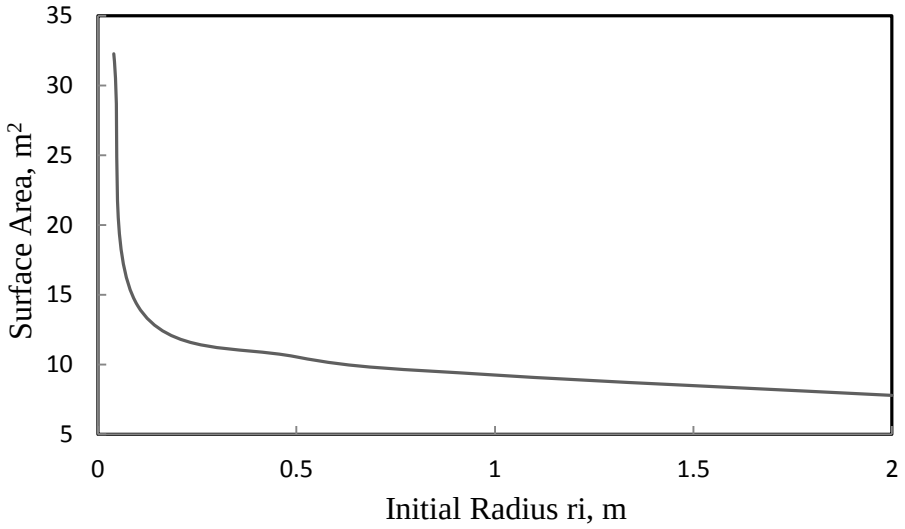

Figure 59 : Surface area of reflecting surface for various values of r_i

Thus, by changing the value of r_i, reflecting surface of various sizes and shapes can be achieved to satisfy same flux distribution.

Collector can secure the flux distribution even if the incoming flux changes. This property can be ensured by analyzing Eq. (7.3). Suppose a solar collector is constructed according to the inputs of present case study. Once the collector is constructed, all of its geometrical properties become constant and cannot be changed. Thus, the value of r_i,r_{ab} and variation of r and t with respect to x becomes constant. The only thing that can change is the incoming solar flux and the flux being achieved over the surface of absorber. Analyzing the Eq. (7.3) and Eq. (7.8), it can be seen that Eq. (7.8) is purely a geometric relationship that does not change once the collector is made. Thus, any change in the incoming solar flux is going to disturb Eq. (7.3) directly. Suppose incoming solar flux decreases to half of its value in present case study. This decrease is going to multiply

the R.H.S. of Eq. (7.3) by 0.5 and this equation will not be satisfying the collector obtained in the present case study anymore. For this equation to satisfy the developed collector, L.H.S. side must be multiplied by 0.5 as well. This multiplication on L.H.S. side is going to affect B_x directly as r_{ab} is constant. This multiplication of 0.5 with the B_x is not going to change the distribution at all but it will just decrease the achieved flux at each point by 0.5 securing the distribution. Thus, it is concluded that any change in the incoming solar radiation does not change the flux distribution. A case is solved by using inputs of present case study with incoming flux of 500 W/m^2. The Required flux distribution is $0.5B_x$. The reflecting surface obtained is exactly the one achieved for present case study shown in Figure 53. Comparison of non-dimensional achieved fluxes is shown in Figure 60. It can be seen that flux distribution is completely secured.

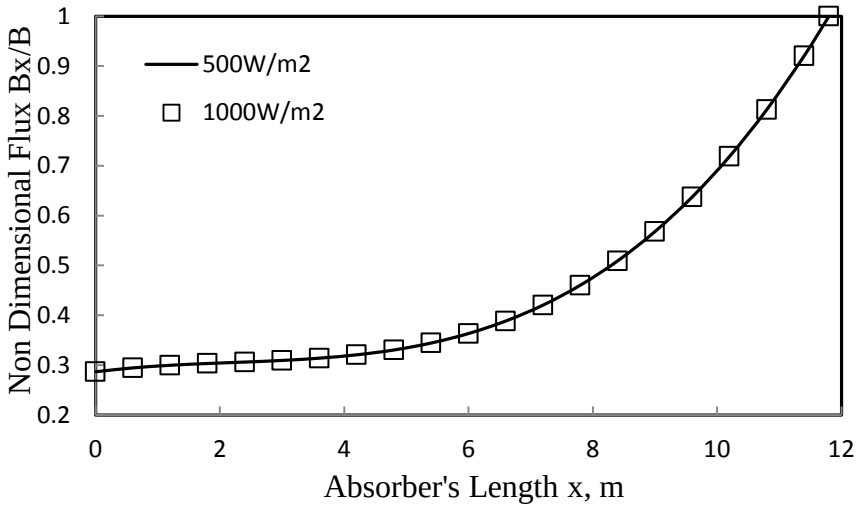

Figure 60 : Comparison of achieved fluxes for incoming solar fluxes of 500 and 1000 W/m^2

7.4 CONCLUSION

The present work is a step towards fulfillment of need of a solar collector that can give required flux distribution. An algorithm is developed that gives the data points for designing the reflecting surface. These data points can be used as input to numerically controlled manufacturing mechanism. This algorithm needs simple inputs such as local solar flux density, required profile of heat flux, initial radius of reflecting surface, radius and length of absorber. The absorbing surface is of standard tubular type. To satisfy a specific flux distribution, collectors of different sizes and shapes can be achieved. Collector also has an ability to secure the flux distribution even if the incoming solar flux changes. A case study for optimal heat flux profile for SMR is also presented to highlight the features of developed collector.

CHAPTER 8

OPTIMAL D/L RATIO FOR TUBULAR REFORMER AND OPTIMAL SOLAR COLLECTOR

The optimal operating conditions of the steam methane reformers have always been the main concern for the researchers due to its complex dependence on large number of variables. For this purpose, full scale optimizations, involving all variables, are usually performed. Nandasana et al. [80] has optimized the SMR to get the constant hydrogen supply by varying the inlet feed temperature, inlet feed rate of natural gas and operating temperature. The SMR is also optimized to maximize the flow rate of carbon monoxide in the syngas [137]. The SMR process has also been optimized to get the maximum hydrogen yield at the expense of heat supplied at the wall of reformer. For example, Pantoleontos et al. [60] has optimized the SMR reaction to obtain the maximum hydrogen supply by varying the profile of the heat flux applied at the wall of tubular reformer. Thus, in optimization of SMR either the outputs are maximized for constant inputs or the inputs are minimized for constant outputs.

In most of studies, the geometry of the reformer is kept constant. These types of optimization are important when Steam methane reformers are alone in operation. Mostly, the steam methane reformers operate in a complex cycle of processes. In this cycle, it is very difficult to change the flow variables just to obtain the optimized outcome from the reformer because the large numbers of processes are taking place. Any change in the flow variables will affect the efficiency of other processes. Therefore, the maximum expected outcome cannot be obtained. Thus, to get the maximum conversion from steam methane reformer at the specific operating parameters of the certain operating cycle, the geometry of the reformer must be optimized prior to put it into the processes' cycle.

A reformer of tubular shape is considered in the present study. The tubular shape is characterized by its length, diameter and thickness. The thickness of the reformers depends on the structural strength and heat transfer limitations. It does not vary too much. Thus, only length and diameter of the reformer are considered to study the effect of geometry. A ratio of diameter to length of reformer is defined as the representative of geometry of reformer.

Methane conversion of SMR reaction is either kinetically or thermodynamically limited. Kinetically limited conversion is always less than thermodynamically limited conversion. Thermodynamic limit is the maximum conversion that can be obtained under certain operating conditions. Thus, to get the maximum conversion by varying the geometry of tubular reformer, the thermodynamically limited conversion should be studied as the function of diameter to length ratio of the reformer. Thus, general operating

conditions for SMR reaction are used to simulate a tubular reformer. Diameter to length (D/L) ratio of the reformer is varied. Approach towards equilibrium of three reactions of SMR is monitored. The value of D/L ratio at which reactions are the closest to equilibrium is selected as the optimal value.

8.1 OPERATING CONDITIONS' RANGES OF SMR

The SMR reaction strongly depends on the pressure, temperature and velocity fields that vary considerably inside the reformer. The reaction also depends on the inlet feed to the reformer and mass of the catalyst. Overall, SMR reaction has large number of variables with complex dependence on methane conversion. The simulations are performed at the general operating ranges of these variables. To decide the general operating range of the variables, a literature survey is performed. The operating pressure of the reformer is found to vary from 1 bar to 30 bar [138,139]. Average heat flux applied at the wall has its value in the range of 45 to 80 kW/m^2 [60]. The steam to carbon and hydrogen to methane molar ratio does not vary too much. Most commonly, a value of 3 is used for steam to carbon molar ratio and the value around 1 is used for hydrogen to methane molar ratio [62,67,140]. The porosity of catalyst does not vary to a large extent. In most of studies, a value close to 0.5 is observed [62]. The diameter of the reformers is found to vary from 0.003 m to 0.06 m [62,140]. The length of reformer is found to vary from 0.062 m to 10 m [110,141]. Diameter of the catalyst particle is also found to vary little. In most of the reformers, inlet feed temperature don't vary too much. It is usually around 500 to 600 K [77].

Thus, for the present simulations, a reformer of diameter 0.06 m is simulated with the exit pressure fixed at 25.7 bar. Applied wall heat flux is fixed at 80 kw/m^2. Inlet feed velocity is fixed at 1m/s. Steam to carbon ratio is fixed to a value of 3 and hydrogen to methane ratio is fixed to value of 1.25. The inlet feed temperature is fixed at 600 K. The porosity of catalyst bed is fixed at 0.528 with the catalyst particle size of 0.23 mm. The density of catalyst is fixed at 2355.5 kg/m^3. The D/L ratio is varied from the value of 0.004 to 0.41. The approach towards the equilibrium of three SMR reactions is monitored separately. The approach toward equilibrium of these reactions is calculated by the following formulae

$$\gamma_1 = 1 - \frac{P^2 n_{CO} n_{H_2}^2}{K_1 n_{CH_4} n_{H_2O}}$$

$$\gamma_2 = 1 - \frac{n_{CO} n_{H_2O}}{K_2 n_{CO_2} n_{H_2}}$$

$$\gamma_3 = 1 - \frac{P^2 n_{CO_2} n_{H_2}^4}{K_3 n_{CH_4} n_{H_2O}^2}$$

A value of 1 for these parameters indicates that no products are formed. Thus, the reactions are at the farthest position from equilibrium. The value of zero indicates that reactions have reached the equilibrium state. These parameters are dimensionless number and are independent of temperature, pressure and inlet feed to the reformer. As D/L ratio is varied, these parameters also changes due to change of geometry of reformer. The value of D/L ratio where these parameters have the lowest value is the optimal value for reformer.

8.2 OPTIMAL DESIGN OF SOLAR COLLECTOR

Once the optimal D/L ratio is decided for the SMR process under the general operating conditions, optimal solar collectors is designed according to weather conditions of Dhahran. Inputs for designing a solar collector are local solar flux density, radius and length of reformer. Initial radius for solar collector is also one of the inputs. It is reported in literature that average solar flux density for Dhahran is around 1000W/m^2 [142]. So, this value of solar flux density is used for design of solar collector. Using the radius value of 0.06 m, the length for the reformer is calculated. Only remaining input that can have various values is initial radius of collector. It is varied from the 0.001 to 20 m. An objective function that is the surface area of resulting collector is also calculated for each value of initial radius. The value of initial radius that gives the minimum value of surface area is regarded as the optimal value. The main reason for selecting the surface area as the objective function is to select a collector that has minimum material usage. Smaller the surface area, lesser will be the material used. Therefore, the material cost for the collector will be less.

8.3 RESULTS AND DISCUSSION

Simulations are performed for each value of D/L ratio under the selected operating conditions. Fractional methane conversion is found to increase along the direction of flow. This is due to the fact that as the reaction mixture moves over the catalyst, contact time increases producing more products as shown in Figure 61. It can also be seen that as D/L ratio decreases fractional methane conversion increases as shown in Figure 62. For the D/L ratios higher than 0.06, the fractional methane conversion is close to zero. For D/L ratios lower than 0.06, fractional methane conversion increases sharply.

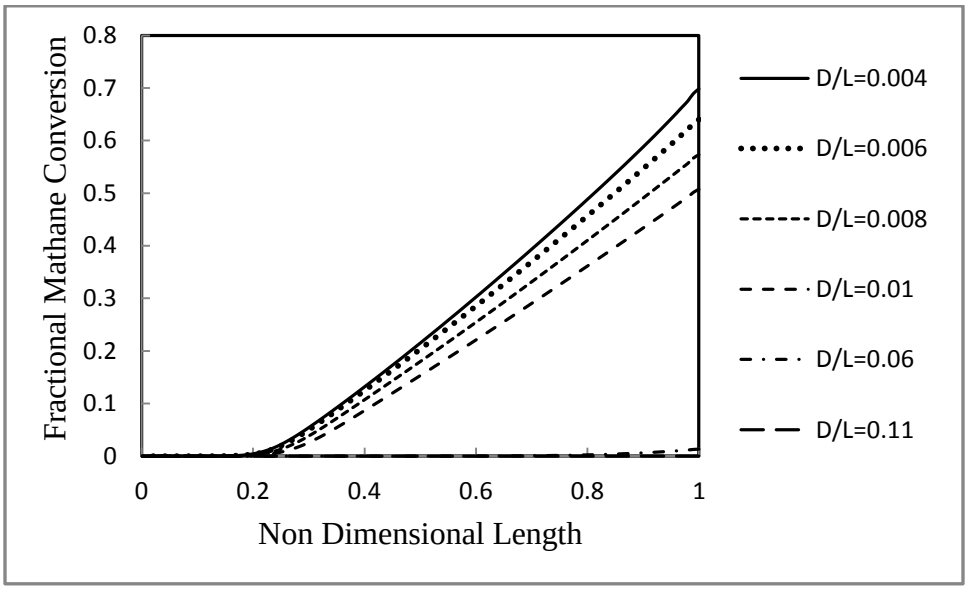

Figure 61 : Fractional methane conversion along the direction of flow for various values of D/L ratio

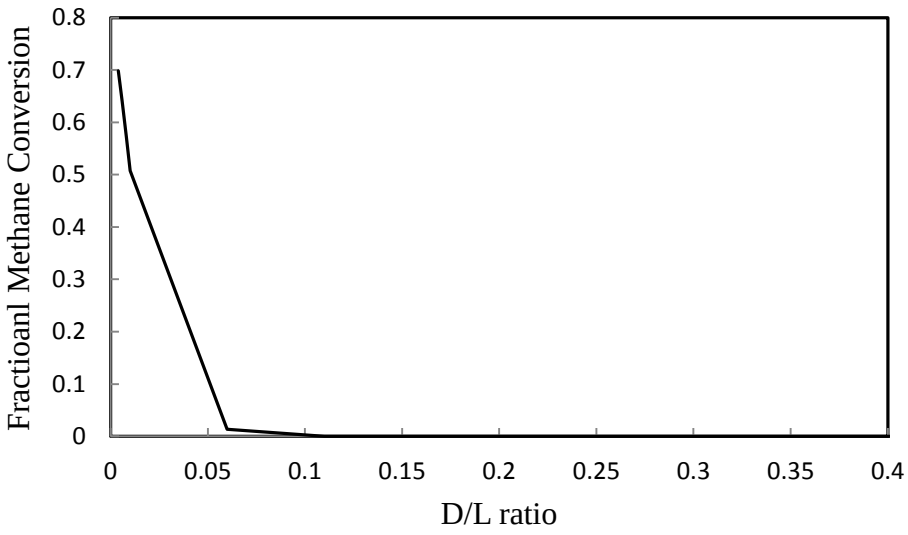

Figure 62 : Fractional methane conversion for various values of D/L ratios

To find the optimal D/L value, three chemical reactions representing the SMR process are studied separately. The parameters that measure the approach of reactions towards the equilibrium are obtained for each value of D/L ratio. For reaction 1, this parameter decreases with decrease in D/L ratio up to a value of 0.008. After that value, it starts to increase indicating the 0.008 value of D/L ratio optimal for reaction 1 as shown in Figure 63. It can also be seen from the graph that the parameter γ_1 does not have value of zero at D/L ratio of 0.008 but it is the minimum value that this reaction can obtain over the entire range of D/L ratio as shown in Figure 64. The graph of γ_1 with various value of D/L ratio has lot of local minima. Therefore, a wide range of D/L ratio varying from 0.004 to 0.41 is studied to find the absolute minima.

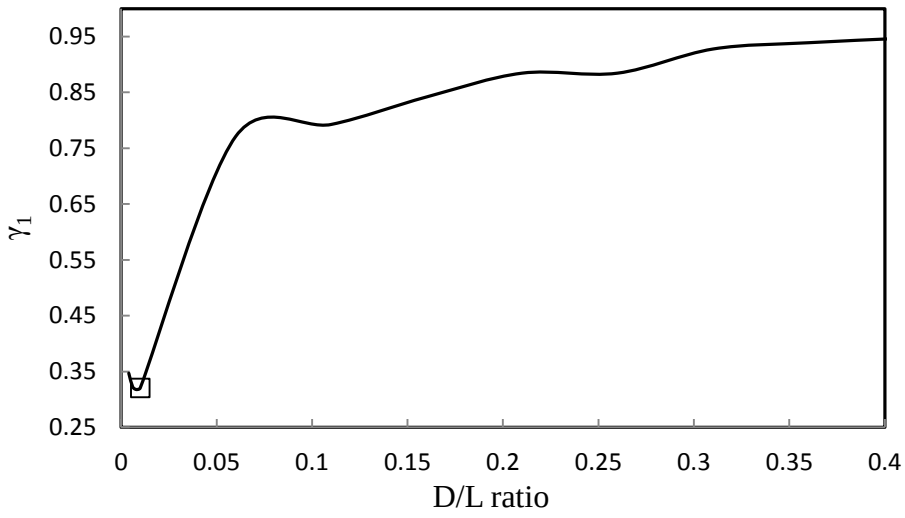

Figure 63 : γ_1 for various values of D/L ratio

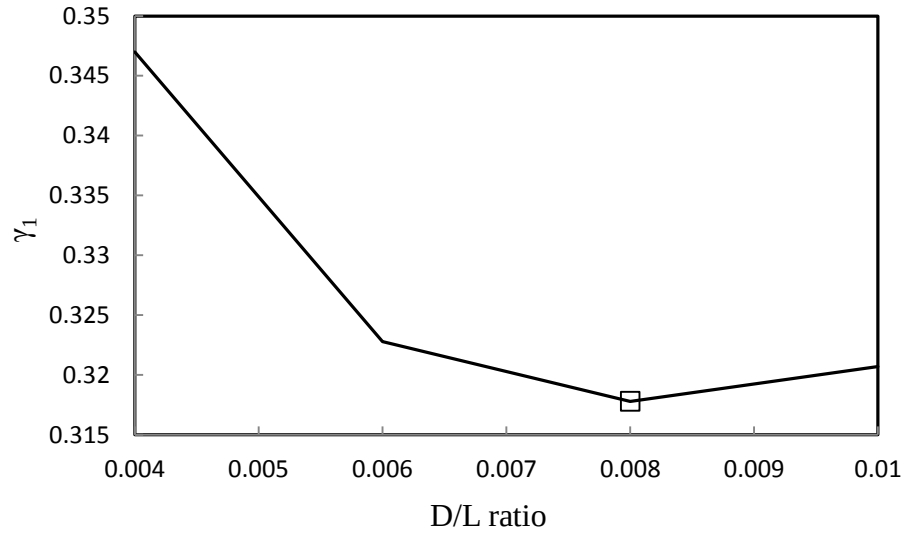

Figure 64 : Enlarged view of variation of γ_1 or various values of D/L ratios

For the reaction 2, γ_2 has similar trend as that of γ_1. It decreases with increase in D/ L ratio lower than 0.008. For D/L ratio higher than 0.008, it increases with increase in D/L

ratio as shown in Figure 65.The γ_2 has its lowest value at D/L ratio of 0.008 as shown in Figure 66.

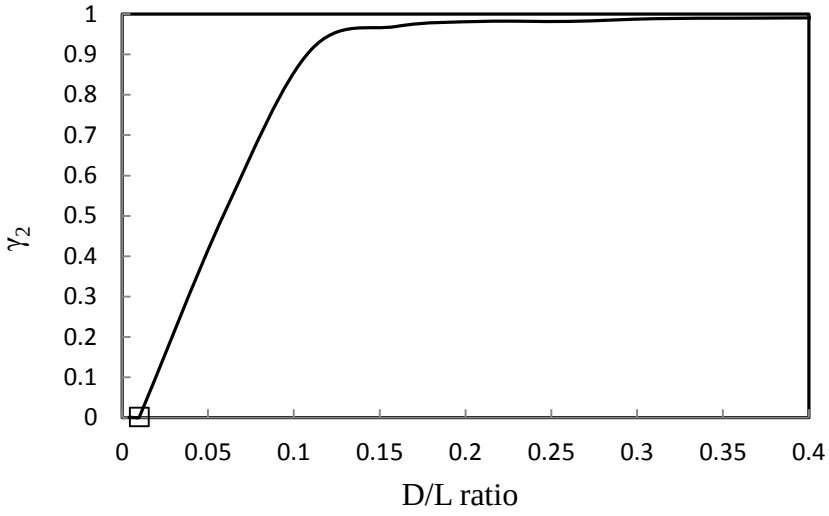

Figure 65 : Variation of γ_2 for various values of D/L ratios

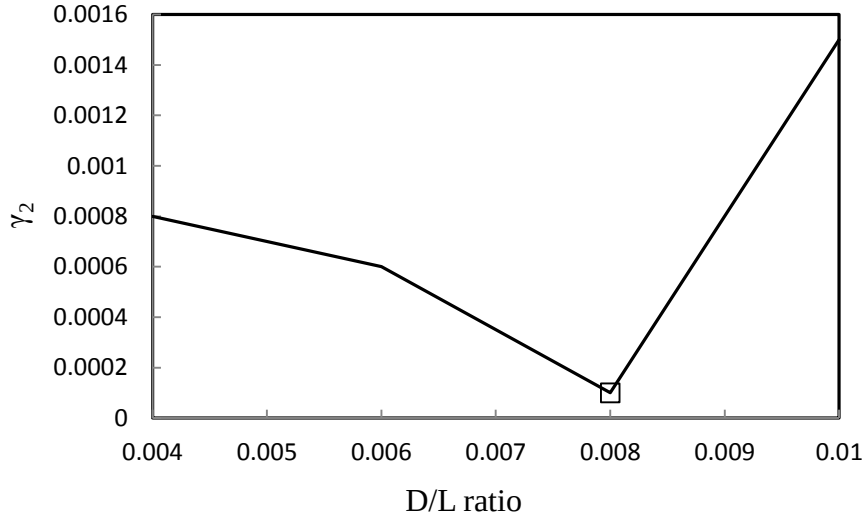

Figure 66 : Enlarged view of variation of γ_2 for various values of D/L ratios

For reaction 3, the variation of γ_3 for various values of D/L ratio is shown in Figure 67. The trend of γ_3 is same as that of γ_1 and γ_2. Enlarged view of the graph in Figure 68 shows that the optimal value for reaction 3 is 0.008.

All of three reactions have their minimum γ values at D/L ratio of 0.008. Therefore, this value is the optimal for SMR reaction under the specified operating conditions. Strong coupling of three SMR reactions can also be seen from above study that all of them are reaching to equilibrium at the same value of D/L ratio.

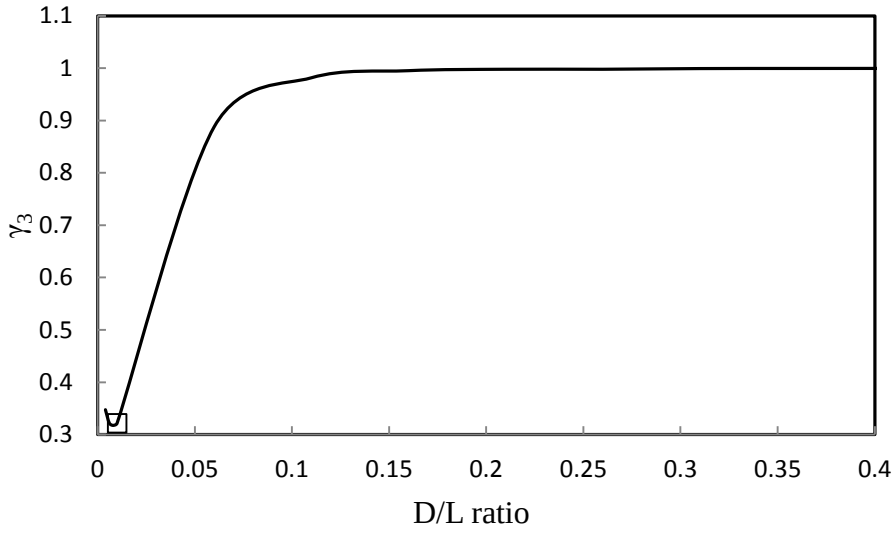

Figure 67 : Variation of γ_3 for various values of D/L ratio

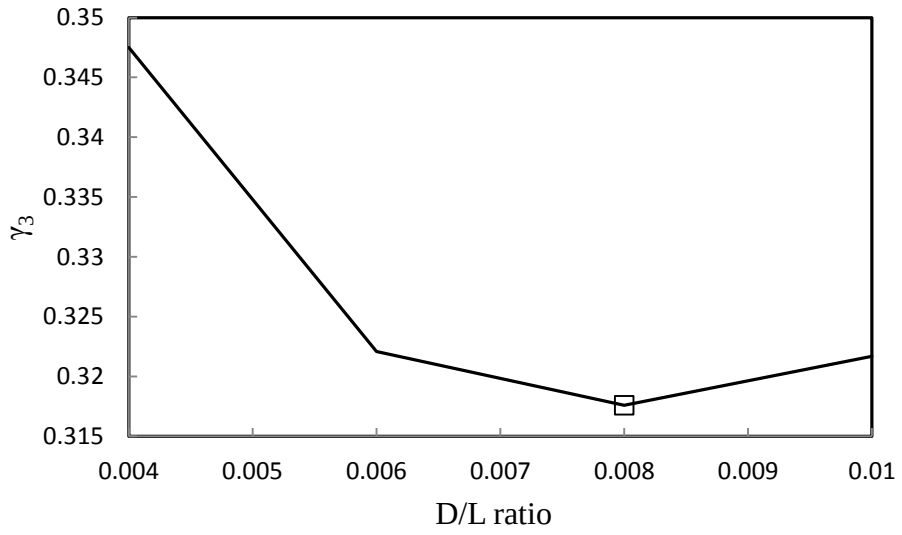

Figure 68 : Enlarged view of variation of γ_3 for various values of D/L ratios

After obtaining the optimal value of D/L ratio from the computational fluid dynamics model of SMR, optimal solar collector is designed under the specified operating conditions of SMR. As stated earlier, a reformer with diameter of 0.06 m is used to obtain the optimal D/L ratio. Thus, diameter of 0.06 m and D/L ratio of 0.008, the length of reformer is calculated. These dimensions of reformer along with local solar flux density are used in the design algorithm for solar collector. The initial radius is varied to get the collectors of various surface areas. It is found that as the initial radius is increased the surface area of reflecting surface decrease as shown in Figure 69.

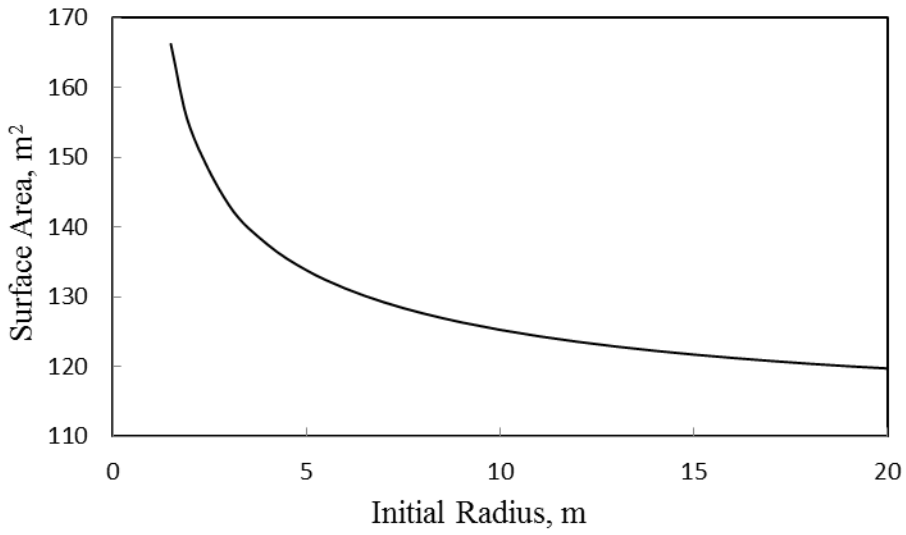

Figure 69 : Variation of surface area of reflecting surface for various values of initial radius

It means that greater the initial radius of the collector lesser will be the surface area. Therefore, less material will be used to build the reflecting surface. It can also be seen that the surface area of reflecting surface is always decreasing with increase in initial radius. Therefore, the value of initial radius that will give the minimum surface area would be very very high. It can also be seen that the increase in surface area for unit increase in initial radius is decreasing with increase in initial radius. Therefore, a compromise is required between the value of initial radius and the cost of material. Depending on one's own limitations, one can decide the value of initial radius for solar collector.

8.4 CONCLUSION

In the present study, optimal tubular reformer and respective optimal of solar collector is studied. General operating conditions for SMR reaction are selected for simulations. It is seen that at these general operating conditions, a value of 0.008 for the D/L ratio for tubular reformer is the value at which three SMR reaction are closest to equilibrium after that reactions start moving away from equilibrium. It can also be seen from the study that all of the three reactions which are studied separately for approach of equilibrium are reaching the equilibrium at the same value of D/L ratio which indicates strong coupling between the reactions.

In the later part of the chapter, optimal design of solar collector is studied. It can be seen from the study that greater the initial radius of the reflecting surface smaller will be the surface area of the reflecting surface. Thus, lesser will be the cost for the material of reflecting surface. It is also seen that at higher value of initial radius, increasing the initial radius produces less change in surface area.

CHAPTER 9

CONCLUSIONS AND RECOMMENDATIONS

Steam methane reforming is a striking solution towards the problems of unclean combustion and storage of solar energy. The process is also used word wide for the production of hydrogen which is used extensively in the process industry and refineries. Therefore, steam methane reforming has been main concern for the researchers over last 50 years.

The steam methane reforming process has complex kinetic dependence. A number of experimental studies have been performed to decide its kinetics. A large number of kinetic models, explaining the reaction paths, have been developed. The main problem with these kinetic models is the range of their applicability. Most of models are developed under limited range of operating conditions, therefore, work within that range only. There is a need to look for a kinetic model that is more general. A kinetic model that is applicable over a long range of operating conditions. It should be able to predict the results of other limited models in their operating ranges. All these kinetic models are catalyst specific and large number of catalyst are used for SMR process. The Ni based catalyst is found to be used more extensively due heat and mass transfer limitations.

Thus, the early part of the thesis is devoted to a thorough literature survey to find a comprehensive kinetic model dealing with Ni based catalyst.

Based on the kinetic model, a comprehensive computational fluid dynamic based two dimensional axisymmetric homogenous steam methane reforming model is developed. The most practical assumptions are made to develop the model. The model is validated against the experimental data. A high validity of model ensured that the model can be used for the further studies of steam methane reforming reaction. To check the influence of operating parameters on the steam methane reforming, a parametric study is performed. Influence of pressure, temperature, inlet feed velocity and inlet feed molar ratios are studied.

The driving heat for steam methane reforming reaction is provided by solar energy. It is seen in the literature that not only the amount of supplied heat but the distribution of heat also controls the efficiency of reaction. This raises the challenge of designing a solar collector that can give the required energy distribution. Thus, a solar collector is developed that can give the required energy distribution with certain specifications.

The two limits on methane conversion also necessitate knowing that under which limit a specific conversion is lying. These conversion limits are the function of geometry as well as the operating variables of steam methane reforming. Therefore, there is a need of study of these conversion limits as the function of geometry as well the operating variables of steam methane reforming. Thus, in the last part of the thesis optimal diameter to length ratio for a tubular reformer is obtained for optimal operation of SMR.

9.1 CONCLUSIONS

From present studies, it is concluded that

- Most commonly used catalyst for steam methane reforming is Ni based due to mass and heat transfer limitations.
- The steam methane reforming reaction gives non monotonic reaction rate order with respect to the partial pressure of steam.
- The kinetic model developed by Xu and Froment [52] is found to the best model for steam methane reforming reaction over Ni based catalysts.
- The steam methane reforming reaction strongly depends on the mass transfer limitations, which is shown by precise modeling of mass diffusion.
- The pressure drop due to porous nature of catalyst of steam methane reforming can easily be modeled by using correlations.
- The use of porosity as the decreasing factor is for the various terms of momentum and energy equations is a valid assumption and captures the true physical phenomena.
- The assumption of modeling the catalyst as the continuum is also a good approach as long as the mass diffusion and pressure drop are modeled precisely.
- It is seen in the parametric study that with increase in the temperature conversion increases and the thermodynamic limit is achieved with lower contact time.

- The methane conversion is found to decrease with increase in pressure and thermodynamic limit is achieved with low contact time, thus, longer reformers are required at low pressure to get thermodynamically limited conversion.
- The steam methane reforming reaction is compressible, thus, instead of mass flow rate the average inlet velocity should be studied to obtain the contact time dependence if pressure dependence is studied separately.
- It is also seen in the parametric studies that change in steam to carbon molar ratio has the more effect on the steam methane reforming reaction than the change in hydrogen to methane molar ratio.
- The design algorithm for solar collector is flexible and takes care of user's limitation such as available space by giving multiple shapes for same flux distribution
- Algorithm also secures the flux distribution even if the incoming solar flux changes
- The Study of optimal Diameter to Length (D/L) ratio showed that methane conversion increases with decrease in D/L ratio.
- This study has also shown that the developed CFD based SMR model captures the strong coupling between the SMR reactions precisely.
- It is also concluded from the study that increase in the initial radius in the design algorithm for solar collector decreases the surface area of reflecting surface of collector.

9.2 RECOMMENDATIONS

In the light of comprehensive study of steam methane reforming reaction, following points can be recommended for future research.

- In the CFD model of steam methane reforming, the assumption of constant porosity should be relaxed.
- The pore structure models should be incorporated in the model to obtain more accurate fractional methane conversion.
- In the design of solar collector, certain assumption should be relaxed such as the constant value of reflectivity.
- The assumption of 100% tracking of solar collector should also be considered in the model and a correction factor depending on the tracking mechanism should be included in the model.
- The designing algorithm should be extended to the non-specular surface with certain modifications

NOMENCLATURE

A	Area, m^2
A_i	Pre exponential factor for Arrhenius equation, dimensions of $k_{o,i}$
$A_{Cp,i}$	Polynomial coefficients for calculation of C_{pi}
A_{abs}	Surface area of absorber, m^2
A_{ref}	Aperture area of absorber, m^2
a_{ii}	Coefficient of products in chemical reaction
a_{ii}	Coefficient of products in chemical reaction
B	Local solar flux, J
B_i	Pre exponential factor for Van't Hoff equation, dimension of K_i
B_x	Required flux over surface of absorber, J
C_p	Specific heat capacity of reaction mixture, $kJ/kg\ K$
C_{pi}	Specific heat capacity of reaction mixture, $kJ/kg\ K$
C_n	Concentration ratio
C_{ideal}	Ideal concentration ratio
$D_{i,e}$	Effective diffusive coefficient of specie i, m^2/s
$D_{i,T}$	Thermal diffusive coefficient of specie i, kg/ms
$D_{n,i}$	Knudsen diffusive coefficient of specie i, m^2/s
$D_{m,i}$	Molecular diffusive coefficient of specie i, m^2/s
DEN	Denominator
d_p	Equivalent particle diameter, m

d	Distance of intercepting surface from source, *m*
E	Energy, *J*
E_i	Activation energy of reaction i, *kJ/mol*
E_{dx}	Energy received by small element dx, *J*
F_i	Molar Flow rate of specie i, *mol/h*
F_{mix}	Molar Flow rate of reaction mixture, *mol/h*
$GHSV$	Gas hour space velocity, $cm^3/g_{cat}\ h$
H_i	Absorption enthalpy of specie i, *kJ/mol*
h	Height of intercepting surface, *m*
h_i	Enthalpy of specie i, *W/mK*
j_i	Diffusive Flux of specie i, kg/m^2s
k_e	Effective heat conduction coefficient, *W/mK*
k_i	Heat conduction coefficient of specie i, *W/mK*
k_f	Heat conduction coefficient of reaction mixture, *W/mK*
k_s	Heat conduction coefficient of catalyst, *W/mK*
$K_{e,i}$	Equilibrium constant for reaction i, bar2 for i=1, 3 and 0 for i=2
k_o	Constant for reaction rate, unit depends on rate equation
$k_{o,i}$	Rate constant of reaction i, Table no. 1
K_i	Van't Hoff constant for specie i, Table no. 2
L	Length of absorber, *m*
M_i	Molecular weight of specie i, *kg/mol*
m	Constant for reaction rate models
n_i	Molar ratio of specie i, F_i/F_{MIX}

n	Constant for reaction rate models
P	Pressure of reaction mixture, N/m^2
p_i	Partial pressure of specie i, *bar*
R	General gas constant, *J/mol K*
R_i	Rate of reaction of specie i, mol/m^3s
r_1,r_2,r_3	Rate of reactions 1, 2 and 3, $kmol/kg_{cat}h$
r_i	Initial radius of reflecting surface, *m*
r_{ab}	Radius of absorber, *m*
r_c	Rate of reaction, *kmol/h*
S/C	Steam to carbon molar ratio
T	Temperature of reaction mixture, *K*
T_o	Reference temperature for viscosity calculation, *K*
T_s	Temperature of sun, *K*
V	Velocity of reaction mixture, *m/s*
W_{cat}	Mass of catalyst, *kg*
xx	Abscissa of global co-ordinate axes, *m*
Y_i	Mass fraction of specie i
yy	Ordinate of global co-ordinate axes, *m*

GREEK SYMBOLS

α	Absorbance
β,θ	Angular rotation, radians
ρ	Reflectance
ρ_f	Density of reaction mixture, kg/m^3
ρ_i	Density of specie i, kg/m^3
$\bar{\bar{\tau}}$	Effective shear stress, N/m^2
τ	Transmittance
ε	Porosity of catalyst bed
ϵ	Emittance
μ_f	Viscosity of reaction mixture, *kg/ms*
μ_i	Viscosity of specie i, *kg/ms*
$\mu_{i,o}$	Viscosity of specie at reference temperature, *kg/ms*
η_i	Effectiveness factor of reaction i
η	Efficiency

REFERENCES

[1] Chamousis R., 2006, Hydrogen : Fuel of the Future.

[2] Armor J. N., 1999, "The multiple roles for catalysis in the production of H_2," Appl. Catal. A Gen., 176(2), pp. 159–176.

[3] Holladay J. D., Hu J., King D. L. and Wang Y., 2009, "An overview of hydrogen production technologies," Catal. Today, 139(4), pp. 244–260.

[4] Rostrup-Nielsen J. R., 1993, "Production of synthesis gas," Catal. Today, 18(4), pp. 305–324.

[5] Gerhard E. R. and Moe M. J., 1965, "Chemical reaction and heat transfer rates in steam methane reforming," AIchE Symp. 56th Natl. Meet.

[6] Hoang D., 2004, "Modeling of a catalytic autothermal methane reformer for fuel cell applications," Appl. Catal. A Gen., 268(1-2), pp. 207–216.

[7] Ceo N., Tang S., Lin J. and Tan K. L., 1998, "Partial oxidation of methane to syngas over Ni/MgO, Ni/CaO and Ni/CeO_2," Catal. Commun., 51, pp. 169–175.

[8] Laosiripojana N. and Assabumrungrat S., 2005, "Catalytic dry reforming of methane over high surface area ceria," Appl. Catal. B Environ., 60(1-2), pp. 107–116.

[9] Ewan B. and Allen R., 2005, "A figure of merit assessment of the routes to hydrogen," Int. J. Hydrogen Energy, 30(8), pp. 809–819.

[10] Steinberg M., 1989, Hydrogen Production form Fossil Fuels.

[11] Bartels J. R., Pate M. B. and Olson N. K., 2010, "An economic survey of hydrogen production from conventional and alternative energy sources," Int. J. Hydrogen Energy, 35(16), pp. 8371–8384.

[12] Abbott D., 2010, "Keeping the Energy Debate Clean: How Do We Supply the World's Energy Needs?," Proc. IEEE, 98(1), pp. 42–66.

[13] Akers W. W. and Camp D. P., 1955, "Kinetics of the methane-steam reaction," AIChE J., 1(4), pp. 471–475.

[14] Allen D. W., Gerhard E. R. and Likins M. R., 1975, "Kinetics of the Methane-Steam Reaction," Ind. Eng. Chem. Process Des. Dev., 14(3), pp. 256–259.

[15] Rakass S., Oudghiri-Hassani H., Rowntree P. and Abatzoglou N., 2006, "Steam reforming of methane over unsupported nickel catalysts," J. Power Sources, 158(1), pp. 485–496.

[16] Sehested J., 2006, "Four challenges for nickel steam-reforming catalysts," Catal. Today, 111(1-2), pp. 103–110.

[17] De Miguel N., Manzanedo J. and Arias P. L., 2012, "Testing of a Ni-Al_2O_3 catalyst for methane steam reforming using different reaction systems," Chem. Eng. Technol., 35(4), pp. 720–728.

[18] Wong C. and Mccabe R. W., 1989, "Effects of high-temperature oxidation and reduction on the structure and activity of Rh/Al_2O_3 and Rh/SiO_2 Catalysts," J. Catal., 64, pp. 47–64.

[19] Ross J., Steel M. C. F. and Zeini-Isfahani A., 1978, "Evidence for the participation of surface nickel aluminate sites in the steam reforming of methane over nickel/alumina catalysts," J. Catal., 52(2), pp. 280–290.

[20] Matsumura Y. and Nakamori T., 2004, "Steam reforming of methane over nickel catalysts at low reaction temperature," Appl. Catal. A Gen., 258(1), pp. 107–114.

[21] Roh H., Jun K., Dong W., Chang J., Park S. and Joe Y., 2002, "Highly active and stable Ni/Ce–ZrO_2 catalyst for H_2 production from methane," J. Mol. Catal. A Chem., 181, pp. 137–142.

[22] Guo X., Sun Y., Yu Y., Zhu X. and Liu C., 2012, "Carbon formation and steam reforming of methane on silica supported nickel catalysts," Catal. Commun., 19, pp. 61–65.

[23] Zhai X., Ding S., Liu Z., Jin Y. and Cheng Y., 2011, "Catalytic performance of Ni catalysts for steam reforming of methane at high space velocity," Int. J. Hydrogen Energy, 36(1), pp. 482–489.

[24] Chen Y. and Ren J., 1994, "Conversion of methane and carbon dioxide into synthesis gas over alumina-supported nickel catalysts. Effect of Ni-$A1_2O_3$ interactions," Catal. Letters, 29, pp. 39–48.

[25] Numaguchi T., Shoji K. and Yoshida S., 1995, "Hydrogen effect on alpha-$A1_2O_3$ supported Ni catalyst for steam methane reforming reaction," Appl. Catal., 133, pp. 241–262.

[26] Young-Sam O., Hyun-Seog R., Ki-Won J. and Young-Soon B., 2003, "A highly active catalyst, Ni/Ce–ZrO_2/θ-Al_2O_3 for on-site H_2 generation by steam methane reforming: pretreatment effect," Int. J. Hydrogen Energy, 28(12), pp. 1387–1392.

[27] Al-Ubaid A. and Wolf E. E., 1988, “Steam reforming of methane on reduced non-stoichiometric nickel aluminate catalysts,” Appl. Catal., 40, pp. 73–85.

[28] Roh H. S., Ki-Won J., Dong W., Baek S. C. and Park S., 2002, “Methane reforming reactions over stable Ni theta-Al_2O_3 catalysts,” J. Chem. Eng., 8(5), pp. 464–471.

[29] Dong W., Roh H., Jun K., Park S. and Young-Sam O., 2002, “Methane reforming over Ni/Ce-ZrO_2 catalysts : effect of nickel content,” Appl. Catal. A Gen., 226, pp. 63–72.

[30] Rostrup Nielsen J., 1984, “Sulfur-passivated nickel catalysts for carbon-free steam reforming of methane,” J. Catal., 85(1), pp. 31–43.

[31] Trimm D. L., 1997, “Coke formation and minimisation during steam reforming reactions,” Catal. Today, 37(3), pp. 233–238.

[32] Ruojun S., Liangqu Z. and Shendu G. U. O., 1991, “Coking resistant nickel catalysts for hydrocarbon steam reforming,” Catal. Deactiv., 68, pp. 243–247.

[33] Trimm D. L., 1999, “Catalysts for the control of coking during steam reforming,” Catal. Today, 49(1-3), pp. 3–10.

[34] Xu J., Chen L., Tan K., Borgna A. and Saeys M., 2009, “Effect of boron on the stability of Ni catalysts during steam methane reforming,” J. Catal., 261(2), pp. 158–165.

[35] Mariana de Mattos V. M. Souza and Schmal M., 2005, “Supported nickel catalysts for steam reforming of mathane,” Chem. Eng. Congress.

[36] Hegarty M. E. S., Connor A. M. O. and Ross J. R. H., 1998, “Syngas production from natural gas using ZrO_2-supported metals,” Catal. Today, 42, pp. 225–232.

[37] Laosiripojana N. and Assabumrungrat S., 2005, “Methane steam reforming over Ni/Ce–ZrO_2 catalyst: Influences of Ce–ZrO_2 support on reactivity, resistance toward carbon formation, and intrinsic reaction kinetics,” Appl. Catal. A Gen., 290(1-2), pp. 200–211.

[38] Kuo H. K., Ganesan P. and Angelis R. J. De, 1980, “The sintering of a silica-supported nickel catalyst,” J. Catal., 319, pp. 303–319.

[39] Sehested J., Carlsson A., Janssens T. V. W., Hansen P. L. and Datye A. K., 2001, “Sintering of nickel steam-reforming catalysts on $MgAl_2O_4$ spinel supports,” J. Catal., 197(1), pp. 200–209.

[40] Hou K. and Hughes R., 2001, “The kinetics of methane steam reforming over a Ni/alpha-Al_2O catalyst,” Chem. Eng. J., 82(May 2000), pp. 311–328.

[41] Munster P. and Grabke H. J., 1981, "Kinetics of the steam reforming of methane with iron, nickel, and iron-nickel alloys as catalysts," J. Catal., 287, pp. 279–287.

[42] Nikolla E., Schwank J. and Linic S., 2009, "Comparative study of the kinetics of methane steam reforming on supported Ni and Sn/Ni alloy catalysts: The impact of the formation of Ni alloy on chemistry," J. Catal., 263(2), pp. 220–227.

[43] Bodrov, N. M., Apel'baum L. O. and T. M. I., 1964, "Kinetics of the reactions of methane with steam on the surface of nickel," Kinet. Karaliz, 5, pp. 696–705.

[44] Bodrov, N. M., Apel'baum L. O. and T. M. I., 1967, "Kinetics of the reaction of methane with water vapor, catalyzed by nickel on a porous carrier," Kinet. Karaliz, 8, pp. 821–828.

[45] Bodrov, N. M., Apel'baum L. O. and T. M. I., 1967, "Kinetics of the reaction of methane with steam on the surface of nickel at 400 to 600 ^{o}C.," Kinet. Karaliz, 8, pp. 821–828.

[46] Murray A. P. and Snyder T. S., 1989, "Steam-methane reformer kinetic computer model with heat transfer and geometry options," Ind. Eng. Chem. Process Des. Dev., 24(1967), pp. 286–294.

[47] Steel M. C. F. and Ross J.R.H., 1972, Mechanism of the steam reforming of methane over a coprecipitated nickel-alumina catalyst.

[48] Ko K. D., Lee J. K., Park D. and Shin S. H., 1995, "Kinetics of steam reforming over a Ni/alumina catalyst," Korean J. Chem. Eng., 12(4), pp. 478–480.

[49] Agnelli M. E., Ponzi E. N. and Yermian A. A., 1987, "Catalytic deactivation on methane steam reforming catalysis. 2. Kinetics study," Ind. Eng. Chem. Res., 26, pp. 1707–1713.

[50] Hyman M. H., 1968, "Simulate methane reformer reactions," Hydrocarb. Process, 47(7), p. 131.

[51] Gover S. S., 1970, "Hydrocarbon process," Hydrocarb. Process, 49(4), p. 109.

[52] Xu J. and Froment G. F., 1989, "Methane steam reforming, methanation and water-gas shift: I. Intrinsic kinetics," AIChE J., 35(1), pp. 88–96.

[53] Wei J. and Iglesia E., 2004, "Reaction pathways and site requirements for the activation and chemical conversion of methane on Ru−based catalysts," J. Phys. Chem. B, 108(22), pp. 7253–7262.

[54] Wei J. and Iglesia E., 2004, "Isotopic and kinetic assessment of the mechanism of reactions of CH_4 with CO_2 or H_2O to form synthesis gas and carbon on nickel catalysts," J. Catal., 224(2), pp. 370–383.

[55] Hoang D. L., Chan S. H., and Ding O. L., 2005, "Kinetic and modelling study of methane steam reforming over sulfide nickel catalyst on a gamma alumina support," Chem. Eng. J., 112(1-3), pp. 1–11.

[56] Soliman M. A., Adris A. M., Al-Ubaid A. S. and El-Nashaie S. S. E. H., 2007, "Intrinsic kinetics of nickel/calcium aluminate catalyst for methane steam reforming," J. Chem. Technol. Biotechnol., 55(2), pp. 131–138.

[57] Wei J. and Iglesia E., 2009, "Steam methane reforming in a Ni/Al_2O_3 catalyst: Kinetics and diffusional limitations in extrudates," Can. J. Chem. Eng., 87(6), pp. 945–956.

[58] Jun H. J., Park M. J., Baek S. C., Bae J. W., Ha K. S. and Jun K.-W., 2011, "Kinetics modeling for the mixed reforming of methane over $Ni\text{-}CeO_2/MgAl_2O_4$ catalyst," J. Nat. Gas Chem., 20, pp. 9–17.

[59] Jones G., Jakobsen J., Shim S., Kleis J., Andersson M., Rossmeisl J., Abildpedersen F., Bligaard T., Helveg S. and Hinnemann B., 2008, "First principles calculations and experimental insight into methane steam reforming over transition metal catalysts," J. Catal., 259(1), pp. 147–160.

[60] Pantoleontos G., Kikkinides E. S. and Georgiadis M. C., 2012, "A heterogeneous dynamic model for the simulation and optimization of the steam methane reforming reactor," Int. J. Hydrogen Energy, 37(21), pp. 16346-16358.

[61] Numaguchi T. and Kikuchi K., 1988, "Intrinsic kinetics and design simulation in a complex reaction network: Steam methane reforming," Chem. Eng. Sci., 43(8), pp. 2295–2301.

[62] Froment G. F. and Xu J., 1989, "Methane steam reforming : II . Diffusional limitations and reactor simulation ","AIChE J., 35(1), pp. 97–103.

[63] Adris A. M., Elnashie S. S. E. H., AL-Ubaid A. S. and Soliman M. A., 1990, "On the non-monotonic behavior of methane-steam reforming kinetics," Chem. Eng. Sci., 45(2), pp. 491–501.

[64] De Deken. J. C., Devos. E. F. and Froment. G. F., 1982, "Steam reforming of natural gas," Chem. React. Engng ACS Symp. Ser. 196., pp. 1–28.

[65] Khomenko A. A., Apelbaum L. O., Shub F. S., Yu S. and Snagovsky M. I. T., 1971, "Mechanism of steam and dry reforming of methane over nickel catalysts," Kinet. i Katal., 12, pp. 423–431.

[66] Avetisov A. K., Rostrup-Nielsen J. R., Kuchaev V. L., Bak Hansen J. H., Zyskin A. G. and Shapatina E. N., 2010, "Steady-state kinetics and mechanism of methane reforming with steam and carbon dioxide over Ni catalyst," J. Mol. Catal. A Chem., 315(2), pp. 155–162.

[67] Seo Y. S., Seo D. J., Seo Y. T. and Yoon W. L., 2006, "Investigation of the characteristics of a compact steam reformer integrated with a water-gas shift reactor," J. Power Sources, 161(2), pp. 1208–1216.

[68] Zhai X., Ding S., Cheng Y., Jin Y. and Cheng Y., 2010, "CFD simulation with detailed chemistry of steam reforming of methane for hydrogen production in an integrated micro-reactor," Int. J. Hydrogen Energy, 35(11), pp. 5383–5392.

[69] Irani M., Alizadehdakhel A., Pour A. N., Hoseini N. and Adinehnia M., 2011, "CFD modeling of hydrogen production using steam reforming of methane in monolith reactors: Surface or volume-base reaction model?," Int. J. Hydrogen Energy, 36(24), pp. 15602–15610.

[70] Vakhshouri K. and Hashemi M. M. Y. M., 2007, "Simulation study of radial heat and mass transfer inside a fixed bed catalytic reactor," World accedamy of eng. and tech., 34, pp. 180-187.

[71] Shayegan J., Hashemi M. M. Y. M. and Vakhshouri K., 2008, "Operation of an industrial steam reformer under severe condition: A simulation study," Can. J. Chem. Eng., 86(4), pp. 747–755.

[72] Alberton L., Schwaab M., Fontes C. E., Bittencourt R. C. and Pinto C. j., 2009, "Hybrid modeling of methane reformers. 1. A metamodel for the effectiveness factor of a catalyst pellet with complex geometry," Ind. Eng. Chem. Res., 48, pp. 9369–9375.

[73] Schwaab M., Alberton L., Fontes C. E., Bittencourt R. C., Pinto C. and Mu L., 2009, "Hybrid modeling of methane reformers . 2 . Modeling of the Industrial reactors," Ind. Eng. Chem. Res., 48, pp. 9376–9382.

[74] De Wilde J. and Froment G. F., 2012, "Computational Fluid Dynamics in chemical reactor analysis and design: Application to the ZoneFlow^{TM} reactor for methane steam reforming," Fuel, 100, pp. 48–56.

[75] Zanfir M. and Gavriilidis A., 2003, "Catalytic combustion assisted methane steam reforming in a catalytic plate reactor," Chem. Eng. Sci., 58(17), pp. 3947–3960.

[76] Soliman M. A., El-Nashaie S. S. E. H., Al-Ubaid A. and Adris A., 1889, "Simulation of steam reformer For methane," Chem. Eng. J., 13(8), pp. 1801–1806.

[77] Pedernera M. N., Piña J., Borio D. O. and Bucalá V., 2003, "Use of a heterogeneous two-dimensional model to improve the primary steam reformer performance," Chem. Eng. J., 94(1), pp. 29–40.

[78] Pin J., Schbib S. and Borio D. O., 2001, "Influence of the heat flux profiles on the operation of primary steam reformers," Ind. Eng. Chem. Res., 40(2), pp. 5215–5221.

[79] Froment G. F., 2000, "Production of synthesis gas by steam- and CO_2-reforming of natural gas," 163, pp. 147–156.

[80] Nandasana A. D., Ray A. K. and Gupta S. K., 2003, "Dynamic model of an industrial steam reformer and its use for multiobjective optimization," Ind. Eng. Chem. Res., 42(17), pp. 4028–4042.

[81] Sehested J., 2004, "Sintering of nickel steam-reforming catalysts: effects of temperature and steam and hydrogen pressures," J. Catal., 223(2), pp. 432–443.

[82] Paramaliana A., Frusteri F., Arena F., Mondello N. and Giordano N., 1989, "Activity and characterization of alkali doped Ni/MgO catalysts," Struct. React. Surfaces, 48, pp. 739–748.`

[83] Bernardo C. A. and Trimms D. L., 1979, "The kinetics of gasification of carbon deposited on nickel catalysts," Carbon N. Y., 17, pp. 115–120.

[84] Bernardo C. A., Alstrup I. and Rostrup-Nielsen J. R., 1985, "Carbon deposition and methane steam reforming on silica-supported Ni-Cu catalysts," J. Catal., 96(2), pp. 517–534.

[85] Chen W. J., Sheu F. R. and Savage R. L., 1987, "Catalytic activity of coal ash on steam methane reforming and water-gas shift reactions," Fuel Process. Technol., 16(3), pp. 279–288.

[86] Sehested J., 2003, "Sintering of nickel steam-reforming catalysts," J. Catal., 217, pp. 417–426.

[87] Snoeck J. and Froment G. F., 2002, "Steam/CO_2 reforming of methane. Carbon formation and gasification on catalysts with various potassium contents," Ind. Eng. Chem. Res., 41, pp. 3548–3556.

[88] Teixeira A. C. S. C. and Giudici R., 1999, "Deactivation of steam reforming catalysts by sintering: experiments and simulation," Chem. Eng. Sci., 54(15-16), pp. 3609–3618.

[89] Barbieri G. and Maio F. P. Di, 1997, "Simulation of the methane steam reforming process in a catalytic Pd-membrane reactor," Ind. Eng. Chem. Res., 5885(96), pp. 2121–2127.

[90] Adris A. M., Lim C. J. and Gracc J. R., 1997, "The fluidized-bed membrane reactor for steam methane reforming: model verification and parametric study," Chem. Eng. J., 52(10), pp. 1609–1622.

[91] Barbieri G., Marigliano G., Perri G. and Drioli E., 2001, "Conversion−temperature diagram for a palladium membrane reactor. Analysis of an endothermic reaction: Methane steam reforming," Ind. Eng. Chem. Res., 40(9), pp. 2017–2026.

[92] Barbieri G., Violante V., Maio F. P. Di, Criscuoli A. and Drioli E., 1997, "Methane steam reforming analysis in a palladium-based catalytic membrane reactor," Ind. Eng. Chem. Res., 36(8), pp. 3369–3374.

[93] Catalano J., Guazzone F., Mardilovich I. P., Kazantzis N. K. and Ma Y. H., 2011, "Hydrogen production in a large scale water gas shift Pd-based catalytic membrane reactor," Ind. Eng. Chem. Res.

[94] Gallucci F., Comite A., Capannelli G. and Basile A., 2006, "Steam reforming of methane in a membrane reactor: An industrial case study," Ind. Eng. Chem. Res., 45(9), pp. 2994–3000.

[95] Gallucci F., Paturzo L., Fama A. and Basile A., 2004, "Experimental study of the methane steam reforming reaction in a dense Pd/Ag membrane reactor," Ind. Eng. Chem. Res., 43, pp. 928–933.

[96] Galuszka J., Pandey R. and Ahmed S., 1998, "Methane conversion to syngas in a palladium membrane reactor," Catal. Today, 46(2-3), pp. 83–89.

[97] Grace J. R., Li X. and Jim Lim C., 2001, "Equilibrium modelling of catalytic steam reforming of methane in membrane reactors with oxygen addition," Catal. Today, 64(3-4), pp. 141–149.

[98] Kikuchi E., 2000, "Membrane reactor application to hydrogen production," Catal. Today, 56(1-3), pp. 97–101.

[99] Kikuchi E., Nemoto Y., Kajiwara M., Uemiya S. and Kojima T., 2000, "Steam reforming of methane in membrane reactors: comparison of electroless-plating and CVD membranes and catalyst packing modes," Catal. Today, 56(1-3), pp. 75–81.

[100] Mahecha-Botero A., Chen Z., Grace J. R., Elnashaie S. S. E. H., Jim Lim C., Rakib M., Yasuda I. and Shirasaki Y., 2009, "Comparison of fluidized bed flow regimes for steam methane reforming in membrane reactors: A simulation study," Chem. Eng. Sci., 64(16), pp. 3598–3613.

[101] Nam S. W., Yoon S. P., Ha H. Y., Hong S.A. and Maganyuk A. P., 2000, "Methane steam reforming in a Pd-Ru membrane reactor," Korean J. Chem. Eng., 17(3), pp. 288–291.

[102] Nielsen P. E. H. and Lehrmann P., 1995, "Steam reforming of methane in a membrane reactor," Catal. Today, 25(3), pp. 303–307.

[103] Oklany J. S., Hou K. and Hughes R., 1998, “A simulative comparison of dense and microporous membrane reactors for the steam reforming of methane,” Appl. Catal., 170, pp. 13–22.

[104] Patel K. and Sunol a, 2007, “Modeling and simulation of methane steam reforming in a thermally coupled membrane reactor,” Int. J. Hydrogen Energy, 32(13), pp. 2344–2358.

[105] Shu J., Grandjean B. P. A. and Kaliaguine S., 1994, “Methane steam reforming in asymmetric Pd- and Pd-Ag / porous SS membrane reactors,” Science, 119(2), pp. 305–325.

[106] Tong J. and Matsumura Y., 2006, “Pure hydrogen production by methane steam reforming with hydrogen-permeable membrane reactor,” Catal. Today, 111(3-4), pp. 147–152.

[107] Tong J., Su L., Kashima Y., Shirai R., Suda H. and Matsumura Y., 2006, “Simultaneously depositing Pd−Ag thin membrane on asymmetric porous stainless steel tube and application to produce hydrogen from steam reforming of methane,” Ind. Eng. Chem. Res., 45(2), pp. 648–655.

[108] Uemiya S., Sato N., Ando H. and Matsuda T., 1991, “Steam reforming of methane in a hydrogen-permeable membrane reactor,” Appl. Catal., 67, pp. 223–230.

[109] Adris A. E. M., 1994, “A fluidized bed membrane reactor for steam methane reforming: Experimental verification and model validation.”

[110] Chen D., Lødeng R., Svendsen H. and Holmen A., 2011, “Hierarchical multiscale modeling of methane steam reforming reactions,” Ind. Eng. Chem. Res., 50(5), pp. 2600–2612.

[111] Snoeck J. W., Froment G. F. and Fowles M., 1997, “Kinetic study of the carbon filament formation by methane cracking on a nickel catalyst,” J. Catal., 169(1), pp. 250–262.

[112] Snoeck J. W., Froment G. F. and Fowles M., 1997, “Filamentous carbon formation and gasification: Thermodynamics, driving force, nucleation, and steady-state growth,” J. Catal., 169(1), pp. 240–249.

[113] Muhammad-sukki F., Ramirez-iniguez R., Mcmeekin S. G., Stewart B. G. and Clive B., “Solar concentrators,” Int. J. Appl. Sci., 1(1), pp. 1–15.

[114] Rabl A., 1976, “Comparison of solar concentrators,” Sol. Energy, 18(2), pp. 93–111.

[115] Kalogirou S. A., 2004, “Solar thermal collectors and applications” Progress in Energy and Combustion Science, 30, pp. 231-295.

[116] Winston R., 1974, “Principle of solar concentrators of a novel design,” Sol. Energy, 16(1), pp. 89–95.

[117] Piatkowski N., Wieckert C., Weimer A. W. and Steinfeld A., 2011, “Solar-driven gasification of carbonaceous feedstock—a review,” Energy Environ. Sci., 4(1), p. 73.

[118] Muir J. F., Hogan R. E., Skocypec R. D. and Buck R., 1994, “Solar reforming of methane in a direct absorption catalytic reactor on a parabolic dish: I—Test and analysis,” Sol. Energy, 52(6), pp. 467–477.

[119] Anikeev V. I., Bobrin A. S., Ortner J., Schmidt S., Funken K. H. and Kuzin N. A., 1998, “Catalytic thermochemical reactor/receiver for solar reforming of natural gas: Design and performance,” Sol. Energy, 63(2), pp. 97–104.

[120] Li Z., Tang D., Du J. and Li T., 2011, “Study on the radiation flux and temperature distributions of the concentrator–receiver system in a solar dish/Stirling power facility,” Appl. Therm. Eng., 31(10), pp. 1780–1789.

[121] Rabl A., 1976, “Solar Concentrators with Maximal Concentration for Cylindrical Absorbers,” Appl. Opt., 15(7), pp. 1871–1873.

[122] Shuai Y., Xia X. L. and Tan H. P., 2008, “Radiation performance of dish solar concentrator/cavity receiver systems,” Sol. Energy, 82(1), pp. 13–21.

[123] Meier R. H., Ana S. and Calif, 1987, “Ellipdoidal solar dish concentrator.”

[124] Hockman V. J., Ridge O. and Tenn, 1975, “Solar radiation collector and concentrators.”

[125] Hines B. E., and Jhnson R. L., 2010, “Hybrid primary optical component for optical concentrators.”

[126] Zalusky J. T., 2010, “Placement of solar collector.”

[127] Jones T. M., 1994, “System for deicing dish mounted antenne.”

[128] Tripanagnostopoulos Y., Georgostathis P. and Iliopoulou A., 2009, “Optical study of new designs for CPVT systems. ”

[129] Tuchelt M. J., 2008, “Solar energy collection apparatus and method.”

[130] Polk D. E., 2011, “Concentrating solar energy collector system with photovoltic cells.”

[131] S.Ergun, 1952, “Fluid Flow through Pacekd columns,” Chem. Eng. Prog., 48(2), pp. 89–94.

[132] Wilke C. R. and Chang P., 1955, “Correlation of diffusion coefficients in dilute solutions,” AIChE J., 1(2), pp. 264–270.

[133] A. J. Chorin., 1968, “Numerical solution of navier-stokes equations,” Math. Comput., 22, pp. 745–762.

[134] ANSYS, Inc., 2009, ANSYS FLUENT 13.0 User's Guide.

[135] Ross B. Y. J. R. H., 1982, “Metal catalysed methanation and steam reforming,” 2(39).

[136] Duffie J. A. and Beckman W. A., 2006, Solar engineering and thermal processes.

[137] Rajesh J. K., Gupta S. K., Rangaiah G. P. and Ray A. K., 2000, “Multiobjective optimization of steam reformer performance using genetic algorithm,” Ind. Eng. Chem. Res., 39(3), pp. 706–717.

[138] Levent M., Budak G. and Karabulut A., 1998, “Estimation of concentration and temperature profiles for methane-steam reforming reaction in a porous catalyst,” Fuel Process. Technol., 55(3), pp. 251–263.

[139] De Groote A. M. and Froment G. F., 1995, “Reactor modeling and simulations in synthesis gas production,” Rev. Chem. Eng., 11(2).

[140] El-Bousiffi M. A., and Gunn D. J., 2007, “A dynamic study of steam-methane reforming,” Int. J. Heat Mass Transf., 50(3-4), pp. 723–733.

[141] Oliveira E. L. G., Grande C. A., and Rodrigues A. E., 2010, “Methane steam reforming in large pore catalyst,” Chem. Eng. Sci., 65(5), pp. 1539–1550.

[142] Shaahid S. M. and Elhadidy M. A., 1994, “Wind and solar energy at Dhahran, Saudi Arabia,” Renew. Energy, 4(4), pp. 441–445.

VITAE

Name: Muhammad Ibrar Hussain

Date of Birth: April 1, 1988

Present Address: KFUPM P. O. Box 8637, King Fahd University of Petroleum and Mineral, Dhahran-31261, Saudi Arabia

Permanent Address: House No. 8, Opposite to Municipal Park, Tulamba Road, Mian Channu, Punjab, Pakistan

Email Address: mibrarhussain@kfupm.edu.sa

ibrarhm@gmail.com

Educational Qualification:

M.S (Mechanical Engineering)

January, 2014

King Fahd University of Petroleum & Minerals,

Dhahran, Saudi Arabia.

B.E. (Mechanical Engineering)

June, 2010

University of Engineering and Technology,

Lahore, Pakistan.